November 27, 1961

To the Graduate Council:

I am submitting herewith a dissertation written by William Joseph Carnes entitled "Flame Photometric Studies: Part A: Studies of the Extraction and Flame Emission of Yttrium; Part B: Droplet Size of Aerosols in Flame Photometry; Part C: Studies of the Reaction Zone of an Oxygen-Acetylene Flame." I recommend that it be accepted in partial fulfillment of the requirements for the degree of Doctor of Philosophy, with a major in Chemistry.

John A. Dean
Major Professor

We have read this dissertation and recommend its acceptance:

Geo. K. Schweitzer

[illegible]

William H. Fletcher

E. E. Stansbury

Accepted for the Council:

Hilton A. Smith
Dean of the Graduate School

FLAME PHOTOMETRIC STUDIES

PART A: STUDIES OF THE EXTRACTION AND FLAME EMISSION OF YTTRIUM

PART B: DROPLET SIZE OF AEROSOLS IN FLAME PHOTOMETRY

PART C: STUDIES OF THE REACTION ZONE OF AN OXYGEN-ACETYLENE FLAME

A Dissertation

Presented to

the Graduate Council of

The University of Tennessee

In Partial Fulfillment

of the Requirements for the Degree

Doctor of Philosophy

---

by

William Joseph Carnes

December 1961

ACKNOWLEDGEMENT

The author wishes to express his sincere appreciation to Professor John A. Dean for the suggestions and encouragement he has given during the course of this research.

505984

TABLE OF CONTENTS

CHAPTER		PAGE
PART A. STUDIES OF THE EXTRACTION AND FLAME EMISSION OF YTTRIUM		
I.	INTRODUCTION	1
	A. Historical Introduction	1
	B. Organic Solvents and Flame Photometry	2
	C. Early Work on Yttrium and the Rare Earths	2
	D. Statement of the Problem	3
II.	APPARATUS AND REAGENTS	4
	A. Apparatus	4
	1. Flame Spectrophotometer	4
	2. Rotameter	4
	3. Precision Wet-Test Meter	5
	B. Instrument Settings	5
	C. Reagents	5
	1. Demineralized Water	5
	2. 4-Methyl Pentan-2-One	5
	3. 2-Thenoyltrifluoroacetone Solution	5
	4. Standard Yttrium Solutions	6
	5. Buffer Solutions	6
	6. Anion Solutions	7
	7. Cation Solutions	7
III.	EXPERIMENTAL RESULTS AND DISCUSSION	9
	A. Flame Spectrum	9

CHAPTER PAGE

III. (Continued)

1. Background Correction 11
2. Emission Sensitivity. 11
B. Working Curve 11
C. Slit Width. 13
D. Effects of Flows of Acetylene and Oxygen on Emission Intensities 13
1. Burner Height 15
2. Aspiration Rate 15
E. Extraction of Yttrium 16
1. Extraction Curve. 16
2. Aqueous-Organic Volume Ratio. 17
F. Interference Studies on the Emission of Yttrium 20
1. Calcium Interference. 23
2. Cerium Interference 23
3. Cobalt Interference 23
4. Copper Interference 25
5. Iron(III) Interference. 25
6. Lanthanum Interference. 25
7. Manganese Interference. 25
8. Thorium Interference. 29
9. Vanadium, Zinc, and Zirconium Interferences 29
10. Rare Earth Interferences. 29
11. Anionic Interferences 29

CHAPTER PAGE

IV. SUMMARY 30

BIBLIOGRAPHY. 32

PART B. DROPLET SIZE OF AEROSOLS IN FLAME PHOTOMETRY

I. INTRODUCTION. 36

A. Atomization in Flame Photometry 36

B. Mechanism of Pneumatic Atomization. 37

C. Experimental Methods for Obtaining Drop Size. 40

1. Microscopic Methods 40

2. Frozen Droplet Methods. 41

3. Photographic Methods. 41

4. Optical Methods 42

5. Electronic Methods. 42

6. Cascade Impactors 42

D. Mathematical Expression of Droplet Size Distribution. . . 43

1. Empirical Functions 43

2. Log-Normal Distribution Functions 44

3. Upper-Limit Function. 46

E. Mean Diameters. 48

1. Aqueous Versus Organic Solvents 49

2. Evaporation Rates 50

G. Statement of the Problem. 51

II. APPARATUS AND REAGENTS. 52

A. Apparatus 52

1. Chemical Microscope 52

CHAPTER PAGE

II. (Continued)

2. Atomizer. 52

3. Sampling Device 52

B. Reagents. 52

1. Chloroform. 52

2. Demineralized Water 53

3. 4-Methyl Pentan-2-One 53

III. EXPERIMENTAL RESULTS. 54

A. Measurement of Droplet Sizes. 54

B. Distribution Studies. 55

C. Mean Diameters. 59

IV. DISCUSSION OF RESULTS 62

A. Observed Droplet Sizes. 62

B. Distribution Studies. 64

C. Mean Diameters. 65

D. Correlation of Droplet Size to Evaporation Rates. 66

V. SUMMARY 69

BIBLIOGRAPHY. 70

PART C. STUDIES OF THE REACTION ZONE OF AN OXYGEN-ACETYLENE FLAME

I. INTRODUCTION. 74

A. Spectra of Hydrocarbon Flames 74

1. The CH Bands. 74

2. The Swan Bands of C_2. 74

3. The Atomic Carbon Line. 74

CHAPTER PAGE

I. (Continued)

4. The OH Bands 75

5. Other Band Systems 75

B. Abnormal Excitation in Flames 76

C. Causes for Abnormal Excitation 77

D. Excitation Processes in Flame Photometry 78

E. Statement of the Problem 79

II. APPARATUS AND REAGENTS 80

A. Apparatus 80

1. Flame Spectrophotometer 80

2. Gas Flows 80

B. Reagents 80

1. Demineralized Water 80

2. 4-Methyl Pentan-2-One 80

3. Hydrobromic Acid 81

4. Arsenic Solutions 81

5. Antimony Solutions 81

6. Bismuth Solutions 81

7. Calcium Solutions 82

8. Cadmium and Zinc Solutions 82

9. Mercury(II) Solutions 82

10. Platinum Solutions 83

11. Tin Solutions 83

CHAPTER PAGE

III. EXPERIMENTAL RESULTS. 84

A. Development of the Light-Pipe 84

B. Study of Transmission Properties of the Light-Pipe. . . . 85

1. Effect of the Light Source Diameter 87

2. Effect of the Light Source Diameter with a Non-Reflecting Tube 90

3. Photoresponse Without the Use of a Light Pipe 90

C. Mounting the Light-Pipe 93

D. Alignment Procedure 93

E. Emission Zones of Flame Spectra 95

1. Carbon Line 95

2. CH and C_2 Band Emission 98

3. OH Band Emission. 98

F. Flame Spectra of Metals in the Reaction Zone. 101

1. Procedure 101

2. Instrument Settings 101

3. Arsenic Spectrum. 101

4. Antimony Spectrum 101

5. Bismuth Spectrum. 104

6. Tin Spectrum. 104

7. Zinc Spectrum 109

8. Cadmium Spectrum. 109

9. Mercury Spectrum. 109

10. Platinum Spectrum 109

CHAPTER PAGE

III. (Continued)

G. Interference Studies of Arsenic, Antimony, and Bismuth. . 110

1. Self-Absorption Studies 110

2. Mutual Interferences. 110

3. Effect of Tin and Zinc on the Emission Intensity of Arsenic 112

H. Ratio of Signal-to-Background Using the Light-Pipe. . . . 114

I. Observations on the Emission Intensity Distribution of Calcium 118

IV. DISCUSSION OF RESULTS 122

A. Application of the Light-Pipe to Flame Photometry 122

B. Flame Spectra of Metals in the Reaction Zone. 122

C. Interference Studies of Arsenic, Antimony, and Bismuth. . 125

D. Observations on the Emission Intensity Distribution of Calcium 126

E. Suggestions for Further Study 127

V. SUMMARY 128

BIBLIOGRAPHY. 129

LIST OF TABLES

TABLE PAGE

PART A. STUDIES OF THE EXTRACTION AND FLAME EMISSION OF YTTRIUM

I. Effect of Aqueous-Organic Volume Ratio on the Recovery of Yttrium 19

II. Tolerance Limits for Diverse Cations Upon the Emission Intensity of Yttrium. 21

III. Tolerance Limits for Anions Upon the Emission Intensity of Yttrium 22

PART B. DROPLET SIZE OF AEROSOLS IN FLAME PHOTOMETRY

IV. Representation of Distribution. 56

PART C. STUDIES OF THE REACTION ZONE OF AN OXYGEN-ACETYLENE FLAME

V. Signal-to-Background Ratios as Observed with the Light-Pipe and Without the Light-Pipe. 119

VI. Emission Lines Observed for Some Elements in the Reaction Zone. 123

LIST OF FIGURES

FIGURE PAGE

PART A. STUDIES OF THE EXTRACTION AND FLAME EMISSION OF YTTRIUM

1. Flame Spectrum of Yttrium Showing Band Heads at 597 mμ and 613 mμ 10
2. Emission of Yttrium as a Function of the Concentration of Yttrium in 4-Methyl Pentan-2-One 12
3. Emissivity of the 597 mu Band Head of Yttrium as a Function of the Ratio of Oxygen Flow to Acetylene Flow 14
4. Per Cent Yttrium Extracted as a Function of pH 18
5. Calcium Spectrum from 580 mμ to 620 mμ from a Solution of 100 μg. of Calcium Per Ml. of 4-Methyl Pentan-2-One. 24
6. Iron Spectrum from 580 mμ to 620 mμ from a 4-Methyl Pentan-2-One Solution Which Contained 200 μg. of Iron Per Ml. 26
7. Lanthanum Spectrum from 580 mu to 620 mμ from a 4-Methyl Pentan-2-One Solution Which Contained 200 μg. of Lanthanum Per Ml.. 27
8. Manganese Spectrum from 580 mμ to 620 mμ from a 4-Methyl Pentan-2-One Solution Which Contained 200 μg. of Manganese Per Ml.. 28

PART B. DROPLET SIZE OF AEROSOLS IN FLAME PHOTOMETRY

9. Drop Size Distribution of Water. 58
10. Drop Size Distribution of Chloroform 60
11. Drop Size Distribution of 4-Methyl Pentan-2-One. 61
12. Histogram Showing the Per Cent of the Total Number of Drops Observed Versus the Diameter in Microns of Each Size Group . 63

FIGURE PAGE

PART C. STUDIES OF THE REACTION ZONE OF AN OXYGEN-ACETYLENE FLAME

13. Device for Measuring Transmission Properties of the Light-Pipe 86

14. Plot of Relative Light Intensity Versus the Position of the Light Source for Three Light Source Diameters. Light Source 0.7 cm. from Entrance of Light-Pipe. 88

15. Plot of Relative Light Intensity Versus the Position of the Light Source for Three Light Source Diameters. Light Source 3.0 cm. from Entrance of Light-Pipe. 89

16. Plot of Relative Light Intensity with a Non-Reflecting Light-Pipe Versus the Position of the Light Source for Three Light Source Diameters. Light Source 3.0 cm. from Entrance of Light-Pipe 91

17. Plot of Relative Light Intensity With and Without the Light-Pipe Versus the Position of the Light Source for Two Light Source Diameters 92

18. Light-Pipe Mounting Bracket for Beckman Model DU Spectrophotometer with Flame Attachment. 94

19. Flame Spectrum of Carbon Showing the Atomic Line at 247.8 mμ . 96

20. Plot of Emission Intensity of the 247.8-mμ Carbon Line Versus Relative Flame Region Viewed 97

21. Plot of Emission Intensities of the 431.1-mμ CH Band Head and the 516.5-mμ C_2 Band Head Versus Flame Region Viewed 99

FIGURE PAGE

22. Plot of Emission Intensity of the 306.7-mμ OH Band Head Versus Flame Region Viewed 100

23. Flame Spectrum of Arsenic Showing the Atomic Line at 234.9 mμ. 102

24. Plot of Emission Intensities of Arsenic, Antimony and Bismuth Versus Flame Region Viewed 103

25. Flame Spectrum of Antimony Showing the Atomic Line at 252.8 mμ 105

26. Flame Spectrum of Bismuth Showing the Atomic Lines at 222.8 mμ and 223.0 mμ 106

27. Plot of Emission Intensities of Tin and Carbon as a Function of Flame Region Viewed 107

28. Plot of Emission Intensities of Tin and Carbon as a Function of Flame Region Viewed 108

29. Plot of Emission Intensity Versus Concentration on Logarithmic Coordinates for Arsenic, Antimony, and Bismuth 111

30. Flame Spectrum of Arsenic and Tin Showing the Degree of Resolution of the 234.9-mμ Arsenic Line and the 235.5-mμ Tin Line 113

31. Plot of Emission Intensity of the 247.8-mμ Carbon Line as a Function of the Flame Region Viewed. 115

32. Plot of Emission Intensity of the 520-mμ Chromium Triplet Versus Relative Flame Region Viewed. 117

33. Plot of Emission Intensities of the 422.7-mμ Calcium Line and the 247.8-mμ Carbon Line Versus Flame Region Viewed. 120

PART A

STUDIES OF THE EXTRACTION AND FLAME EMISSION OF YTTRIUM

CHAPTER I

INTRODUCTION

A. Historical Introduction

It is somewhat of a paradox that part of the earliest recorded work on flame spectra involved the discovery by Kirchhoff and Bunsen of two new elements, cesium in 1860 and rubidium in 1861.[1] From that time until the early 1930's, a period of nearly three-quarters of a century, the usefulness of flame spectroscopy was restricted largely to qualitative applications. The major difficulties which were encountered in quantitative analysis were in burner design and in methods of reproducibly introducing samples into the flame. Lundegardh[2] is credited with recognizing the quantitative applications of flame excitation as a useful and convenient method of analysis. This was due mainly to his improved method of introducing samples into the flame with a discharge type atomizer. Lundegardh-type spray chambers are still utilized on some commercial flame photometers.[3] Modern electronic circuits and the introduction of the electron multiplier phototube have permitted comparatively weak signals from the flames to be suitably amplified and recorded.

B. Organic Solvents and Flame Photometry

A major contribution to the utility of flame-spectrophotometric methods has been the use of organic solvents. Aqueous-organic solutions and nonaqueous organic solvents aspirated directly into a flame have become accepted techniques for flame-photometric analysis. Smit, Alkemade, and Verschure[4] were the first to take advantage of the increased emission sensitivities of sodium and potassium when organic solvents, such as the low molecular weight alcohols and ketones, were mixed with aqueous solutions.

Purely nonaqueous solvent systems were first reported by Conrad and Johnson[5] in the analysis of metal additives in lubricating oils. A common method of analysis for lead in gasolines was developed by Gilbert[6] whereby the gasoline samples were aspirated directly into a flame.

Solvent extraction systems are becoming widespread in their usefulness for flame photometry. A judicious choice of chelating agent, pH, and solvent gives a high degree of versatility to this method of analysis. Many interfering elements can be eliminated. The atomization of a combustible solvent produces a larger flame and metal emissions are increased many-fold, bringing many elements with weak flame emission within the realm of flame-photometric methods of analysis.[7]

C. Early Work on Yttrium and the Rare Earths

Piccardi[8] and Piccardi and Sberna,[9] in classifying the yttrium oxide bands in the flame, reported a good spectrum with 0.001 per cent

yttrium oxide. Plantinga and Rodden,[10] using the spark-in-flame method of Hultigren,[11] gave 0.0001 M. of yttrium as its limit of detection, but reported an unsteady emission below 0.001 M. (equivalent to 89 µg. of yttrium per ml.). An approximate analysis scheme was employed in which the emission of yttrium solutions were measured after successive dilution until the yttrium bands were no longer detectable. Pinta[12] examined the flame spectra of dilute solutions of the rare earths using a small prism spectrograph and air-acetylene flames. Sensitivities ranged from 4 µg. per ml. for europium to 50 µg. per ml. for praseodymium. In a later study, Pinta[13] studied the eluate fractions from an ion exchange column. Concentrations of rare earth oxide up to 0.5 per cent were determined.

Rains, House, and Menis[14] reported the flame spectra of yttrium and the rare earths from an organic aerosol with an oxy-hydrogen flame. Direct-current arc procedures for yttrium are limited to the 50- to 100-µg. per ml. range.[15]

D. Statement of the Problem

Although the flame spectrum of yttrium has been well defined in previous work, very little information was available in regard to the effect of spectral and radiation interferences, other than the rare earths, upon the emission of yttrium. Information regarding the optimum conditions for the flame-photometric determination of yttrium was lacking also. The main objective of this phase of work was clarification of these points. Development of a suitable method of analysis for yttrium was also considered.

CHAPTER II

APPARATUS AND REAGENTS

A. Apparatus

1. Flame Spectrophotometer

A Beckman Model DU spectrophotometer with a modified Model 9220 flame attachment and Model 4304 photomultiplier unit was used. The modification on the flame attachment consisted of a rack-and-pinion burner mount whereby the burner could be raised and lowered at will. A Beckman Energy Recording Attachment (ERA), Model 5800, coupled the photomultiplier output to a Bristol Dynamaster Recorder, Model 1PH560-51. The recorder had a 10-mv., full-scale response with a 2/3-second pen response. The chart was driven at a rate of 4 inches per minute. The wavelength positioning knob on the Beckman Model DU was replaced with a motor-driven gear train which rotated the wavelength shaft at approximately 0.17 revolutions per minute. A 10.5-to-1 gear reduction knob permitted fast manual positioning to the wavelength region desired.

A Beckman Model 4030 integral aspirator-burner, designed for use with acetylene and oxygen, was used as the excitation source.

2. Rotameter

A pair of Brooks, Sho-Rate "150", Model 1356 rotameters were used to meter the flows of oxygen and acetylene to the burner. Tube number 3-15-4 was used to regulate the oxygen flow and tube number 4-15-2 was used to regulate the acetylene flow. The rotameters were calibrated

under operating conditions by the use of a Precision Wet-test Meter.

3. Precision Wet-Test Meter

The Precision Wet-test Meter provided a means of calibrating the rotameters used to regulate the flow of gases under operating conditions. The aspirating capillary was sealed to insure that all of the gases flowing through the burner would be measured by the Wet-test Meter.

B. Instrument Settings

The following instrument settings were employed:

ERA, per cent adjust	60
Selector switch, position	0.1
Phototube resistor, megohms	22
Phototube (RCA 1P28), volts per dynode	60
Acetylene flow, cu. ft. per hr.	2.25
Oxygen flow, cu. ft. per hr.	7.38
Slit width, mm.	0.030
Spectral (half) band width (at 600 mμ), mμ	1.05

C. Reagents

1. Demineralized Water

Demineralized water was used in the preparation of all solutions. This was prepared by passing ordinary distilled water through a column of Amberlite MB-3 resin.

2. 4-Methyl Pentan-2-One

Practical grade 4-methyl pentan-2-one was used without further purification.

3. 2-Thenoyltrifluoroacetone Solution

A 0.1 M. solution of 2-thenoyltrifluoroacetone (TTA) was prepared by dissolving 5.5 g. of technical grade 2-thenoyltrifluoroacetone in 4-methyl pentan-2-one and then diluting to 250 ml. with additional solvent. The solution was stored in a cool place and protected from light.

4. Standard Yttrium Solutions

Yttrium nitrate, c. p. grade, was precipitated as the oxalate, washed with boiling water, and ignited to the oxide, Y_2O_3. A standard solution of yttrium, 1.00 ml. equivalent to 4.00 mg. of yttrium, was prepared by dissolving 1.270 g. of yttrium oxide in a minimum amount of concentrated nitric acid and 30 per cent hydrogen peroxide to cause dissolution. The solution was boiled to remove excess hydrogen peroxide and the volume was adjusted to 250 ml. with demineralized water. Less concentrated standards were prepared by appropriate dilutions.

5. Buffer Solutions

Reagent grade acetic acid (0.5 mole) was diluted with ammonium hydroxide until the desired pH value was attained. The solution was diluted to 500 ml., giving a buffer solution 1.0 M. in total acetate. Solutions 0.5 M. and 1.5 M. in total acetate were prepared in an analogous manner.

6. Anion Solutions

The following reagent grade compounds were dissolved in demineralized water to give an anion concentration of 10,000 µg. per ml. Other concentrations of anion used were prepared by appropriate dilution.

Anion	Compound	Grams per 500 ml. of Solution
Br^-	NH_4Br	6.1286
Cl^-	NH_4Cl	7.5443
F^-	NaF	11.053
HPO_4^{-2}	$(NH_4)_2HPO_4$	6.8800
I^-	NH_4I	5.7107
NO_3^-	NH_4NO_3	6.4557
$C_2O_4^{-2}$	$(NH_4)_2C_2O_4 \cdot H_2O$	8.075
ClO_4^-	$NaClO_4$	6.1559
SO_4^{-2}	$(NH_4)_2SO_4$	6.8775

7. Cation Solutions

The following reagents were dissolved in demineralized water by conventional means to give a cation concentration of 10,000 µg. per ml. Other concentrations of cation used were prepared by appropriate dilution.

Cation	Compound	Grams per 500 ml. of Solution
Al^{+3}	Al metal	5.000
Ba^{+2}	$Ba(NO_3)_2$	9.512
Ca^{+2}	$Ca(NO_3)_2 \cdot 4H_2O$	29.460
Ce^{+4}	$Ce(SO_4)_2$	11.858
Co^{+2}	$Co(NO_3)_2 \cdot 6H_2O$	24.690

Cr^{+3}	$Cr(NO_3)_3 \cdot 9H_2O$	38.472
Cu^{+2}	Cu metal	5.000
La^{+2}	$La(NO_3)_2 \cdot 6H_2O$	14.876
Mg^{+2}	MgO	8.290
Mn^{+2}	Mn metal	5.000
Ni^{+2}	$Ni(NH_4)_2(SO_4)_2 \cdot 6H_2O$	33.651
K^{+}	KNO_3	12.830
Na^{+}	$NaNO_3$	18.480
Th^{+4}	$Th(NO_3)_4 \cdot 4H_2O$	11.895
UO_2^{+2}	$UO_2(C_3H_3O_2)_2 \cdot 2H_2O$	8.909
VO_2^{+}	NH_4VO_3	10.964
Zn^{+2}	Zn metal	5.000
ZrO^{+2}	$ZrO(NO_3)_2 \cdot 2H_2O$	14.650

CHAPTER III

EXPERIMENTAL RESULTS AND DISCUSSION

A. Flame Spectrum

The flame spectrum of yttrium comprises several molecular band systems, each rather narrow. Heads of the band systems are located at 468, 484, 506, 509, 597, and 613 mμ.[8,9,12,14,16] The first five bands, being rather less sensitive than those at 597 and 613 mμ, were not investigated. The bands at 597 and 613 mμ are very intense, quite narrow, and only slightly degraded toward the red. They arise from the transition between the first molecular excited state and the ground state and belong to the orange system.[17] The general appearance of the flame spectrum of yttrium over the wavelength region 580 to 630 mμ is shown in Figure 1. The dashed line represents the oxygen-acetylene flame background when aspirating solvent only.

The 597-mμ and 613-mμ bands rest on the slope of the intense C_2 continuum associated with the Swan C_2 band systems. The background in this region is free of band emissions from the flame gases and is, consequently, quite smooth in appearance. However, in very fuel-rich flames or near the highly luminous reaction zone, the background becomes rather erratic, with increasing slope, and creates some difficulty in determining background corrections. The unresolved yellow doublet of sodium, apparent as a single peak, unavoidably appears as an impurity element in laboratory solutions.

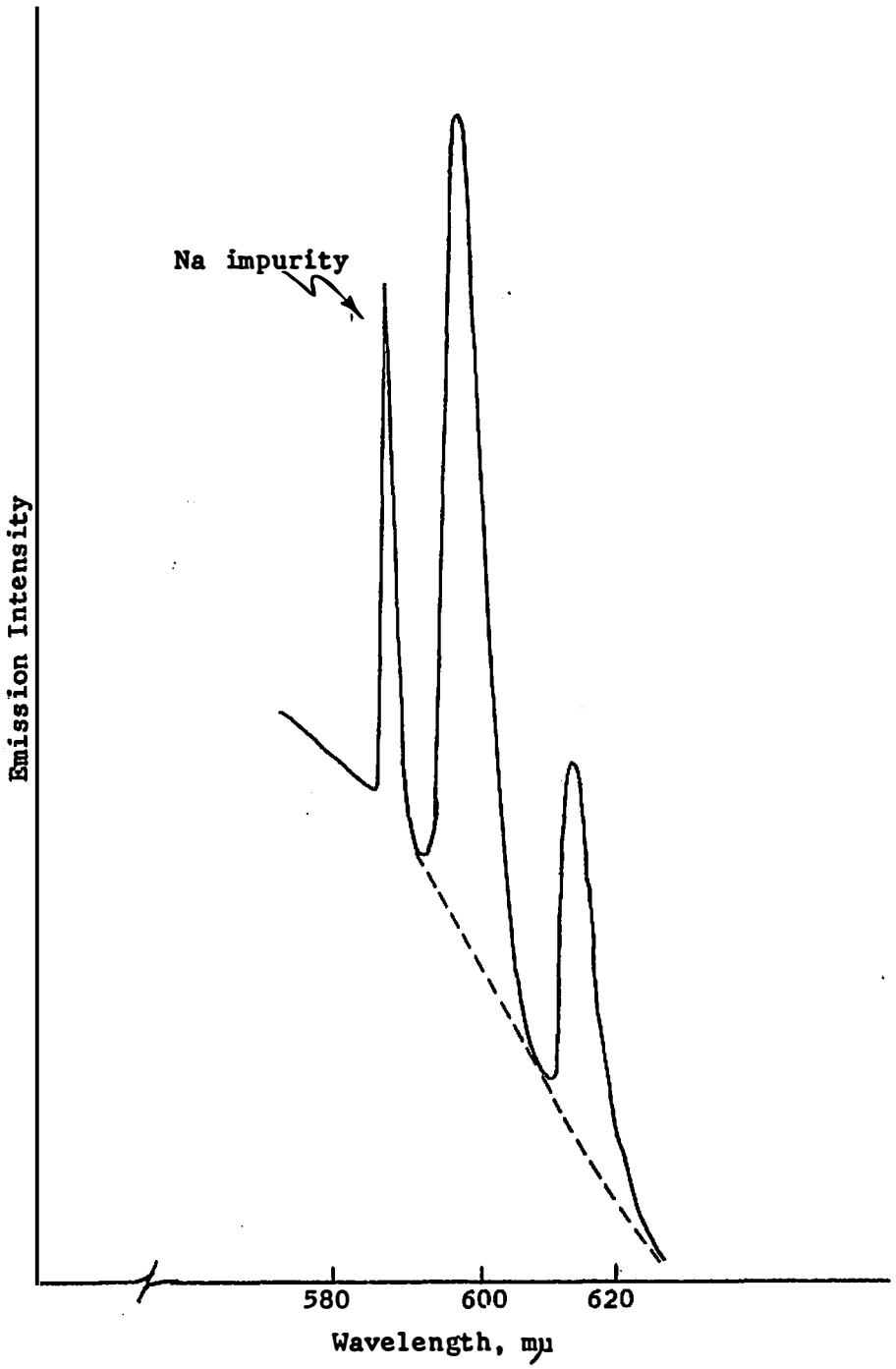

Figure 1. Flame spectrum of yttrium showing band heads at 597 mμ and 613 mμ.

1. Background Correction

A correction was made for the flame background emission at the wavelengths 597 and 613 mμ. The background emission in the vicinity of the 597-mμ band was read at 593 and 608 mμ, the minimum readings on either side of the crest. The average of these readings was then subtracted from the reading at the crest of the band. In like manner, the 613-mμ band was corrected by taking background readings at 608 and 625 mμ.

2. Emission Sensitivity

For the instrument settings employed and the particular photomultiplier tube installed, the emission sensitivity was 0.25 μg. of yttrium per ml. per 0.1 mv. at 597 mμ. The 613-mμ band was about one-half as sensitive as the 597-mμ band and had an emission sensitivity of 0.55 μg. of yttrium per ml. per 0.1 mv. These values were for a 4-methyl pentan-2-one solution of yttrium and represented a 400-fold enhancement over values obtained under optimum conditions for an aqueous solution of yttrium.

B. Working Curve

The band heads at 597 and 613 mμ were very sensitive. At these wavelengths an ERA setting of 50 per cent gave a chart reading of approximately 4,0 mv. when using a 4-methyl pentan-2-one solution of yttrium containing 12.5 μg. per ml. The calibration curve was linear up to 20 μg. per ml., the largest concentration investigated, as shown in Figure 2.

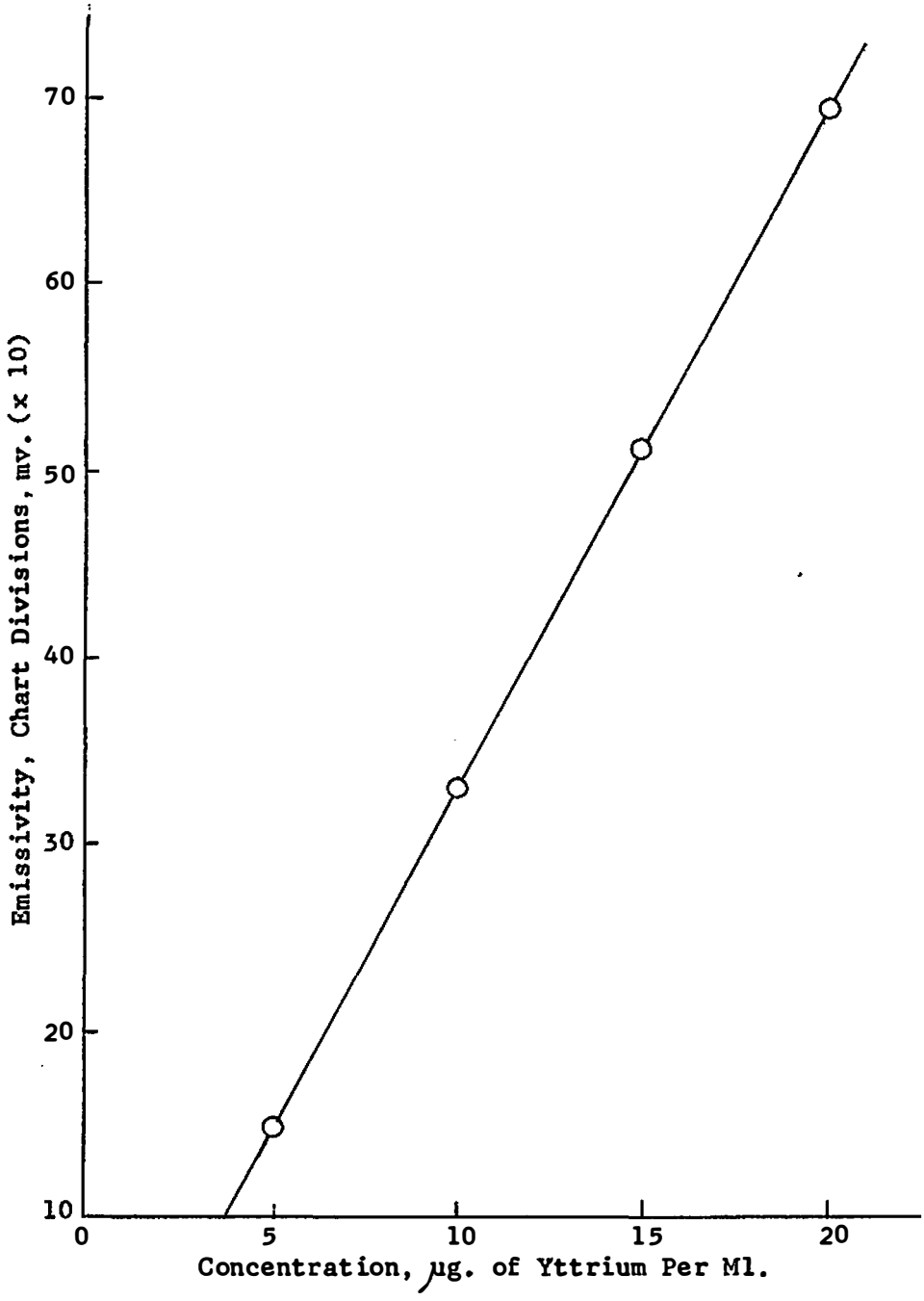

Figure 2. Emission of yttrium as a function of the concentration of yttrium in 4-methyl pentan-2-one.

C. Slit Width

The slit width used was 0.030 mm. which corresponded to a spectral band width (width at one-half the net peak height) of 1.05 mμ at 597 mμ. At larger slit widths the two bands at 597 and 613 mμ were incompletely resolved from each other and from the sodium doublet at 589.0 and 589.6 mμ. The one-half band widths of the yttrium bands were 6 and 5 mμ for the 597 and 613-mμ band heads, respectively.

D. Effects of Flows of Acetylene and Oyxgen on Emission Intensities

The variation of the intensity of the 597-mμ band of yttrium as a function of the ratio of oxygen flow to acetylene flow for a number of fixed oxygen (and acetylene) flows when injecting an aerosol of 4-methyl pentan-2-one is shown in Figure 3. For fuel-rich flames, as the oxygen flow increased, a definite maximum occurred in the emission intensity. The increase in emission intensity probably resulted from a concurrent increase in aerosol aspirated which in turn increased the time-concentration of yttrium in the flame and thus effectively increased the amount of yttrium available for excitation and emission. High acetylene flows produced luminous and unsteady flames, consequently, the flame background stability became the determining factor in the choice of the optimum acetylene flow.

At lower acetylene flows the emission intensity decreased. This resulted from a marked decrease in flame size and a lowering of the energy content of the flame due to the decrease in the combustible

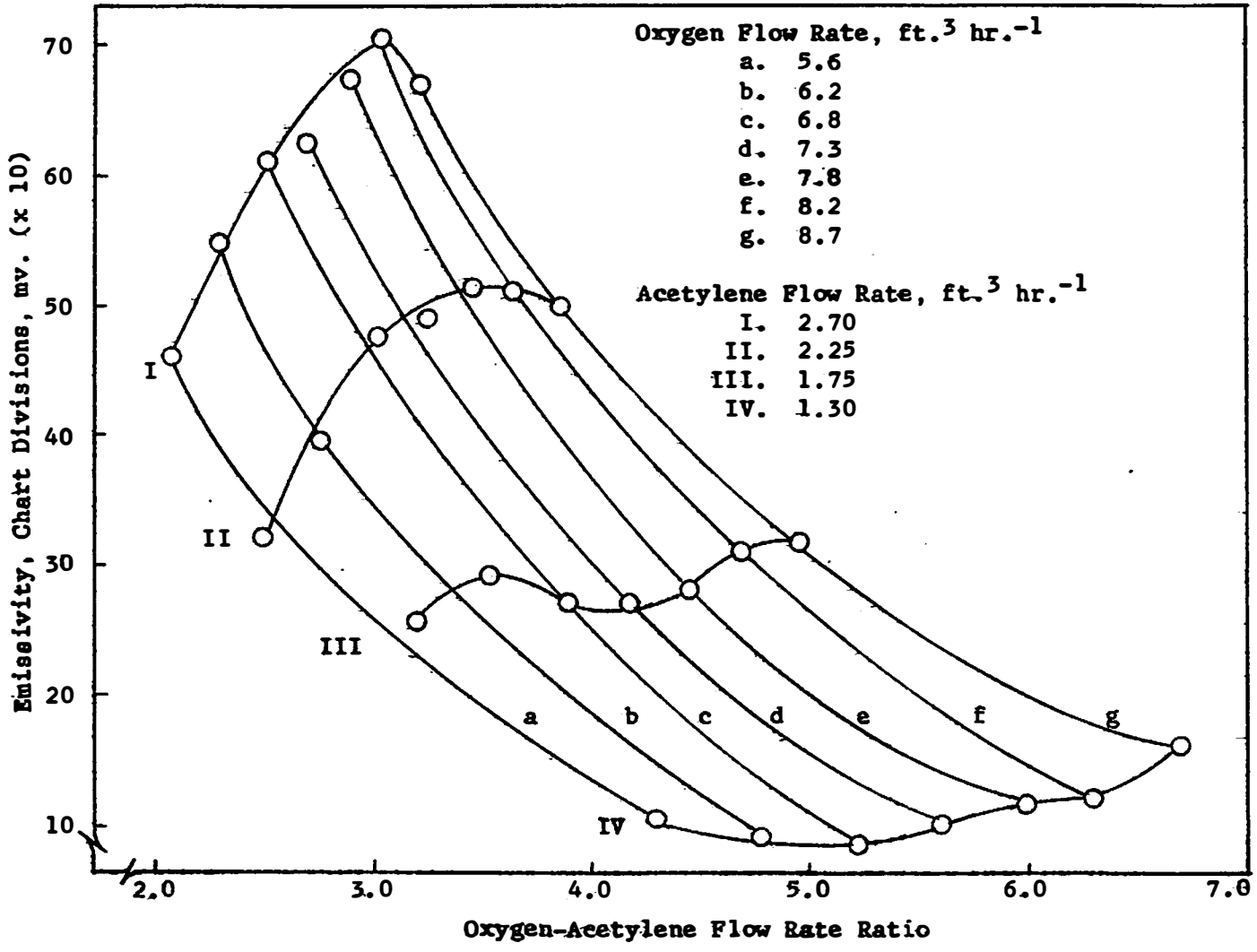

Figure 3. Emissivity of the 597 mμ band head of yttrium as a function of the ratio of oxygen flow to acetylene flow.

component of the gases. At the lower limit of acetylene flow (1.3 cu. ft. per hr.) the slight increase in emission intensity, as the oxygen flow was increased, was again due to the resulting increase in aspiration rate. At high ratios of oxygen flow to acetylene flow, the aerosol itself became the major source of fuel. The flame was usually extinguished when the burner capillary was withdrawn from the solution. The optimum ratio of oxygen flow to acetylene flow were 3.0-3.8, and tended toward the lower ratio as the oxygen flow increased concomittantly with the acetylene flow. In many respects the excitation conditions resembled those recommended for aluminum[18] and lanthanum,[19] other members of Periodic Group III.

1. Burner Height

A cursory study of the emission intensity as a function of the flame region viewed revealed the region of maximum emission intensity occurred immediately above the inner cone. An extensive treatment was precluded by the unstable character of the flame background in the vicinity of the inner cone. The normal position of the burner was used. Thus a region of the flame mantle which extends from 10 to 16 mm. above the burner tip was viewed.

2. Aspiration Rate

The volumetric aspiration rates of the 4-methyl pentan-2-one solution for a particular oxygen flow, as shown in Figure 3, are tabulated below:

Oxygen Flow (Liters per Minute)	Volumetric Aspiration Rate (Milliliters per Minute)
2.38	0.63
2.82	0.93
3.14	1.10
3.56	1.38

E. Extraction of Yttrium

The extraction of yttrium from an aqueous solution into 4-methyl pentan-2-one was studied. 2-Thenoyltrifluoroacetone was used as the chelating agent since it was known to extract yttrium.[20] No investigation of other chelating agents was made.

The extraction was carried out in the following manner. Five milliliters of a buffer solution, 1 M. in total acetate concentration, was added to a solution of yttrium; the combined solution was then diluted to a volume of 20 ml. The final concentration of yttrium was 15 µg. per ml. Twenty milliliters of 4-methyl pentan-2-one, 0.1 M. with respect to 2-thenoyltrifluoroacetone, was added and the phases equilibrated for 2 minutes. The 4-methyl pentan-2-one layer was decanted into a 10-ml. beaker and aspirated directly into the flame.

1. Extraction Curve

The pH of the aqueous layer was measured after extraction to insure that no change in pH occurred during the equilibration step. At a pH value which corresponded to apparently complete extraction, the aqueous layer was equilibrated again with 20 ml. of fresh 4-methyl pentan-2-one, 0.1 M. in 2-thenoyltrifluoroacetone and the extract was

aspirated. No residual yttrium was detected in the second extract, which provided assurance that the yttrium was completely extracted by one equilibration with the extractant. Varying the total acetate concentration from 0.1 M. to 0.3 M. in the aqueous solution did not affect the position or shape of the extraction-pH curve. The equilibration time was not critical; extractions were complete after 2 minutes of gentle shaking. Vigorous agitation was avoided as it produced emulsions which persisted for 30 minutes or more.

The nature of the extraction-pH curve is shown in Figure 4. Extraction began at pH 1.3 and was complete at pH 4.2 and up to at least pH 10. A pH of 5 was chosen as a suitable pH value for further extractions. The pH value at 50 per cent extraction, $pH_{\frac{1}{2}}$, was 2.8. This should be compared with the $pH_{\frac{1}{2}}$ value of 3.20 which is reported for 0.2 M. TTA in benzene. It seems to be a general rule that oxygenated solvents markedly enhance the extraction of some cations.[21]

2. Aqueous-Organic Volume Ratio

The effect of the aqueous-organic volume ratio was found to be a factor in the apparent concentration of yttrium in the organic phase. In Table I the per cent recovery of yttrium is shown for some aqueous-organic volume ratios. A total of 200 µg. of yttrium was initially present in the aqueous phase. The volume of the organic phase was 10 ml. The apparent increase in concentration was due to the decrease in the volume of the organic phase after equilibration. The amount of yttrium extracted was not effected, but the concentration of yttrium

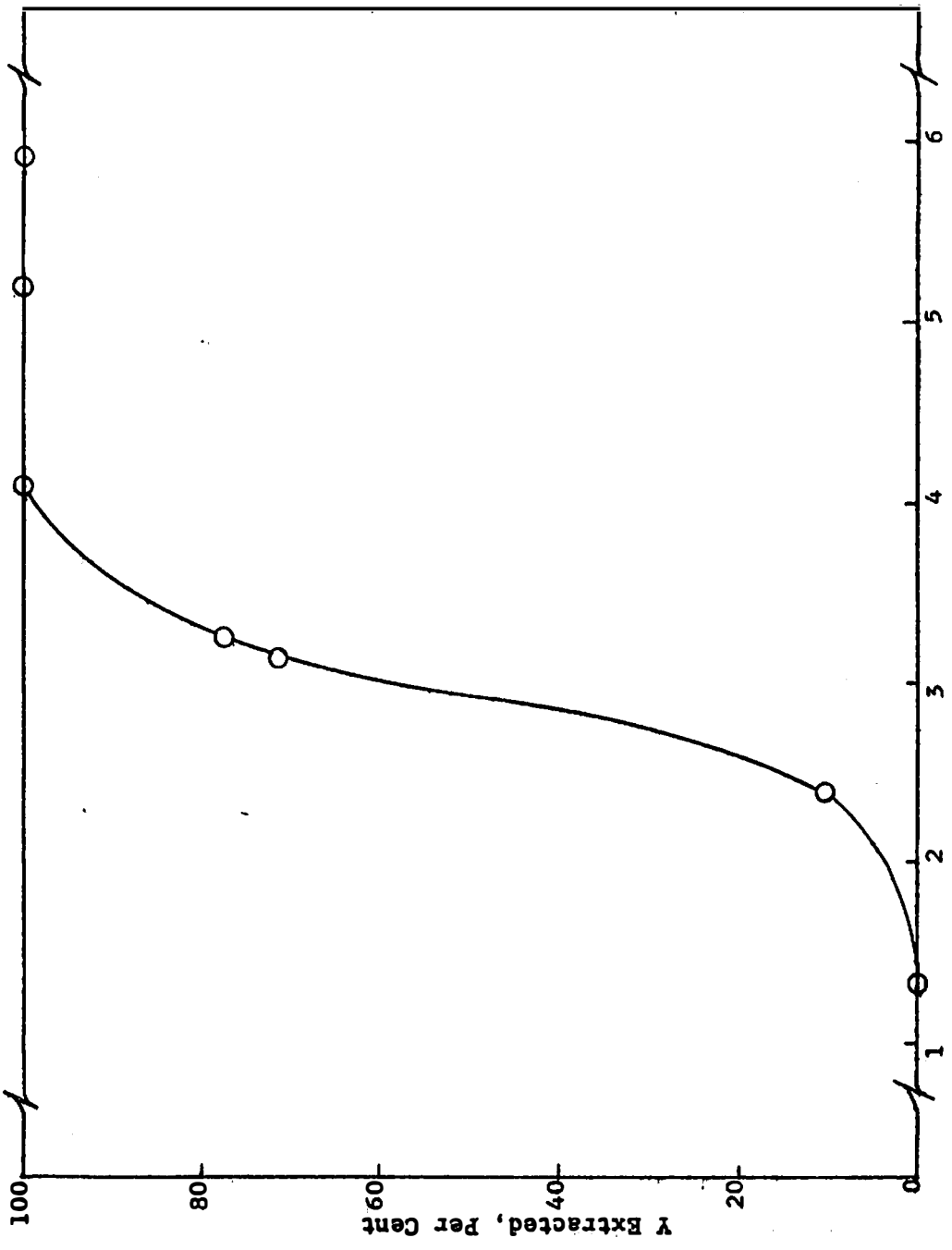

Figure 4. Per cent yttrium extracted as a function of pH.

TABLE I

EFFECT OF AQUEOUS-ORGANIC VOLUME RATIO ON THE RECOVERY OF YTTRIUM

Volume Ratio: Aqueous to Organic Phase[a]	Per Cent Recovery of Yttrium	
	Organic Phase Not Pre-equilibrated	Organic Phase Pre-equilibrated
1	100	100
5	111	107
10	127	119
15	144	135
20	169	
25	202	

[a]Ten milliliters of organic phase was initially present. The aqueous phase contained an initial weight of 200 µg. of yttrium.

increased in the organic phase due to the loss in volume of the organic phase. A prior equilibration of the extracting solution with the acetate buffer reduced the volume loss of the organic phase, however, the acetate buffer apparently dissolves an appreciable quantity of the 4-methyl pentan-2-one. A similar effect was observed by Eshelman, Dean, Menis, and Rains[18] for the extraction of aluminum with 2-thenoyltrifluoro-acetone dissolved in 4-methyl pentan-2-one. A prior equilibration of the acetate buffer with the organic phase was recommended.

F. Interference Studies on the Emission of Yttrium

The extent to which other elements interfere with the emission intensity of yttrium is given in Tables II and III. The quantities indicated for the individual elements represent initial amounts present in the aqueous solution before extraction. No attempt was made to determine the degree of coextraction of a diverse element with yttrium, although data are available oftentimes.[21] Solutions of the test ion in the absence of yttrium were carried through the extraction procedure to ascertain the extent of spectral interference. The degree of interference as tabulated would then apply to the 4-methyl pentan-2-one solution containing a total of 200 µg. of yttrium and perhaps an undetermined amount of interferant. The tolerance limits are of practical value for ascertaining the maximum permissible level of interferant that will not be detrimental to the extraction procedure or to the emission spectrum of yttrium. Interferences encountered are discussed specifically for each element.

TABLE II

TOLERANCE LIMITS FOR DIVERSE CATIONS UPON THE EMISSION INTENSITY OF YTTRIUM

Diverse Ion Present	Tolerance Limit, Mg.	
	597 mμ	613 mμ
Aluminum	20[a]	20[a]
Barium	20[a]	20[a]
Calcium	20[a]	20[a]
Cerium(III)	2	4
Cobalt	2	2
Chromium	20[a]	20[a]
Copper	0.05	0.05
Iron(III)	2	2
Lanthanum	0.2	20[a]
Magnesium	20[a]	20[a]
Manganese	0.2	20[a]
Nickel	20[a]	20[a]
Potassium	20[a]	20[a]
Sodium	20[a]	20[a]
Thorium	1	2
Uranium	20[a]	20[a]
Vanadium	2.5	2.5
Zinc	0.2	20
Zirconium	0.1	0.05

[a]Maximum quantity tested.

TABLE III

TOLERANCE LIMITS FOR ANIONS UPON THE EMISSION INTENSITY OF YTTRIUM

Diverse Ion Present	Tolerance Limit, Mg.
Bromide	20[a]
Chloride	20[a]
Fluoride	0.2
Iodide	20[a]
Nitrate	20[a]
Oxalate	<0.05
Perchlorate	20[a]
Phosphate	<0.1
Sulfate	20[a]

[a]Maximum quantity tested.

1. Calcium Interference

Calcium accompanied yttrium in the extraction and presented serious spectral interference. Calcium possesses strong oxide bands of the orange system with prominent heads from 598 to 636 mμ.[17] The appearance of this band system in the flame spectrum is shown in Figure 5. Fortunately, the interference from calcium was circumvented by a backwashing step. The 4-methyl pentan-2-one solution containing yttrium and calcium was equilibrated with an equal volume of a buffer solution, 0.1 M. in total acetate and having a pH value of 5. This effectively removed all traces of calcium from the 4-methyl pentan-2-one solution without any detectable loss of yttrium.

2. Cerium Interference

Cerium(IV) destroyed the chelating agent. Cerium(III) coextracted and showed a continuum in the region of the yttrium bands, which rendered a background correction impossible above a tolerance limit of 2 mg. of cerium(III) at the 597 mμ band head. A tolerance limit of 4 mg. was permissible when the 613 mμ band head was used.

3. Cobalt Interference

The presence of cobalt produced a general increase in background reading. A background correction was impossible above a tolerance limit of 2 mg. of cobalt. There was no direct spectral interference from bands or lines.

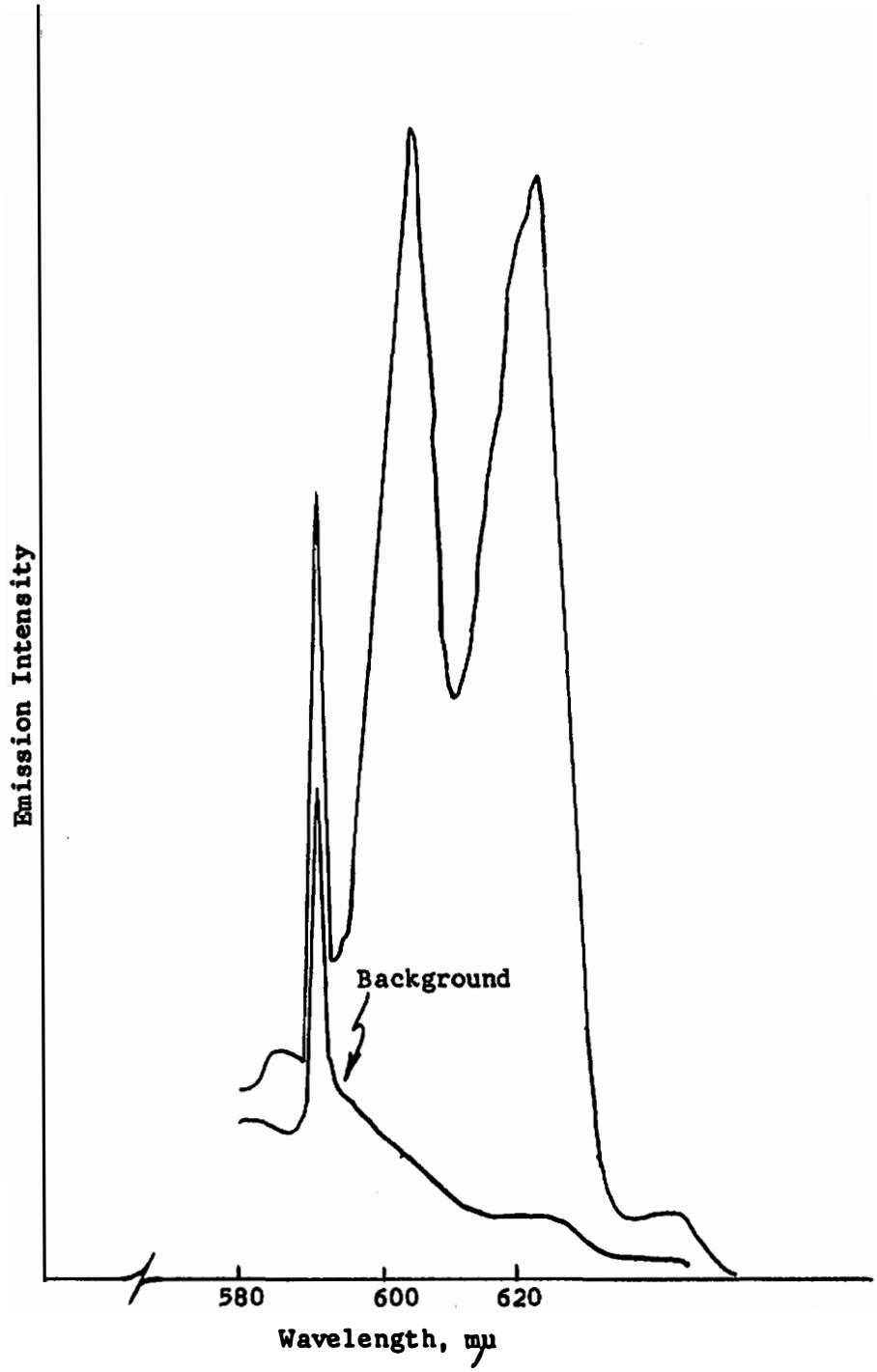

Figure 5. Calcium spectrum from 580 mμ to 620 mμ from a solution of 100 μg. of calcium per ml. of 4-methyl pentan-2-one.

4. Copper Interference

Although copper did not exhibit either a pronounced continuum or direct spectral interference, its presence had a severe quenching action on the yttrium emission.

5. Iron(III) Interference

Iron(III) was coextracted with yttrium. A series of oxide bands with heads at 597, 610, 611, 618, and 622 mμ offered direct spectral interference. Figure 6 illustrates the emission character of the oxide bands of iron. Since the relative intensity of the iron oxide bands was rather weak, some iron could be tolerated or it could be reduced to the divalent state which does not extract.

6. Lanthanum Interference

Figure 7 illustrates the strong oxide band system for lanthanum which is centered around 590 mμ. This band constituted a serious spectral interference for the 597-mμ band of yttrium; however, the 613-mμ band was free from lanthanum interference.

7. Manganese Interference

A strong MnO band at 586/589 mμ is shown in Figure 8. Direct spectral interference was encountered for the 597-mμ band of yttrium. No difficulty was met in the use of the 613-mμ band to record emission intensities for yttrium.

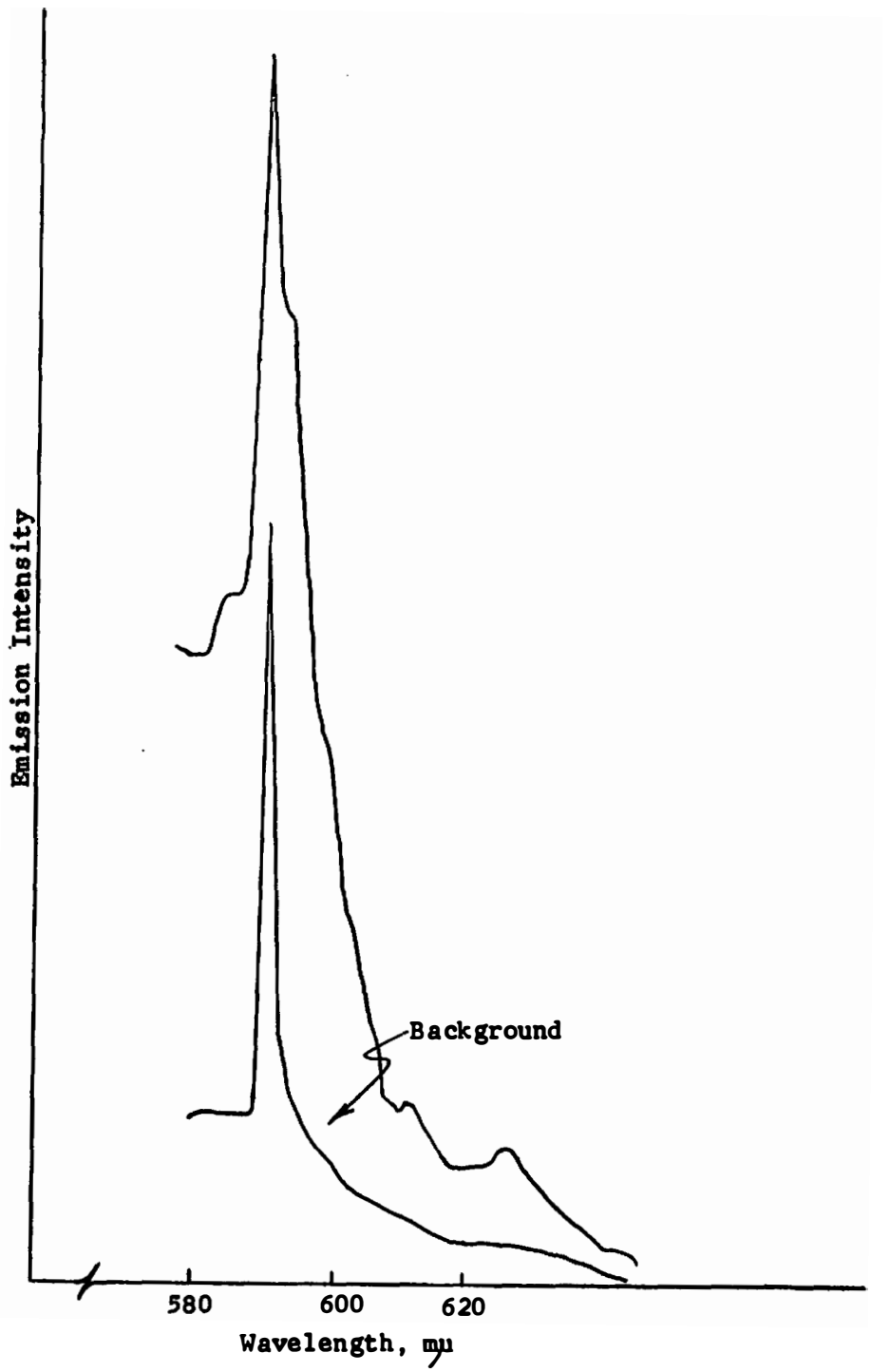

Figure 6. Iron spectrum from 580 mμ to 620 mμ from a 4-methyl pentan-2-one solution which contained 200 μg. of iron per ml.

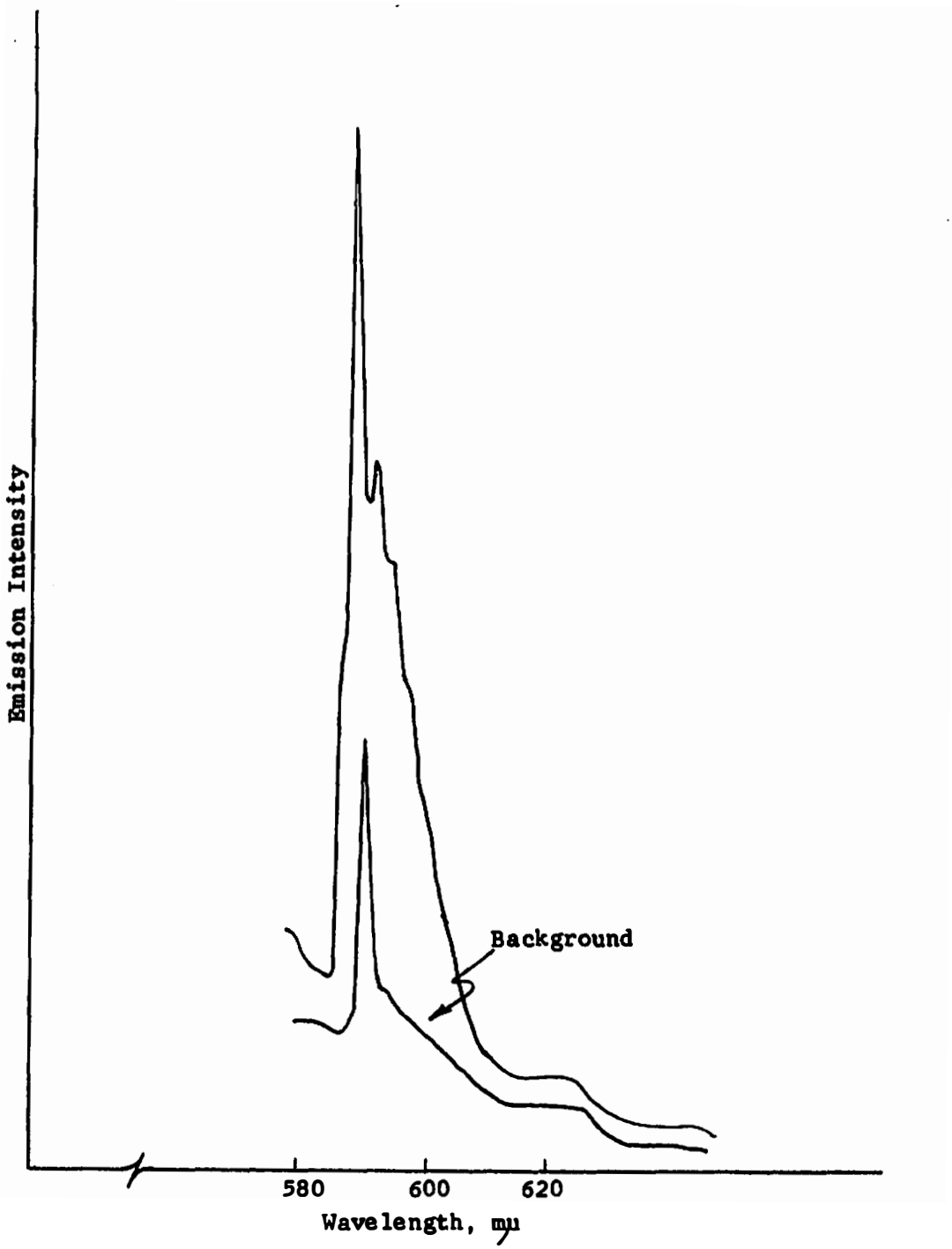

Figure 7. Lanthanum spectrum from 580 mμ to 620 mμ from a 4-methyl pentan-2-one solution which contained 200 μg. of lanthanum per ml.

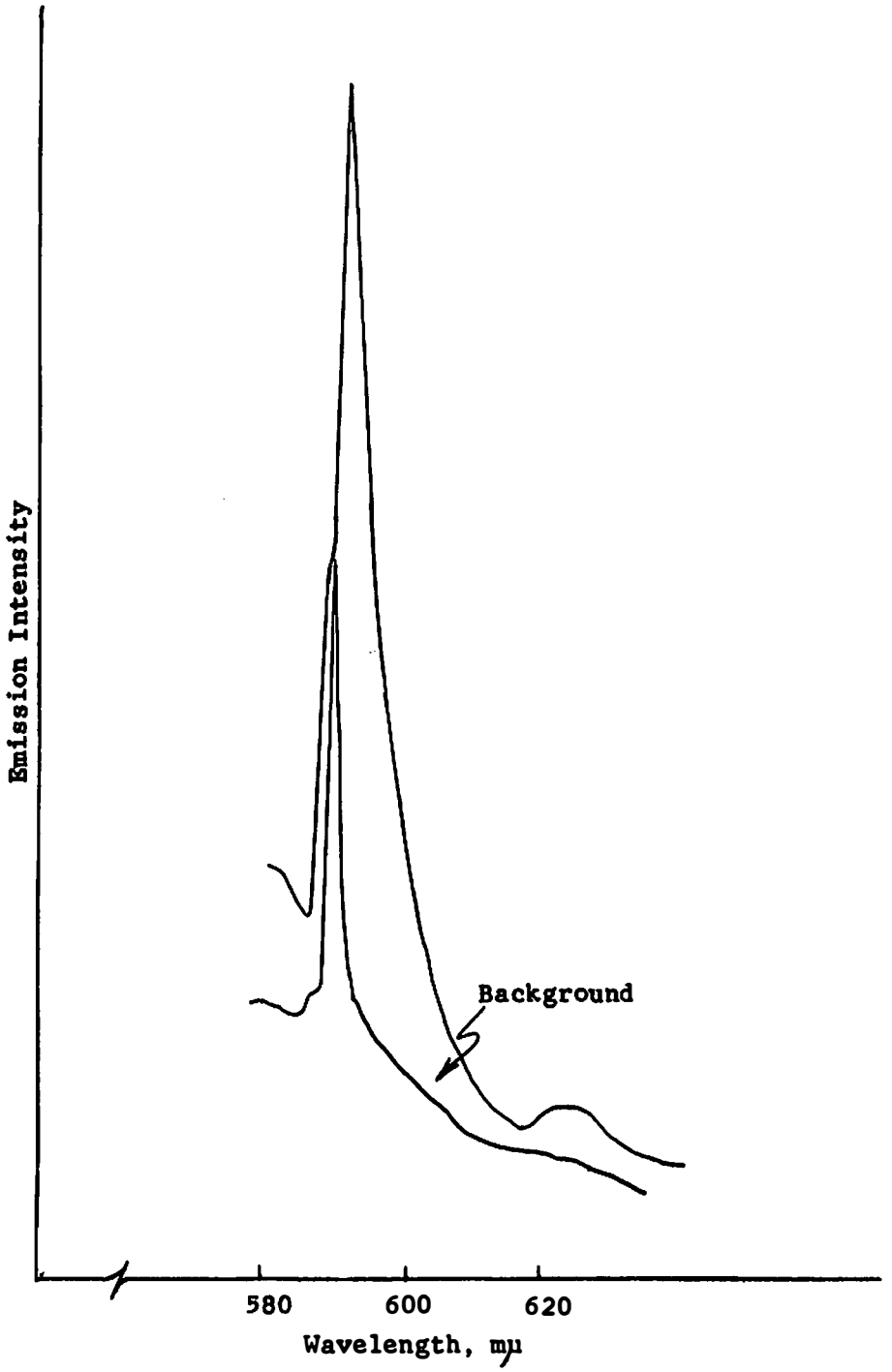

Figure 8. Manganese spectrum from 580 mμ to 620 mμ from a 4-methyl pentan-2-one solution which contained 200 μg. of manganese per ml.

8. Thorium Interference

Thorium produced a general increase in the background radiation level. When a correction was applied for the increase in background, satisfactory results were obtained for the emission intensity of yttrium.

9. Vanadium, Zinc, and Zirconium Interferences

Vanadium, zinc, and zirconium did not exhibit spectral interference and the flame background was essentially unaltered. However, these elements seriously quenched the yttrium emission.

10. Rare Earth Interferences

Interferences from the rare earths have been summarized by Rains, House, and Menis.[14] Gadolinium, europium, and terbium possess strong band systems in the region of the yttrium bands at 597 mμ and 613 mμ which would offer direct spectral interference.

11. Anionic Interferences

Of the anionic substances that were tested, fluoride, oxalate, and phosphate interferred seriously by precipitating yttrium from the aqueous solution and thereby preventing the extraction of yttrium.

CHAPTER IV

SUMMARY

The Beckman DU flame spectrophotometer has been employed in a study of the flame emission characteristics of yttrium. The yttrium oxide bands which crest at 597 and 613 mμ are very sensitive in the oxygen-acetylene flame. A 400-fold enhancement in the emission sensitivity of yttrium is obtained when a 4-methyl pentan-2-one solution of yttrium is aspirated in place of an aqueous solution. The emission sensitivities of the two band heads are 0.25 μg. of yttrium per ml. per 0.1 mv. (per cent T) at 597 mμ and 0.55 μg. per ml. per 0.1 mv. at 613 mμ, using 4-methyl pentan-2-one as the solvent.

The optimum ratio of oxygen to acetylene flows range between 3.0 and 3.8 for maximum emission and a favorable flame and background stability. In many respects the excitation conditions resemble those recommended by Eshelman, Dean, Menis, and Rains[18] and Menis, Rains, and Dean[19] for aluminum and lanthanum, respectively.

An extraction procedure was utilized using a 0.1 M. solution of 2-thenoyltrifluoroacetone dissolved in 4-methyl pentan-2-one. The extraction was made from an aqueous solution buffered at pH 5. A variation in the total acetate concentration of the buffer did not affect the extraction curve.

The effect of numerous cationic and anionic species upon the extraction and subsequent emission intensity of yttrium was determined. Tolerance limits were delineated in instances where interferences were

encountered. Calcium, iron, lanthanum, and manganese were the only cationic species studied which offered spectral interference. Calcium interference was circumvented by a back extraction with a solution buffered at pH 5. Fluoride, oxalate, and phosphate ions precipitated yttrium from the aqueous solution and thereby prevented the extraction of yttrium. Interference from the rare earths has been summarized by Rains, House, and Menis.[14]

Several applications of a flame-photometric method of analysis for yttrium in the 2- to 10-parts-per-million range are suggested. The development of a flame spectrophotometric method for the rapid determination of yttrium should be of interest to workers in the fields of nuclear chemistry and metallurgy. The use of a non-radioactive form of yttrium would permit the use of yttrium as a marker in biological studies. The determination of yttrium in the past has been seriously limited by the lack of sensitive analytical methods, other than by radiotracer techniques.

BIBLIOGRAPHY

BIBLIOGRAPHY

1. J. A. Dean, "Flame Photometry," McGraw-Hill Book Co., Inc., New York, 1960, p. 3.

2. H. Lundegardh, "Die Quantitative Spektralanalyse der Elemente," Vols. 1 and 2, Gustave Fischer Verlagsbuchhandlung, Jena, 1929, 1934.

3. J. A. Dean, op. cit., p. 73.

4. J. A. Smit, C. Th. J. Alkemade, and J. C. M. Verschure, Biochim. et Biophys. Acta, 6, 508-523 (1951).

5. A. L. Conrad and W. C. Johnson, Anal. Chem., 22, 1530 (1950).

6. P. T. Gilbert, Jr., Am. Soc. Testing Materials, Spec. Tech. Publ., 116, 77 (1951).

7. J. A. Dean, op. cit., p. 55.

8. G. Piccardi, Gazz. Chim. ital., 63, 127-128 (1933); C. A., 27, 3667 (1933).

9. G. Piccardi and A. Sberna, Atti. accad. Lincei, 15, 309-312 (1932); C. A., 26, 5869 (1932).

10. O. S. Plantinga and C. J. Rodden, Ind. Eng. Chem., Anal. Ed., 8, 232 (1936).

11. R. Hultigren, J. Am. Chem. Soc., 54, 2320 (1932).

12. M. J. Pinta, J. recherches centre natl. recherche sci. Labs. Bellevue (Paris), 21, 260-270 (1952); C. A., 47, 8511 (1953).

13. M. J. Pinta, J. recherches centre natl. recherche sci. Labs. Bellevue (Paris), 22, 19-35 (1953); C. A., 47, 7936 (1953).

14. T. C. Rains, H. P. House, and O. Menis, Anal. Chim. Acta, 22, 315-327 (1960).

15. C. L. Grant, Anal. Chem., 33, 401-404 (1961).

16. C. J. Rodden and O. S. Plantinga, Phys. Revs., 45, 280 (1944).

17. R. W. B. Pearse and A. G. Gaydon, "The Identification of Molecular Spectra," 2nd Ed., John Wiley and Sons, Inc., New York, 1950.

18. H. C. Eshelman, J. A. Dean, O. Menis, and T. C. Rains, Anal. Chem., 31, 183-187 (1959).

19. O. Menis, T. C. Rains, and J. A. Dean, Anal. Chem., 31, 187-192 (1959).

20. R. A. Bolomy and L. Wish, J. Am. Chem. Soc., 72, 4483 (1950).

21. H. J. Bronaugh and J. F. Suttle, U. S. Atomic Energy Comm. Rept. LA-1561 (1953).

PART B

DROPLET SIZE OF AEROSOLS IN FLAME PHOTOMETRY

CHAPTER I

INTRODUCTION

A. Atomization in Flame Photometry

Mavrodineanu and Boiteux[1] have summarized the early methods of introducing samples into the flame. In one method, solutions were fed into the flame from a glass tube along a bundle of platinum wires. Rotating a platinum-gauze disk successively from the solution into the flame was another method. Dry samples have been finely powdered and blown into the flame, and rolls of filter paper containing evaporated salts have been fed at uniform rates into the flame. The most satisfactory method of introducing samples into the flame involves aerosol production from solution media. An aerosol, by its gaseous nature, can be intermingled with fuel components and uniformly distributed throughout the flame.

Two types of atomizer are used in flame photometry.[2] In the discharge type of atomizer, a high speed jet of air is directed at right angles to a gravity-fed liquid stream. The impact of the air stream with the liquid stream shatters the liquid into a multitude of drops. The droplet-laden air stream is usually directed through a condensing chamber before reaching the burner to allow larger droplets a chance to coalesce on the chamber walls and drain away. As a result, only a fine mist is fed to the burner which is usually a Meker-type burner.

The aerosol-air mixture also supplies the oxidant for the fuel combustion. Although extremely fine liquid-air dispersions can be obtained using the discharge type of atomizer, only a small percentage of the aspirated sample actually reaches the flame.

The second, and perhaps more popular, type of atomizer is the total consumption atomizer. The burner and atomizer are an integral unit. Three concentric annuli are used. The outer annulus is for passage of fuel gas, the middle annulus is for the passage of air or oxygen, and the center capillary is for the introduction of the sample to the flame. A high velocity oxygen flow, concentric to the capillary, will create a region of lowered pressure in the capillary and draw the liquid sample out into the oxygen stream as a fine ligament. The effects of turbulence of the oxygen stream and the stretching of the ligament causes it to shatter into fine droplets. All of the sample is fed into the flame, regardless of droplet size. The attractive feature of the total consumption atomizer is the smaller amount of sample used per unit time as compared with the discharge type of atomizer.

B. Mechanism of Pneumatic Atomization

Rayleigh[3] made the first theoretical investigation into the break-up of liquid jets. He considered the problem as an instability effect caused by two factors. The first was the unstable character of a liquid cylinder due to the forces of surface tension acting to cause the liquid to detach itself into masses of larger diameter. A second instability effect was a consequence of the translational movement of the liquid

cylinder. The surface of the liquid cylinder is disturbed in a wave-like manner as a result of a velocity differential between the liquid and air stream.

Lee and Spencer[4] made a number of photomicrographs of fuel sprays. These showed very clearly the nature of the breakup of a ligament of liquid. The effect of surface tension was shown at low jet velocities as the ligament of liquid broke up into spherical drops. At higher jet velocities the photomicrographs indicated a ruffling of the liquid jet surface until a point was reached where the surface tension and viscosity of the fluid were overcome by the turbulent action of the air stream, resulting in a random shatter of the fluid jet. Schweitzer[5] emphasized the effect of turbulence on atomization and claimed that the surface tension was of minor importance at high jet velocities and that viscosity was the controlling liquid property.

From studies of photomicrographs of jet-stream breakup, Nukiyama and Tanasawa[6] observed three stages in the atomization of liquid streams: (1) At low air velocities the characteristic swelling and contraction of the jet stream resulted in the formation of a series of drops which separated from the ligament of the liquid. (2) At intermediate air velocities the fluid jet became distorted and portions of the fluid jet were detached and drawn out into finer ligaments. (3) High air velocities produced films from the fluid jet segments which subsequently broke up into an extremely fine mist.

Lane,[7] using flash and spark photography, clearly illustrated the nature of the breakup of water droplets in a steady stream of moving air.

This type of atomization is independent of the nature of the breakup of the original fluid stream and constitutes a secondary process of atomization where large droplets are shattered to form smaller droplets. The water droplet is flattened and eventually blown out into a bag-like film with a ridge of thicker liquid at the neck of the bag. The film bursts and produces a mist of fine droplets, leaving the circular ring at the neck of the bag intact. This heavier ring later disintegrates into a necklace of large droplet beads. One significant feature of Lane's study was the fact that at least 70 per cent of the mass of the original drop was retained in the liquid at the neck of the bag, and eventually in the larger drops after the ring had disintegrated. This characteristic is borne out by experience in that with most sprays a larger percentage of material is distributed among the largest drops.

Mechanisms of atomization are very complex to treat mathematically and are subject to the nature of the liquid being atomized, the construction of the atomizer, and the relative velocities of the gas-liquid streams. Generally the overall process can be considered as occurring in three steps:[8]

1. The development of a disturbance along the surface of the fluid stream due to instability. The possible causes of the disturbance are:

   (a) surface tension

   (b) inertial forces

   (c) imperfection of the nozzle orifice

   (d) vibration of the nozzle

(e) turbulent flow conditions.

2. The formation of ligaments, films, or threads by the action of the air stream on the initial point of disturbance. The ligaments will fragment and under the influence of surface tension the fragments will form spherical drops.

3. The final breakup of large drops into smaller droplets, if the velocity of the drop is still high with respect to the surroundings. This can be instantaneous for extremely high velocities, or involve a slower distortion of the droplet with the formation and ultimate shattering of the bag-like film.

C. Experimental Methods for Obtaining Drop Size

The measurement of droplet size in an aerosol spray involves the statistical distribution of numerous size classes. It is, therefore, necessary to obtain a true representation of all size classifications and, in particular, to tabulate accurately the frequency of occurrence of a size group. Pilcher[9] has given an excellent review of the handicaps and methods of measuring droplet sizes and has classified 40 different treatments under six main classes of methods.

1. Microscopic Methods

The most general method for determining drop sizes with a minimum of equipment is to collect a spray sample on a glass slide and count the various sized drops. A serious difficulty is that the smaller droplets will tend to follow the air flow around the slide and not be collected

by impact on the slide. For volatile liquids, evaporation must be considered, also the flattening and spreading of the drops upon impact. The slide may be coated with a variety of substances to facilitate the collection of the spray. Oil coatings have been used for water droplets.[10,11,12] Two common procedures are to coat the slide with lampblack from a fuel-rich flame or magnesium oxide from a burning magnesium ribbon.[13] The impact of the droplet will leave a well defined hole which corresponds to the diameter of the droplet. Sprays have been injected into liquids and photomicrographs taken of the suspended droplets.[14]

2. Frozen Droplet Methods

Longwell[15] developed a method of freezing the spray droplets from a fuel-oil spray and, while still frozen, the droplets were sieved. The relative weights of oil retained in each sieve were then determined by dissolving the droplets in benzene and measuring colorimetrically the solutions.

3. Photographic Methods

Photographic methods offer the advantage that sprays are caught in free flight and the errors introduced by placing objects in their path to sample them are eliminated. York and Stubbs[16] used a box-type camera with fixed optics and open shutter. Exposure times were varied by the use of a short-duration background light source. The volume of spray photographed was determined by knowing the depth of field and angular view of the lens system.

4. Optical Methods

Indirect optical methods, based on light-scattering methods, have been developed for extremely fine mists. These include measurements made by light transmission, intensity of scattered light, color of the scattered light, and polarization of the scattered light.[17]

5. Electronic Methods

Guyton[18] developed an electronic counter based upon the electrostatic charging of small particles. These particles were forced to impinge upon a metallic collector where the electrostatic charges were amplified and made to operate a mechanical timer. Electronic discriminators were used to determine the droplet size, dependent upon the charge each size droplet would carry.

6. Cascade Impactors

A number of cascade impactors[13,19,20] have been developed. In principle a spray is allowed to impinge on a slide with a relatively low velocity. The larger droplets will be impacted on the slide while the smaller droplets are swept around the target. Increasing the velocity of the spray stream by using smaller orifices of passage causes each succeeding stage to collect increasingly smaller droplets. Each slide is then given a microscopic examination to determine the range of droplet sizes. For highly volatile liquids considerable success has been achieved by coating the slides with a layer of magnesium oxide.[13] The techniques for determining droplet sizes are identical with those used in simple microscopic methods.

D. Mathematical Expression of Droplet Size Distribution

1. Empirical Functions

The mechanism of atomization is yet but little understood. As a result, there is no theoretically sound method of predicting the distribution of droplet sizes. Consequently, various statistical treatments have been developed for particular types of sprays. The general representation of the drop-size distribution involves a distribution function, f(x), with two evaluable parameters, the mean diameter and an index of precision representing the deviation from the mean. Mugele and Evans[21] have critically reviewed the various functions that have been proposed for treating the droplet sizes.

A strictly empirical function was proposed by Rosin and Rammler.[22]

$$V = 1 - e^{-(x/\bar{x})^{\sigma}} \qquad (1)$$

where

V = volume fraction of the spray of drop of diameter less than x

x = drop diameter

$\bar{x}$ = size parameter

σ = distribution parameter.

The function was originally conceived for the distribution of particle size in grinding mills, but it has been applied successfully to analysis of sprays.

Another completely empirical function was proposed by Nukiyama and Tanasawa[6] from their studies on sprays formed by air atomization.

$$\frac{dv}{dx} = \frac{b^{6/\sigma}}{\Gamma(6/\sigma)} \; x^5 \; e^{-b\,x^{\sigma}} \qquad (2)$$

where

$\frac{dv}{dx}$ = volume distribution

x = droplet diameter

b = size parameter of dimensions of $x^{-\sigma}$

$\Gamma(6/\sigma)$ = generalized gamma function.

$$= \int_0^{\infty} U^{6/\sigma - 1} \; e^{-U} \, dU$$

The distribution functions of Rosin and Rammeler and of Nukiyama and Tanasawa are very difficult to manipulate mathematically. As indicated by Marshall,[23] no theoretical basis exists for accepting or rejecting any particular distribution function. The mathematical simplicity and ease of computation of a distribution function are logical reasons for a selection, as long as the function is consistent with the data.

2. Log-Normal Distribution Functions

Another distribution function which has proven to be applicable to sprays and crushed powders is the log-normal distribution function. This is a purely statistical function, based on the premise that if the data are consistent with the log-normal distribution, then the natural logarithm of the drop diameter is distributed in a normal (Gaussian) distribution. Following the notation used in Mugele and Evans,[21] the application of the log-normal distribution is developed as follows:

The volume distribution of a spray can be represented by

$$\frac{dv}{dy} = \phi(y) = \frac{\sigma}{\sqrt{\pi}} \; e^{-\sigma^2 y^2} \qquad (3)$$

where

$y = \ln \frac{x}{\bar{x}}$

ϕy = normal distribution function

x = droplet diameter

$\bar{x}$ = size parameter

σ = size distribution parameter.

Then

$$\frac{dv}{dx} = \frac{\sigma}{x\sqrt{\pi}} \; e^{-\sigma^2 y^2} \tag{4}$$

The relation of the parameter σ to the standard deviation of the log-normal distribution function is given by:

$$\sigma = \frac{1}{\sigma\sqrt{2}} \; . \tag{5}$$

The substitution of σ and y in Equation 4 gives the standard log-normal distribution function:

$$\frac{dv}{dx} = \frac{1}{x\sigma\sqrt{2\pi}} \; e^{-\ln^2(\frac{x}{\bar{x}})/2\sigma^2} \tag{6}$$

The cumulative volume, V, is obtained by integration of Equation 6:

$$V = \frac{1}{\sqrt{2\pi}} \int_0^x \frac{1}{\sigma x} \; e^{-\frac{1}{2\sigma^2}(\ln x/\bar{x})^2} \; dx \tag{7}$$

To facilitate the integration of Equation 7, a substitution of

$$U = \frac{1}{\sigma\sqrt{2}} \ln (\frac{x}{\bar{x}}) \tag{8}$$

and

$$dx = x\sqrt{2}\,\sigma\, dU \tag{9}$$

in Equation 7 gives

$$V = \frac{1}{\sqrt{\pi}} \int_{-\infty}^{U} e^{-U^2} \, dU \tag{10}$$

Equation 10 is the normal distribution function and can be evaluated by the use of tables of the probability function. A much more convenient method is to plot x, droplet diameter, versus the cumulative volume fraction, V, on log-probability paper, where the ordinate is log x and the abscissa is the volume fraction on a probability scale. This type of plot will yield a straight line if the drop sizes are distributed in a log-normal distribution.

The size distribution parameter, σ, can be found from the slope of the line. Equation 10 can be integrated to obtain the total cumulative volume, V:

$$V = \tfrac{1}{2} \left[1 + \text{erf}(U)\right] \tag{11}$$

where erf(U) is the error function of U. If Equation 11 is solved for U, an equation is obtained which is linear in ln x:

$$U = \text{erf}^{-1} \left[2V - 1\right] = \sigma \ln x/\bar{x} \tag{12}$$

where $\text{erf}^{-1} \left[2V - 1\right]$ is the inverse error function of $\left[2V - 1\right]$.

3. Upper-Limit Function

Mugele and Evans[21] introduced into the log-normal distribution function a third parameter, x_m, which represented a maximum drop diameter. They suggested that such an upper limit, x_m, was more realistic than the concept of an infinitely large drop of infinitely small probability of occurrence. The mathematical treatment is identical with that developed

for the log-normal distribution except now the distribution function is given by:

$$y = \ln \frac{ax}{x_m - x} \tag{13}$$

where a = a parametric constant.

The application of the log-normal and upper-limit function is treated in some detail by Miesse and Putnam[24] and Mugele and Evans.[21] A good approximation of x_m can be obtained by plotting the data as log x versus 100 V on probability paper and drawing a smooth curve to fit the points. From this curve the 90th, 50th, and 10th percentiles, x_{90}, x_{50}, and x_{10}, respectively, are determined. Then x_m is calculated as shown below:

$$x_m = \frac{x_{50}^2 (x_{90} + x_{10}) - 2x_{90}\, x_{50}\, x_{10}}{x_{50}^2 - x_{90}\, x_{10}} \tag{14}$$

The parameter a is determined from the plot of $u = \frac{x}{x_m - x}$ versus 100 V. At the 50th percentile we have:

$$y = 0 = \ln \frac{a\, x_{50}}{x_m - x_{50}}$$

or

$$a = \frac{x_m - x_{50}}{x_{50}} \tag{15}$$

Using the 90th and 50th percentiles:

$$\sigma = \frac{0.394}{\log (u_{90}/u_{50})} \tag{16}$$

E. Mean Diameters

Mugele and Evans[21] have summarized the various methods of expressing mean diameters and their usefulness in different fields of application. The different mean diameters depend largely upon the type of measurement taken. Microscopic tabulations furnish number averages. Diameters measured from sedimentation or impaction techniques will give volume or mass averages. Optical methods, in turn, are based upon the surface area of the droplets.[23] Mugele and Evans[21] developed a general expression for computing any mean diameter:

$$(\bar{x}_{qp})^{q-p} = \frac{\int_{x_o}^{x_m} x^q f(x)\, dx}{\int_{x_o}^{x_m} x^p f(x)\, dx} \tag{17}$$

The terms q and p are usually assigned integral values, although there is no restriction on q or p from having zero or fractional values. The other terms in the general equation have been previously defined. For example, the Sauter, or volume-surface diameter, would be given by:

$$\bar{x}_{32} = \frac{\int_{x_o}^{x_m} x^3 f(x)\, dx}{\int_{x_o}^{x_m} x^2 f(x)\, dx} = \frac{\bar{x}_v^3}{\bar{x}_s^2} \tag{18}$$

Thus the Sauter mean diameter can be visualized as the diameter obtained by dividing the volume of a particle by its surface area. No inferences are drawn as to the exact geometrical configuration of the particle, although for liquid sprays a spherical shape is usually assumed for the droplet.

The mean diameters which are commonly used are tabulated below (from Mugele and Evans[21]):

p	q	Name of Mean Diameter
0	1	Linear
0	2	Surface
0	3	Volume
1	2	Surface - diameter
1	3	Volume - diameter
2	3	Volume - surface (Sauter)

F. Significance of Droplet Size in Flame Photometry

1. Aqueous Versus Organic Solvents

Nukiyama and Tanasawa[25] were able to correlate droplet diameters with properties of liquids:

$$d_o = \frac{585\sqrt{\sigma}}{v\sqrt{\rho}} + 597\left(\frac{\mu}{\sqrt{\rho\sigma}}\right)^{0.45}\left(1000\,\frac{Q_l}{Q_a}\right)^{1.5} \qquad (19)$$

where

d_o = diameter in microns of a single drop having the same volume/surface ratio as the total sum of the drops

v = relative velocity of air stream and liquid stream in meters per second

Q_l/Q_a = ratio of liquid and air volume flows

ρ = liquid density, grams per cc.

σ = liquid surface tension, dynes per cm.

μ = liquid viscosity in poises.

At very small values of Q_l/Q_a, the first term in Equation 19 becomes significant, and thus the surface tension and liquid density become important factors in determining droplet sizes. Smit, Alkemade, and Verschure[26] have demonstrated that the substitution of an organic solvent for water will increase the amount of small diameter droplets in an aerosol spray. Since the amount of atomic and molecular excitation in the flame is dependent upon the number of droplets reaching the flame (spray chamber type of atomizer) and the evaporation of solution droplets, it can be seen that an aerosol containing a greater number of small diameter droplets will be expected to give a higher proportion of excitable metallic species in the flame.

2. Evaporation Rates

The time required for the complete evaporation of a droplet has been related to the square of the initial drop radius.[27] Since for all practical purposes the time allowed for evaporation which leads to excitation in the flame is the same for any solvent system, one factor in flame excitation will be the droplet diameter. The fact that a certain solvent is combustible will not hasten necessarily the evaporation process, other than the solvent combustion providing an additional source of heat to the evaporating droplet. In fact, present theories of droplet combustion recognize the fact that evaporation rates have a controlling influence upon combustion rates of fuel droplets.[28] Probert[29] has concluded that high initial rates of evaporation are favored by small mean diameters and small dispersion constants of the droplet distribution.

G. Statement of the Problem

The droplet size distribution and mean droplet diameters were determined for three solvents commonly used in flame spectrophotometry: water, 4-methyl pentan-2-one, and chloroform. The special upper-limit function of the log-normal distribution function was chosen to represent the droplet size distributions. A qualitative investigation was made to determine the relative amounts of solvent evaporated completely in the flame.

CHAPTER II

APPARATUS AND REAGENTS

A. Apparatus

1. Chemical Microscope

A Bausch and Lomb Type M chemical microscope, with accessories, was used to measure the droplet diameters. The diameters were measured with the aid of a filar micrometer, previously calibrated against a standard stage micrometer.

2. Atomizer

The atomizer was the regular Beckman Model 4030 integral aspirator-burner.

3. Sampling Device

The droplets were allowed to impact upon a standard glass microscope slide which had been uniformly coated with a layer of magnesium oxide.

B. Reagents

1. Chloroform

U. S. P. grade chloroform was used,

2. Demineralized Water

Demineralized water was prepared by passing ordinary distilled water through a column of Amberlite MB-3 resin.

3. 4-Methyl Pentan-2-One

Practical grade 4-methyl pentan-2-one was used.

CHAPTER III

EXPERIMENTAL RESULTS

A. Measurement of Droplet Sizes

The method employed for sampling the spray has been described by May.[13] The impact of a droplet upon a slide coated with magnesium oxide left a well-defined hole which could be observed through a microscope under strong transmitted light. In a later study, May[30] observed that for a large size range and for a wide range of liquids and impact velocities, the ratio of true drop size to impression size was constant and equal to 0.86. It was considered that the certainty in measuring the droplet diameters was no better than $\pm$ 15 per cent; consequently no correction of the impression diameters was made. He also noted that droplets as small as 5 microns in diameter could leave an impression at sufficiently high impact velocities. Droplet diameters were observed below 10 microns and these were included in the distribution of droplet diameters. The measured number of droplets which had a diameter less than 10 microns was probably low, however.

Droplet diameters were grouped together in size groups about a nominal size, x, ($\pm$ 5 microns) and tabulated at intervals of 10 microns over the range of sizes from 0 to 70 microns. The volume of drops in each size group was calculated with an assumed spherical geometry. Also tabulated were the cumulative volume and cumulative volume fraction for

each size group. The data are tabulated in Table IV for water, chloroform, and 4-methyl pentan-2-one.

B. Distribution Studies

When the logarithm of the droplet diameter is plotted versus the cumulative volume fraction on a probability scale, a straight line will result if the distribution of the droplet sizes can be expressed by a log-normal distribution function. Log-probability coordinate paper is commercially available or it may be constructed from ordinary semi-log coordinate paper.

By definition the standard normal curve has a deviation of unity and a zero mean. The total area under the standard normal curve is also unity. To construct a probability scale the midpoint of the coordinate scale is assigned the value 50 per cent of the unit employed (volume, number, etc.), and represents an area of 0.5 of the total area under the standard normal curve. The 60th percentile (area 0.6) is measured a distance of 0.26 linear units, as read from the table of areas under the normal curve, from the 50th percentile point. The 40th percentile is measured 0.26 units in the opposite direction from the 50th percentile point. In a similar manner the points corresponding to 10 and 90 per cent, 20 or 80 per cent, etc., can be located with respect to the midpoint of the coordinate scale. A table of Probits[31] facilitates greatly the construction of a probability scale.

The calculations for water illustrate the treatment of the data. To determine x_m, the maximum droplet diameter, the values of the observed

TABLE IV

REPRESENTATION OF DISTRIBUTION

Nominal Size Group, x, in Microns	Frequency	Volume of Drops, (microns^3 x 10^{-3})	Cumulative Volume, (microns^3 x 10^{-6})	Cumulative Volume Fraction, V
		WATER		
5	154	10	.010	.0025
15	209	370	.380	.095
25	111	910	1.29	.32
35	23	520	1.81	.45
45	15	720	2.52	.63
55	7	610	3.13	.78
65	6	860	4.00	1.00
		4-METHYL PENTAN-2-ONE		
5	295	19	.019	.011
15	165	292	.311	.17
25	40	328	.639	.35
35	5	112	.751	.41
45	8	382	1.13	.62
55	3	262	1.39	.76
65	3	432	1.83	1.00
		CHLOROFORM		
5	169	11	.011	.005
15	220	390	.400	.18
25	81	663	1.06	.48
35	17	382	1.44	.65
45	11	525	1.97	.88
55	3	262	2.23	1.00

diameters are plotted versus the volume fraction, V, as shown in Figure 9. The procedure recommended by Mugele and Evans[21] for arriving at an approximate value of x_m was to read the 90th, 50th, and 10th percentiles and calculate x_m from Equation 14. Miesse and Putnam[24] recommended using an average of several values of x_m calculated from Equation 14; for example, taking values from the curve at x_5 and x_{95}, x_{10} and x_{90}, etc. Employing their method, an average value of x_m was obtained which was not always the best value from which to construct a straight line when log $x/(x_m-x)$ was plotted versus volume fraction. A trial-and-error method was finally used to obtain the best value of x_m, using the average value calculated from Equation 14 as a guide. Using a value of 150 microns for the x_m of water, the diameters were plotted as log $x/(x_m-x)$ versus volume fraction, V, as shown in Figure 9.

The value of a, the parametric constant, was determined at u_{50}, where $u = x/(x_m-x)$. Then from Figure 9:

$$a = \frac{1}{u_{50}} = \frac{1}{0.31} = 3.23 \qquad (20)$$

The size distribution parameter, σ, was determined from the slope of the line given by the plot of log u versus the volume fraction. When the 90th and 50th percentiles were used,

$$\sigma = \frac{0.394}{\log (u_{90}/u_{50})} = \frac{0.394}{\log (0.86/0.31)} = 0.89 \qquad (21)$$

Thus the upper-limit function for water is represented by the following equation:

$$y_{H_2O} = \ln (ax/x_m-x) = \ln \frac{3.23x}{150 - x} \qquad (22)$$

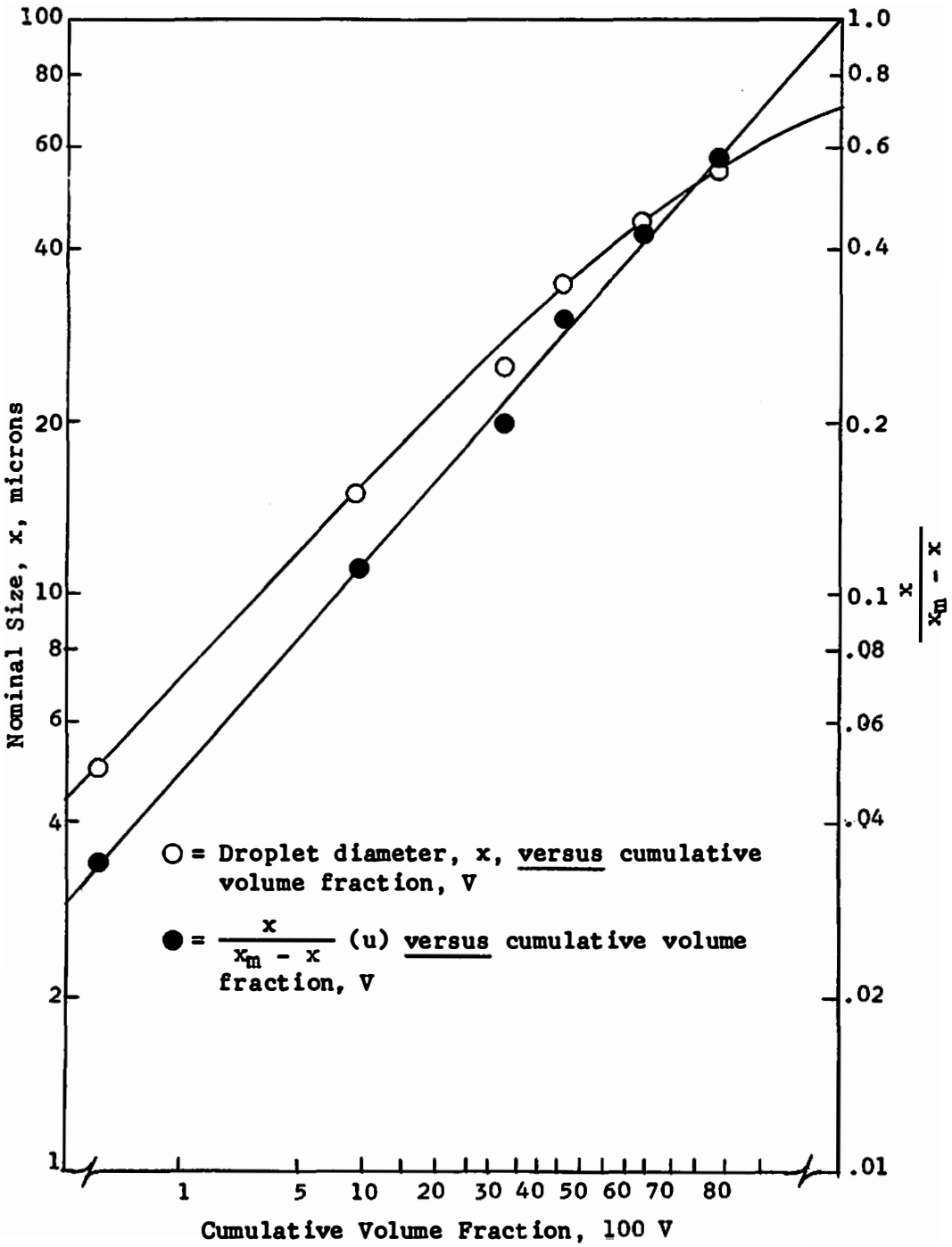

Figure 9. Drop size distribution of water. x_m = 150 μ.

Figures 10 and 11 illustrate the distribution of the droplet diameters for chloroform and 4-methyl pentan-2-one, respectively. The upper-limit functions for chloroform and 4-methyl pentan-2-one (hexone) are given below:

$$y_{CHCl_3} = \ln \left(\frac{2.88\ x}{100 - x}\right) \tag{23}$$

$$y_{Hexone} = \ln \left(\frac{5.0\ x}{200 - x}\right) \tag{24}$$

The values of σ are 0.78 and 0.98 for chloroform and 4-methyl pentan-2-one, respectively.

C. Mean Diameters

Two mean diameters were determined for each of the solvents as a basis for comparing their relative size distributions. Mugele and Evans[21] have solved Equation 17 for the volume mean diameter, $\bar{x}_{31}$, and the Sauter mean diameter, $\bar{x}_{32}$, and the resulting expressions are listed below:

$$\bar{x}_{31} = \frac{x_m}{\left(1 + 2a\, e^{-\frac{1}{4\sigma^2}} + a^2\, e^{1/\sigma^2}\right)^{\frac{1}{2}}} \tag{25}$$

$$\bar{x}_{32} = \frac{1}{\left(1 + a\, e^{\frac{1}{4\sigma^2}}\right)^{\frac{1}{2}}} \tag{26}$$

By the substitution of the proper values of x_m, a, and σ in Equations 24 and 25, the resulting values were obtained:

Mean Diameter	Water	4-Methyl Pentan-2-One	Chloroform
$\bar{x}_{31}$	19.6	16.7	17.6
$\bar{x}_{32}$	27.5	23.4	21.1

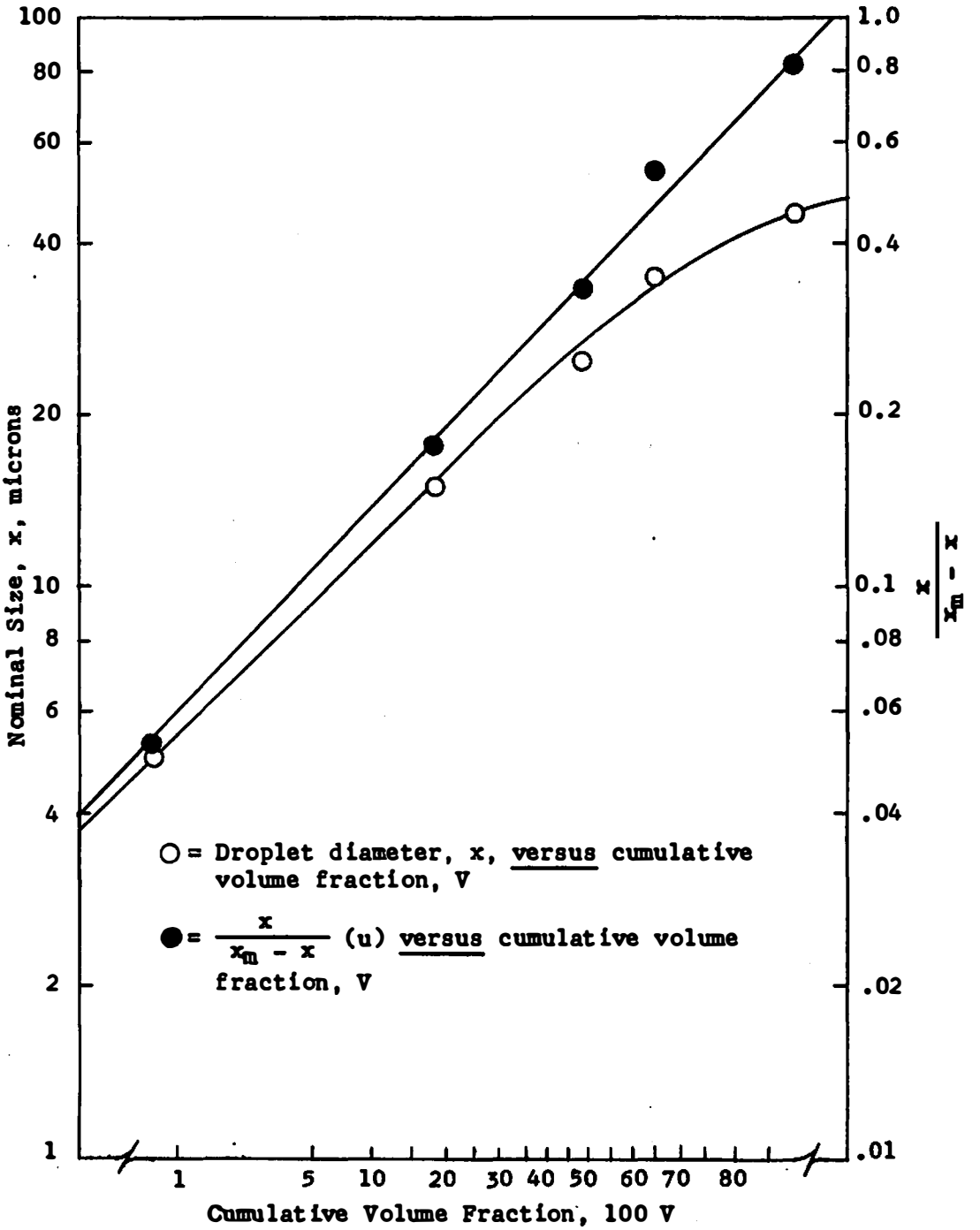

Figure 10. Drop size distribution of chloroform. x_m = 100 μ.

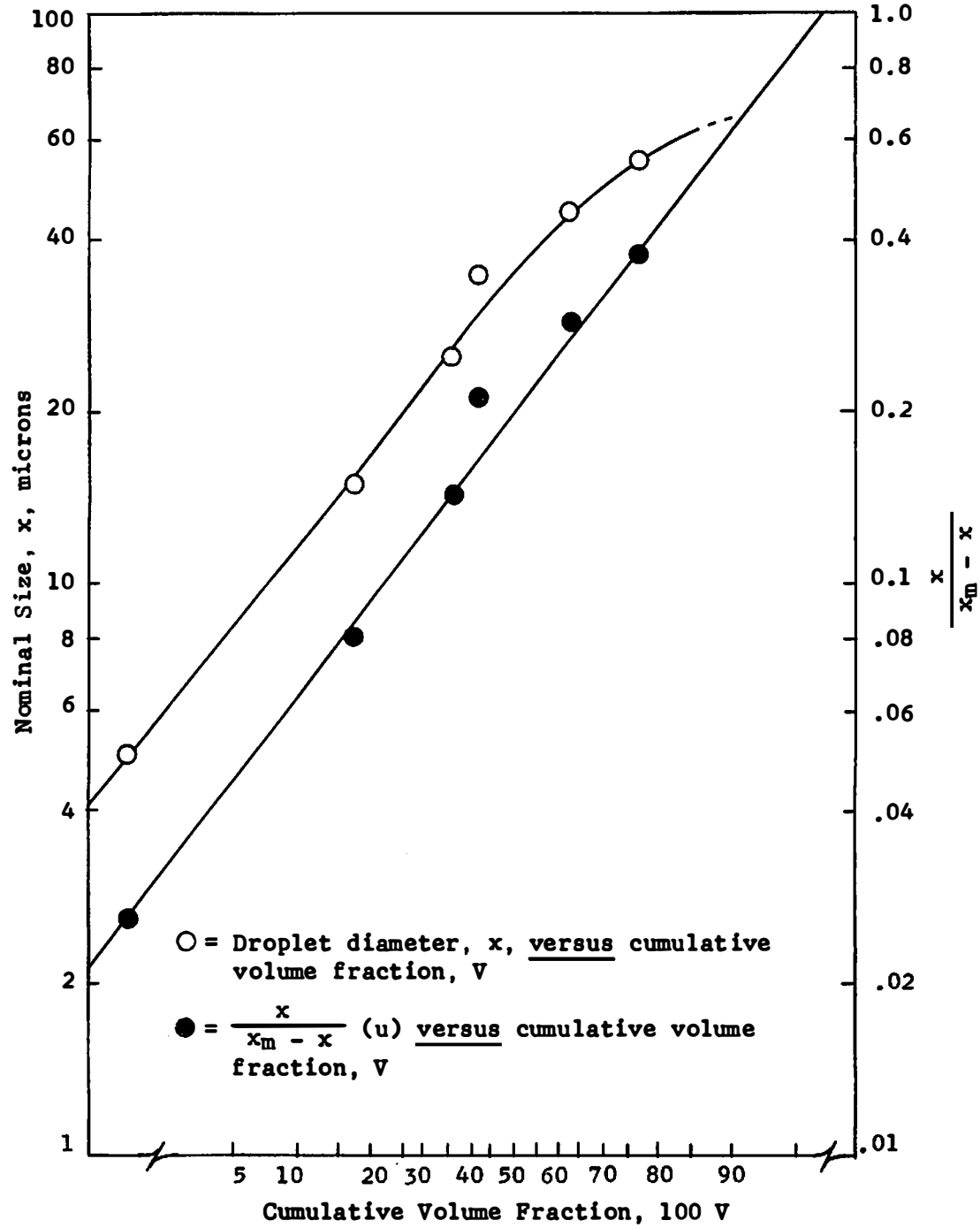

Figure 11. Drop size distribution of 4-methyl pentan-2-one. x_m = 200 μ.

CHAPTER IV

DISCUSSION OF RESULTS

A. Observed Droplet Sizes

The errors in measuring droplet size by microscopic examination of the droplets, or facsimiles thereof, have been discussed in Chapters I and III. Perhaps the most serious error would be the discrimination toward the smallest droplet sizes, due to the fact that extremely small droplets are more subject to evaporation losses. Also the probable failure of the smaller droplets to be impacted on the coated slide would be a serious source of error. Figure 12 represents a histogram which shows the per cent of the total number of droplets observed versus the diameter in microns of each size group. There is an abrupt cutoff in the distribution of the smaller droplets. This is due partly to the manner in which the droplet diameters were grouped. The smallest size increment was from 0 to 10 microns. This increment included all the observed sizes below 10 microns, and for the distribution studies, a nominal size of 5 microns was assigned for this group. The lack of a better counting method precluded a narrower range of size classifications. The plots of log x versus volume fraction, as shown in Figures 9, 10, and 11 are linear except at the larger diameters where the curves bend toward the horizontal axis. The deviation from linearity at large droplet diameters is inherent in the log-normal distribution. It predicts

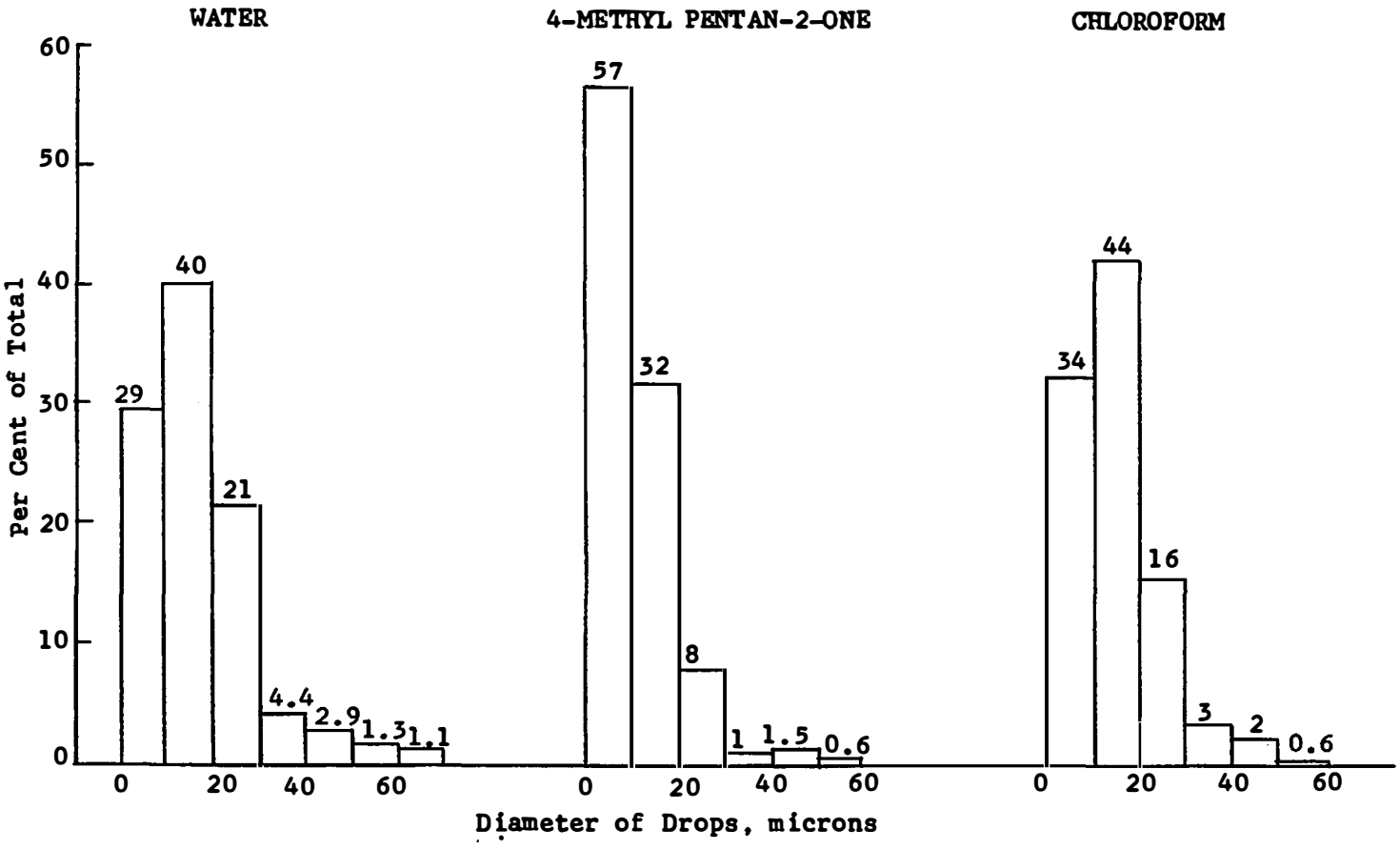

Figure 12. Histogram showing the per cent of the total number of drops observed versus the diameter in microns of each size group.

an infinite drop diameter as the cumulative volume fraction approaches unity. This is contrary to physical reality, thus the basis for the introduction of a maximum drop diameter, x_m, as an upper limit to the droplet diameter size range.

B. Distribution Studies

The upper-limit function of the log-normal distribution was found to be satisfactory for representing the distribution of the observed droplet diameters. The significance of the parameter, α, the size distribution constant, is readily seen by examining the distribution function:

$$dv = \frac{x_m}{x(x_m-x)\sigma\sqrt{2\pi}} \; e^{-\frac{1}{2\sigma^2}\ln^2\left(\frac{ax}{x_m-x}\right)} \; dx \qquad (27)$$

The parameter α has been previously defined by Equation 5:

$$\alpha = \frac{1}{\sigma\sqrt{2}} \qquad (5)$$

The standard deviation is σ, and σ^2 represents the variance of the distribution curve. The parameter α can be associated with the index of precision of the distribution. Large values of α imply that the distribution decreases very rapidly from its maximum value, while the inverse is true for small values of α. Using the calculated values of α from page 59, the relation between α, σ, and σ^2 is shown below:

Aerosol	α	σ	σ^2
Water	0.89	0.79	0.63
4-Methyl Pentan-2-one	0.98	0.73	0.53
Chloroform	0.78	0.90	0.81

There was some degree of uncertainty in determining x_m, the maximum droplet diameter. When Equation 14 was used the average value of x_m which was obtained was too low to give the best straight line when log $x/(x_m-x)$ was plotted versus the cumulative volume fraction. The nature of the curve drawn through the points when log x was plotted versus the cumulative volume fraction had a pronounced effect on the value of x_m thus obtained. There was no basis for drawing any other type of curve except a smooth curve which connected all of the points. A straight line resulted in a very wide range of values for x_m, and a simple average was not felt to be justified. A trial-and-error method proved to be satisfactory for determining the best value of x_m to use in the distribution function.

C. Mean Diameters

The mean diameters tabulated on page 59 are shown only for the comparison of the droplet sizes. The volume mean diameter, $\bar{x}_{31}$, predicts the order of decreasing diameter as water > chloroform > 4-methyl pentane-2-one. The Sauter mean diameter, $\bar{x}_{32}$, and the median diameter (geometric mean diameter), $\bar{x}_{50\%}$, places the order of decreasing diameter as water > 4-methyl pentan-2-one > chloroform. There was a correlation between droplet size and liquid viscosity and surface tension:

Aerosol	Surface Tension (dynes per cm.)	Viscosity (millipoises)	$\bar{x}_{31}$ (microns)	$\bar{x}_{32}$ (microns)	$\bar{x}_{50\%}$ (microns)
Water	72.8	10.09	19.6	27.5	37
4-Methyl pentan-2-one	25.4	5.46	16.7	23.4	35
Chloroform	27.1	5.63	17.6	21.1	27

For the particular type of atomizer used and the range of gas and liquid flows normally encountered in flame photometry, it seemed apparent that liquid viscosity and surface tension might be used to predict the relative degree of dispersion between various aerosols.

D. Correlation of Droplet Size to Evaporation Rates

The determination of evaporation rates of suspended droplets in fast moving air streams still remains in a state of conjecture. The combustibility of a solvent further complicates the process of evaporation. However, a brief resume of the atomization and evaporation of the aerosol in the flame suggests certain restrictions upon the conditions which lead to excitation in the flame. The spray is injected directly into the highly energetic reaction zone of the flame. The distance between the capillary tip and the flame front is only 3 or 4 mm. and, in terms of time, the aerosol certainly has only a minimum amount of time in which to become a fully developed spray. It is quite likely that the full droplet size distribution is never attained before the effects of the high-temperature combustion atmosphere of the flame are felt. The thickness of the reaction zone appears to be 3 or 4 mm. for an oxygen-acetylene flame when the carbon line emission is observed with a slit width of .09 mm.[32] The innerconal region, which includes the reaction zone, extends upward from the base of the flame to a height of approximately 20 mm. The reaction zone is the most energetic region of the flame,[32] and upwards in the flame, where the secondary processes of combustion take place, the energy content of the flame is

steadily decreasing. Although the processes leading to excitation in flames are not fully understood, a solution droplet must be completely evaporated as the first step in the chain of events which ultimately lead to excitation. The larger part of an excited species in the flame will be a result of the complete evaporation of a droplet followed by excitation in the reaction zone. Since the reaction zone is rather thin and the time available for evaporation and excitation is very short, it is reasonable to assume that only the smaller droplets will be evaporated in this time interval. Although intermediate sized drops may be evaporated completely in the innerconal region, the conditions for excitation are less favorable and the contribution of the added material to the flame in this region will not be significant. The largest droplets may be swept through and out of the flame before evaporation is completed. Water droplets have been observed to coalesce on the end of a glass rod which was held near the top and off to the side of an oxygen-acetylene flame when water was being aspirated into the flame.

It might be assumed then that a solvent with a larger percentage of small droplets will lead to a higher degree of excitation in the flame. The fact that a solvent is combustible will further diminish the chance that some of the aerosol might pass through the flame incompletely evaporated. From the work of Wolfhard and Parker[33] it seems reasonably well established that small organic droplets (diameters less than 20 microns) will evaporate with sufficient rapidity so that the fine mist which results will have essentially the same combustion properties as a completely vaporized fuel. From Figure 12, 89 per cent of the droplets

from 4-methyl pentan-2-one possess a diameter less than 20 microns; chloroform has 78 per cent less than 20 microns, while water has 69 per cent less than 20 microns. These percentages are in agreement with the observed emissions of the iron atomic line at 372 mμ when using the three solvents.[34]

Solvent	Per Cent Less Than 20 Microns	Net Emission*
4-Methyl pentan-2-one	89	70
Chloroform	78	21
Water	69	8

The higher net emission of iron when dissolved in 4-methyl pentan-2-one can be attributed to the combustible nature of the solvent.

*Corrected for different aspiration rates.

CHAPTER V

SUMMARY

The droplet-size distributions in aerosols of water, 4-methyl pentan-2-one, and chloroform were determined. The atomizer was the Beckman Model 4030 integral aspirator-burner. The aerosols were allowed to impact upon a microscope slide which had been coated with a uniform layer of magnesium oxide. The slides were viewed under a microscope and the droplet sizes in microns were measured with a filar micrometer which had been calibrated against a standard stage micrometer. The droplet sizes were tabulated in size groups about a nominal size ($\pm$ 5 microns) in intervals of 10 microns over the range from 0 to 70 microns.

The special upper-limit function of the log-normal distribution function was chosen to represent the droplet size distribution in each aerosol. The parameters associated with the upper-limit function were evaluated for the three aerosol systems by a graphic method.

Some mean diameters usually associated with spray analysis were evaluated to compare the relative droplet size between the aerosol systems. The geometric mean diameter placed the aerosols in the order of decreasing diameter: water > 4-methyl pentan-2-one > chloroform. The droplet size was shown to be a significant factor in the extent of excitation in the flame. The observed emission intensity of iron when dissolved in the three solvents followed the trend of the observed droplet diameters.

BIBLIOGRAPHY

BIBLIOGRAPHY

1. R. Mavodineanu and H. Boiteux, "L'Analyse Spectrale Quantitative par la Flamme," Masson et Cie, Paris, 1954.

2. J. A. Dean, "Flame Photometry," McGraw-Hill Book Co., Inc., New York, 1960.

3. Lord Rayleigh, Proc. Math. Soc. (London), 10, 4 (1878); J. M. Pilcher and C. C. Miesse, Chap. 1, p. 2, United States Air Force WADC TR 56-344 (March 1957).

4. D. W. Lee and R. C. Spencer, NACA Report No. 454 (1933); J. M. Pilcher and C. C. Miesse, Chap. 1, p. 5, United States Air Force WADC TR 56-344 (March 1957).

5. P. H. Schweitzer, J. Appl. Phys., 8, 513 (1937).

6. S. Nukiyama and Y. Tanasawa, Trans. Soc. Mech. Engr. (Japan), 6, No. 22, pp. S7-S8 (1940); C. A., 37, 5896 (1943).

7. W. R. Lane, Ind. Eng. Chem., 43, 1312 (1951).

8. J. M. Pilcher and C. C. Miesse, Chap. 1, p. 25, United States Air Force WADC TR 56-344 (March 1957).

9. J. M. Pilcher, op. cit., Chap. 4, Section I.

10. S. Nukiyama and Y. Tanasawa, Trans. Soc. Mech. Engr. (Japan), 4, No. 14, S-13 (1938); J. M. Pilcher, op. cit., Chap. 4, p. 3.

11. S. M. Doble, Engineering, 159, 21-23, 61-63, 103-104 (1945); J. M. Pilcher, op. cit., Chap. 4, p. 4-3.

12. N. A. Dimmock, Nature, 166, 686 (1950).

13. K. R. May, J. Sci. Instr., 22, 187 (1945).

14. K. J. DeJuhasz, O. F. Zahn, and P. H. Schweitzer, Bull. No. 40, Engr. Expt. Sta., Pennsylvania State College, August 22, 1932; J. M. Pilcher, op. cit., Chap. 4, p. 4-2.

15. J. P. Longwell, "Fuel Oil Atomization," D. Sc. Thesis, Massachusetts Institute of Technology, Cambridge, Massachusetts, 1943; J. M. Pilcher, op. cit., Chap. 4, p. 4-6.

16. J. L. York and H. E. Stubbs, Trans. Am. Soc. Mech. Engrs., 74, 1157-1162 (1952); C. A., 46, 11511 (1952).

17. D. Sinclair and V. K. LaMer, Chem. Rev., 44, 245 (1949).

18. A. C. Guyton, J. Ind. Hyg. Toxicol., 28, 133-134 (1946); C. A., 40, 5606 (1946).

19. S. Lasken, U. S. Atomic Energy Comm. Rept. UR-129 (August 1950); N. S. A., 5-649, 103 (1951).

20. J. L. Harp and J. M. Pilcher, U. S. Air Force Contract AF-33(038)-12656, E. O. No. 460-35 S. R.-8, USAF, 13th through 16th Quarterly Progress Reports, July 1953 to July 1954; J. M. Pilcher, op. cit., Chap. 4, p. 4-29.

21. R. A. Mugele and H. D. Evans, Ind. Eng. Chem., 43, 1317-1323 (1951).

22. P. Rosin and E. Rammler, J. Inst. Fuel, 7, 29-36 (1933); C. A., 28, 3870 (1934).

23. W. R. Marshall, Jr., Chem. Eng. Progr. Monograph Ser., 2, 50 (1954).

24. C. C. Miesse and A. A. Putnam, Chap. 4, Section II, pp. 4-68 to 4-78, United States Air Force WADC TR 56-344 (March 1957).

25. S. Nukiyama and Y. Tanasawa, Trans. Soc. Mech. Engr. (Japan), 5, No. 18, 68-75 (1939); C. A., 35, 4258 (1941).

26. J. A. Smit, C. T. J. Alkemade, and J. C. M. Verschure, Biochim. et Biophys. Acta, 6, 508-523 (1951).

27. B. Lewis, R. N. Pease, and H. S. Taylor, Ed., "Combustion Processes," Vol. II, Princeton University Press, New Jersey, 1956.

28. V. K. Gudkov-Belyakov, Dizelestroenie, 7, 10-17 (1940); C. A., 37, 4548 (1943).

29. R. P. Probert, Phil. Mag., 37, 94 (1946).

30. K. R. May, J. Sci. Instr., 27, 128 (1950).

31. R. A. Fisher and F. Yates, "Statistical Tables," 3rd ed., Hafner Publishing Co., New York, 1949.

32. Part C, This Thesis.

33. H. G. Wolfhard and W. G. Parker, J. Inst. Petroleum, 35, 118-125 (1949); C. A., 43, 4840 (1949).

34. J. H. Lady, "Application of Solvent Extraction to Flame Spectrophotometry," Doctoral Thesis, The University of Tennessee, Knoxville, Tennessee, 1955.

PART C

STUDIES OF THE REACTION ZONE OF AN OXYGEN-ACETYLENE FLAME

CHAPTER I

INTRODUCTION

A. Spectra of Hydrocarbon Flames

1. The CH Bands

There are three systems of CH emission found in the reaction zone of hydrocarbon flames. The 431.3 mμ band head is the strongest in the 4300 A system, and is degraded to the violet. The 3900 A system is weaker in intensity, with the 388.9 mμ band head being the most prominent feature of this system. The band is of very open structure and degraded toward the red.[1] The weak 3143 A system appears only in hot flames such as oxygen-acetylene, and even then the bands are usually obscured by the OH bands except for extremely fuel-rich flames.[2]

2. The Swan Bands of C_2

The Swan bands of C_2 are very intense in the reaction zone of hydrocarbon flames. The bands are degraded to the violet and have three prominent band heads at 473.7, 516.5, and 563.5 mμ. The Swan system is the only band system of consequence for C_2 in hydrocarbon flames.[2]

3. The Atomic Carbon Line

Carbon possesses an atomic line at 247.8 mμ. According to Gaydon[2] the emission is found only in very hot flames such as oxygen-acetylene and

requires an excitation energy of 7.7 ev. Rossikhin and Tsykor[3] cite the most probable reaction for the source of atomic carbon as being

$$CH + H \longrightarrow C + H_2 + 1.5 \text{ ev.} \qquad (1)$$

The relatively high excitation energy required for the excitation of the carbon atom indicates the high energy conditions present in the reaction zone, particularly for oxygen-acetylene.

4. The OH Bands

The most prominent band head for the OH system occurs at 306.4 mμ and is degraded to the red.[2] Other band heads are evident from 260 to 347 mμ although they are much weaker in intensity. The OH band emission extends well beyond the reaction zone into the innerconal region of the oxygen-acetylene flame.

5. Other Band Systems

A band has been attributed to HCO[4] although it is predominently associated with cool, low-pressure flames. In hotter flames the band is masked by the strong CH and OH emissions.[2] The "Comet Head" group of bands from C_3 have been reported by Kiess and Bass[5] and more recently by Haser[6] as occurring in oxygen-acetylene flames. These emitters contribute little to the observed spectra of the oxygen-acetylene flame, but their presence is significant when the combustion and excitation mechanisms of flames are considered.

B. Abnormal Excitation in Flames

Line reversal techniques have been successfully used to measure flame temperatures.[7] A line reversal temperature in the reaction zone is dependent upon the excitation energy of the line used.[8] Alekseeva and Mandel'shtam[9] concluded that a non-Boltzmann distribution of energies existed in the reaction zone of an air-acetylene flame. This conclusion was reached by the observations made on several atomic lines of tin. Consideration of the transition probabilities and excitation energies of some tin lines revealed that the observed line intensities were not compatible with the excitation energies of the lines. Furthermore, the line reversal temperatures for sodium, lithium, potassium, and thallium were different in the reaction zone, whereas each element gave the same apparent temperature in the outer mantle of the flame. Gaydon and Wolfhard[10] used the 306.4 mμ band of OH to determine flame temperature from Boltzmann intensity distributions of rotational lines. In all cases these workers obtained temperatures which were much too high. They observed that the OH radiation from oxygen-acetylene flames was about 500 times greater than for oxygen-hydrogen flames with comparable temperatures and OH radical concentrations. The OH radiation from the oxygen-acetylene flame was much stronger in the reaction zone than in the innerconal region. Kane and Broida[11] observed similar high rotational energies of excited OH radicals in flames. Comparable non-thermal rotational energy distributions have been observed for CH and C_2 radicals.[12,13,14]

Instances of abnormal excitation are not restricted to active species formed during the combustion mechanism. Gaydon and Wolfhard,[15] using spectrum line reversal methods, observed that many atomic lines of iron and lead which were obtained in emission against the background of a carbon arc represented a temperature of more than 3800°K. The reversal temperature for the resonance lines increased with decreasing wavelength of the line. This effect was apparent only in the reaction zone of organic flames. No abnormal excitation was observed in flames of hydrogen or carbon monoxide.[15]

A sharp contrast between the spectrum of iron in the reaction zone and in the innerconal gases has been observed. Gaydon and Wolfhard[8] observed the entire spectrum of neutral iron in the reaction zone but only a few resonance lines at the longer wavelengths in the innerconal region. The highest energy level involved corresponded to an energy of 7.53 ev., or 173.5 kcal. per mole. The complete spectrum of neutral lead was also observed in the reaction zone. These effects have been observed in low-pressure premixed flames where the reaction zone is quite thick; at atmospheric pressure the reaction zone is only about 0.02 mm. in thickness.[16] Nevertheless, the abnormal excitation is also evident in the latter flames.[15]

C. Causes for Abnormal Excitation

The cause of abnormal and very high electronic excitation in the reaction zone of organic flames remains unknown.[17] The intensity distribution among the iron lines is independent of the equilibrium flame

temperature, and approximately independent of pressure.[8] This fact has lead Gaydon and Wolfhard to postulate a simple collisional process which is characteristic of the combustion mechanism. There is a strong compulsion to associate the abnormal excitation with the C_2 and CH radicals in the reaction zone.[8,17,18] No known species has yet been identified with the abnormal excitation.

D. Excitation Processes in Flame Photometry

The emission of an element, which includes the oxide or hydroxide bands and the atomic or ionic line spectra, results from the evaporation of a solution aerosol droplet, the dissociation of any molecular species, and excitation of the atoms, ions or molecules formed in the flame. The sequence of events and even the nature of the events leading to emission is still a point of conjecture, especially when using organic solvents.

The steps leading to excitation in an aqueous solution of a metal salt can be considered as follows:[19]

$$MX_{aq} \rightleftharpoons MX_g + H_2O \qquad (2)$$

$$MX_g \rightleftharpoons M_g + X_g \qquad (3)$$

$$M_g \rightleftharpoons M_g^+ + e^- \qquad (4)$$

$$M_g + \begin{bmatrix} OH \\ O \end{bmatrix} \rightleftharpoons \begin{bmatrix} MOH \\ MO \end{bmatrix} \qquad (5)$$

The above equations are feasible from a purely thermal consideration. The formation of MO and MOH is usually considered as a result of Equation 5, although the possibility of the direct formation of MO or MOH from the solvated ions cannot be ruled out. Robinson[20] has suggested

a correlation between the ultraviolet radiation from a flame and the intensity of metallic spectra. The absorption of ultraviolet radiation could conceivably contribute to the breakdown of metal hydrates and oxides or hydroxides. The ultimate picture of the basic mechanisms of flame excitation processes will remain obscure until combustion processes themselves are more fully understood.

E. Statement of the Problem

This investigation was concerned primarily with an exploratory survey of the emission from the reaction zone of an oxygen-acetylene flame. The presence of abnormal excitation in the reaction zone of cool low-pressure flames has been established, and similar excitation conditions are presumed to be present at atmospheric pressure. Particular attention was given to those elements which are only excited with difficulty in the oxygen-acetylene flame. The development and use of a light-pipe for viewing selectively the reaction zone was treated in some detail.

CHAPTER II

APPARATUS AND REAGENTS

A. Apparatus

1. Flame Spectrophotometer

The flame spectrophotometer used in this portion was identical with the equipment described in Part A, except for two features: (1) the wave length shaft was driven at a reduced rate of .05 revolutions per minute by incorporating a larger gear on the wavelength drive shaft; (2) a light-pipe was used to view selected regions of the flame.

2. Gas Flows

The measurement and regulation of gas flows has been described in Part A.

B. Reagents

1. Demineralized Water

Demineralized water was prepared by passing ordinary distilled water through a column of Amberlite MB-3 resin.

2. 4-Methyl Pentan-2-One

Practical grade 4-methyl pentan-2-one was used without further purification.

3. Hydrobromic Acid

Reagent grade fuming hydrobromic acid (49.7 per cent) was used in preparing solutions of the various metals.

4. Arsenic Solutions

A standard solution of arsenic(III) bromide dissolved in 4-methyl pentan-2-one was prepared in the following manner: A 0.6602 gram sample of arsenic(III) oxide was evaporated to dryness with concentrated nitric acid. The residue, arsenic(V) oxide, was allowed to cool, and 10 ml. of fuming hydrobromic acid was added to the residue. Upon standing the arsenic(V) oxide is reduced to arsenic(III) bromide. Ten ml. of methyl alcohol was added to the arsenic solution followed by the addition of 4-methyl pentan-2-one to a final volume of 100 ml. This solution contained 5000 µg. of arsenic per ml. Less concentrated solutions of arsenic were prepared by the appropriate dilution.

5. Antimony Solutions

A 0.5986 gram sample of antimony(III) oxide was dissolved in fuming hydrobromic acid and evaporated to a volume of 10 ml. on a steam bath. The solution was diluted to a final volume of 100 ml. with 4-methyl pentan-2-one which gave a solution containing 5000 µg. of antimony per ml. Less concentrated solutions of antimony were prepared by appropriate dilution.

6. Bismuth Solutions

A solution containing 5000 µg of bismuth per ml. was prepared by dissolving 0.500 grams of bismuth metal in concentrated nitric acid.

Excess hydrobromic acid was added and the solution was boiled until the evolution of bromine had ceased. The volume of the solution was reduced by evaporating to a volume of 10 ml. The solution was then diluted to a final volume of 100 ml. with 4-methyl pentan-2-one. Less concentrated solutions of bismuth were prepared by appropriate dilution.

7. Calcium Solutions

A 2.497 gram sample of calcium carbonate was dissolved in hydrochloric acid and evaporated to dryness. The residue was dissolved in demineralized water and diluted to a final volume of 500 ml., which gave a solution containing 1000 µg. of calcium per ml. Less concentrated solutions were prepared by dilution.

8. Cadmium and Zinc Solutions

Solutions of cadmium and zinc were prepared by dissolving 0.100 gram of each metal in hydrobromic acid and evaporating the solutions to a volume of 10 ml. each. The solutions were each diluted to a final volume of 100 ml. with 4-methyl pentan-2-one, which gave solutions each containing 1000 µg. of the respective metal per ml.

9. Mercury(II) Solutions

A solution which contained 1000 µg. of mercury(II) per ml. was prepared by evaporating a solution that contained 0.1589 gram of mercury(II) acetate with an excess of hydrobromic acid. The volume of the solution was reduced to 10 ml. and the solution was diluted to a final volume of 100 ml. with 4-methyl pentan-2-one. Less concentrated solutions of mercury(II) were prepared by dilution.

10. Platinum Solutions

A 0.100 gram sample of platinum wire was dissolved in aqua regia. The excess nitric acid was removed by boiling with hydrochloric acid. The hydrochloric acid was removed by continued boiling with the addition of hydrobromic acid until fumes of hydrogen bromide were evident. The volume of the solution was reduced to 10 ml. and dissolved in a sufficient volume of 4-methyl pentan-2-one to give a final volume of 100 ml., which gave a solution containing 1000 µg. of platinum per ml.

11. Tin Solutions

A solution which contained 10,000 µg. of tin per ml. was prepared by dissolving 1.000 gram of tin metal in fuming hydrobromic acid. Several hours were required for complete dissolution, with only gentle warming. Five milliliters of methyl alcohol was added to the solution, followed by the addition of 4-methyl pentan-2-one to give a final volume of 100 ml. Less concentrated solutions were prepared by the appropriate dilution.

CHAPTER III

EXPERIMENTAL RESULTS

A. Development of the Light-Pipe

Preliminary work on the emission spectra from the reaction zone involved development of a method for viewing a selected portion of the flame and exclusion of radiation from other regions of the flame. Marr[21] employed a blackened tube with entrance and exit aperatures whose diameters corresponded to the field of view of a quartz lens. In this work a device was needed that could be easily attached and removed. Space limitations precluded the use of a slit arrangement since it would have required a major modification of the flame housing.

A simple light-pipe, or guide, was found to be quite satisfactory for transmitting the radiation from the flame to the entrance light port of the spectrophotometer. Early work was done with a solid Pyrex rod; later, a glass tube, silvered on the outer surface, was used. A section of aluminum tubing was finally chosen as the most satisfactory material. The major objection to transmission of radiation through a solid rod is the absorption and reflection losses. Reflection losses alone amount to 4 per cent at each glass-air interface.[22] Absorption losses are even larger; they depend upon the thickness and nature of the absorbing medium and the wavelength of the light. The length of rod that would be required in this work (14 to 15 cm.) would seriously limit the transmission of light, particularly in the ultraviolet portion of the spectrum.

A hollow aluminum tube will transmit a light beam by multiple reflections from the inner surface. A highly polished aluminum surface will reflect about 90 per cent of the incident light to as short a wavelength as 200 mμ.

Light-pipes have been used for the transmission of infrared radiation,[23] and a radiation pyrometer has been developed using a sapphire rod light-guide,[24] The mathematical treatment of the nature of the reflection, absorption, and scattering of a light beam traversing a cylindrical rod or tube is quite complex.[23,24,25,26]

B. Study of Transmission Properties of the Light-Pipe

A brief study was made on the photoresponse of a barrier-layer cell which was illuminated by a tungsten light beam transmitted through a light-pipe. The effects of a reflecting and a non-reflecting tube were studied. Also, the photoresponse of the barrier-layer cell was obtained when the light beam was allowed to impinge unrestricted upon an aperature placed in front of the barrier-layer cell. Figure 13 illustrates the device used to obtain these data. A tungsten lamp was mounted on a rack-and-pinion mount to enable the light source to be moved vertically in front of the entrance to the light-pipe. The arrangement was analogous to moving a burner vertically in front of the light-pipe for examination of different regions of the flame. The light beam was considered to emanate from a finite sized light source; the size was determined by various diameter aperatures which were placed in front of the tungsten lamp. The solid angle intercepted by the light-

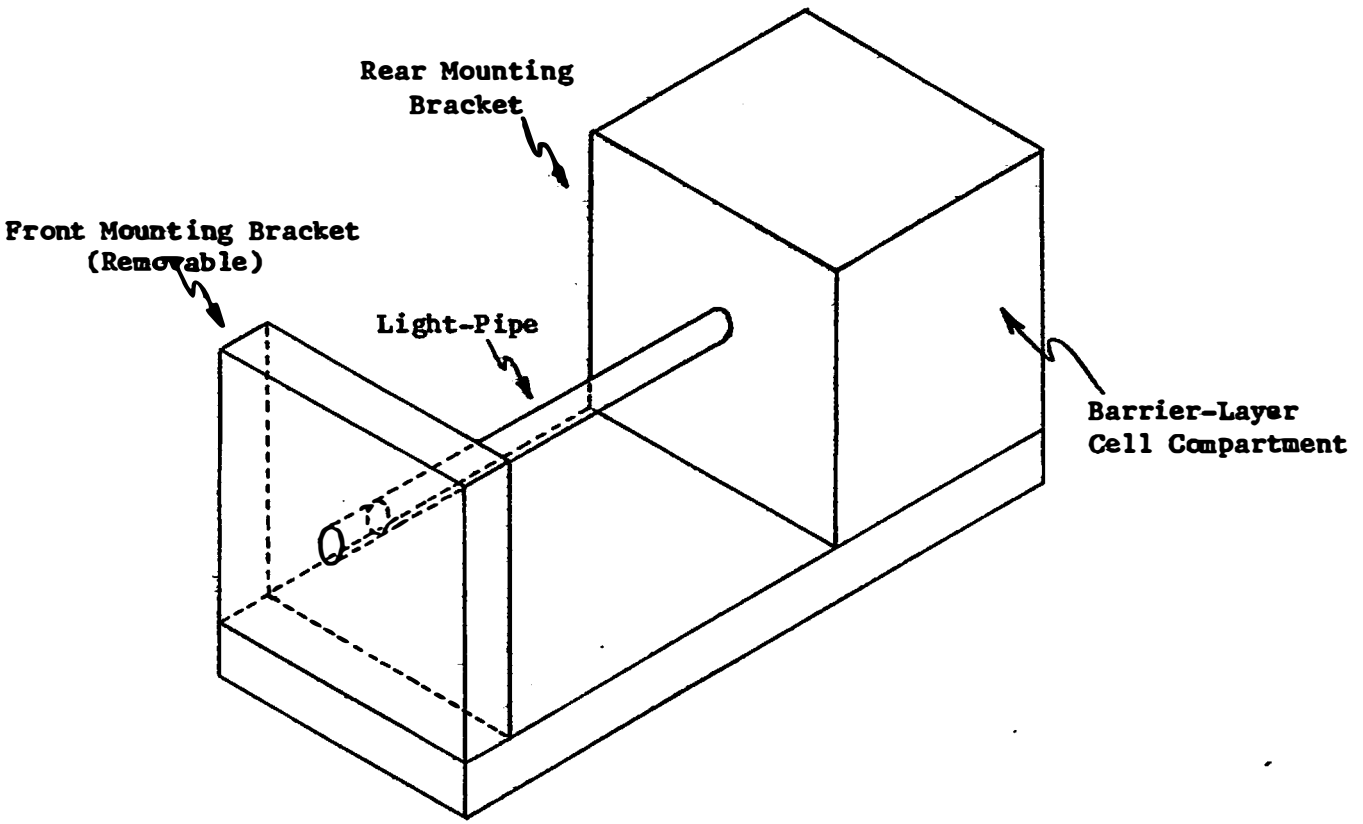

Figure 13. Device for measuring transmission properties of the light-pipe. Not drawn to scale.

pipe was varied by moving the light source away from or closer to the entrance of the light-pipe. The relative intensities of the light flux reaching the barrier-layer cell were obtained from galvanometer readings of the current output of the barrier-layer cell.

1. Effect of the Light Source Diameter

Figure 14 illustrates the effect of increasing the diameter of the light source at a fixed distance from the entrance of the light-pipe. The relative photoresponse of the barrier-layer cell is plotted versus the position of the light source with respect to the axial center of the light-pipe. The axial center of the light pipe is represented by the zero point on the abscissa. Positive and negative distances represented, respectively, the positions of the light source above and below the axial center of the light-pipe. When the smallest diameter light source (0.159 cm.) was used, the photoresponse curve rose to a maximum height and remained constant so long as the light beam filled the light-pipe. The curve was symmetrical about the axial center of the light-pipe. As the diameter of the light source increased, the photoresponse increased likewise although the plateau of the photoresponse curve diminished in length.

Figure 15 illustrates the photoresponse curve when the light-pipe intercepts a smaller solid angle. The curves became broadened and lost their flat plateaus. No difference in the intensity of the light could be detected for the two solid angles represented by the two distances between the light source and the light-pipe entrance.

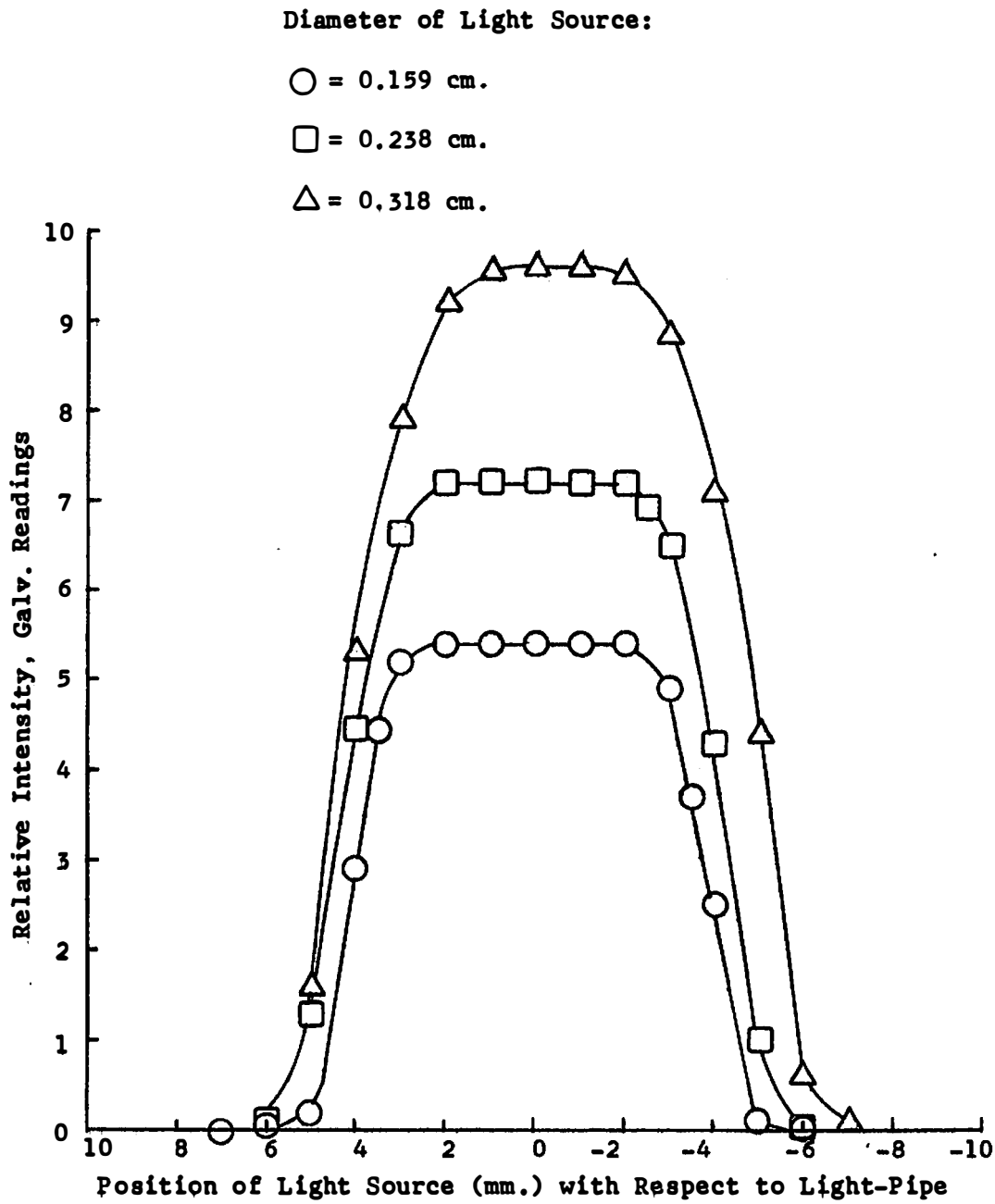

Figure 14. Plot of relative light intensity versus the position of the light source for three light source diameters. Light source 0.7 cm. from entrance of light-pipe.

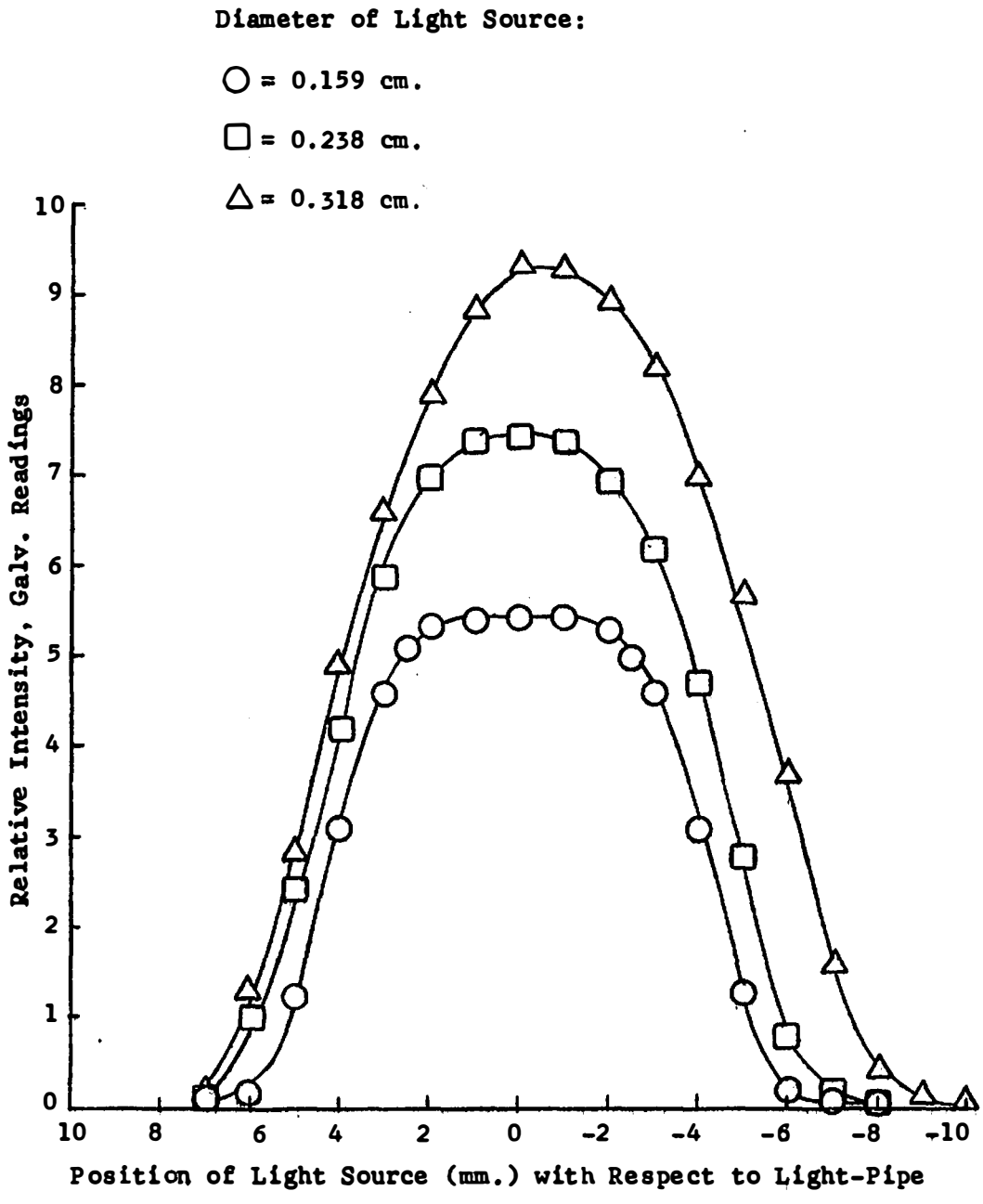

Figure 15. Plot of relative light intensity versus the position of the light source for three light source diameters. Light source 3.0 cm. from entrance of light-pipe.

2. Effect of the Light Source Diameter with a Non-Reflecting Tube

The inner surface of an identical light-pipe was coated with a layer of flat black paint. When dry the inside of the light-pipe was dusted with Norite to further reduce reflections from the inner surface of the light-pipe. Figure 16 illustrates the photoresponse curves obtained under these conditions. The concavity of the curves was the result of some reflection at extremely small incident angles with the walls of the light-pipe as the light source was moved vertically in front of the entrance of the light-pipe. The importance of the reflected light is seen by comparison with Figures 14 and 15.

3. Photoresponse Without the Use of a Light Pipe

The light-pipe and the front mounting bracket were removed (Figure 13) and the light beam was allowed to fall directly on an aperture corresponding to the exit end of the light-pipe in front of the barrier layer cell. The photoresponse curves are shown in Figure 17 with and without the light-pipe. The distance of the light source from the barrier layer cell was the same in both cases. It is readily seen that the light-pipe approximately doubled the relative signal received by the detector and also made the relative vertical position of the light source to the detector very critical as to the point of maximum intensity. The maximum intensity is observed when the light source is at the axial center of the light-pipe.

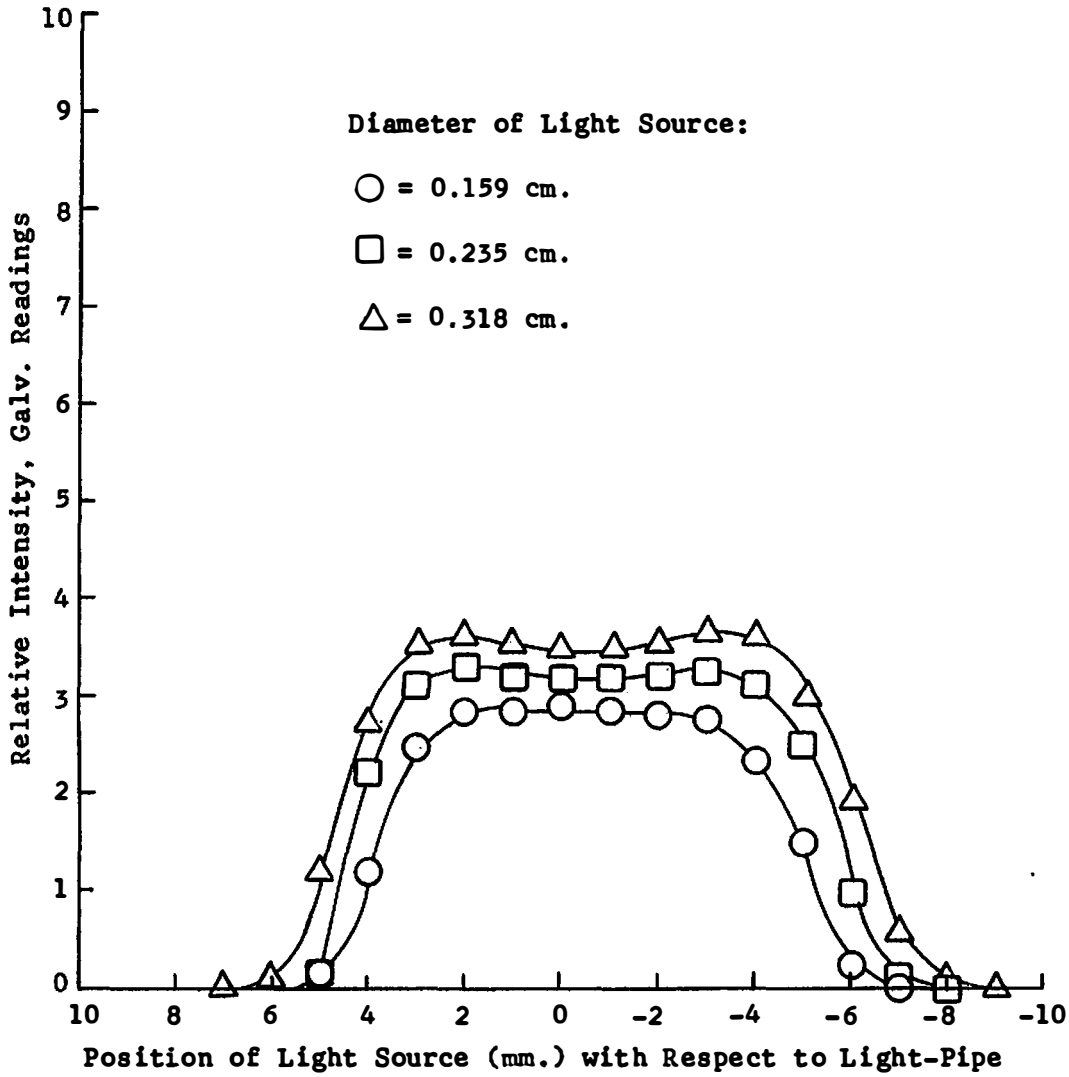

Figure 16. Plot of relative light intensity with a non-reflecting light-pipe versus the position of the light source for three light source diameters. Light source 3.0 cm. from entrance of light-pipe.

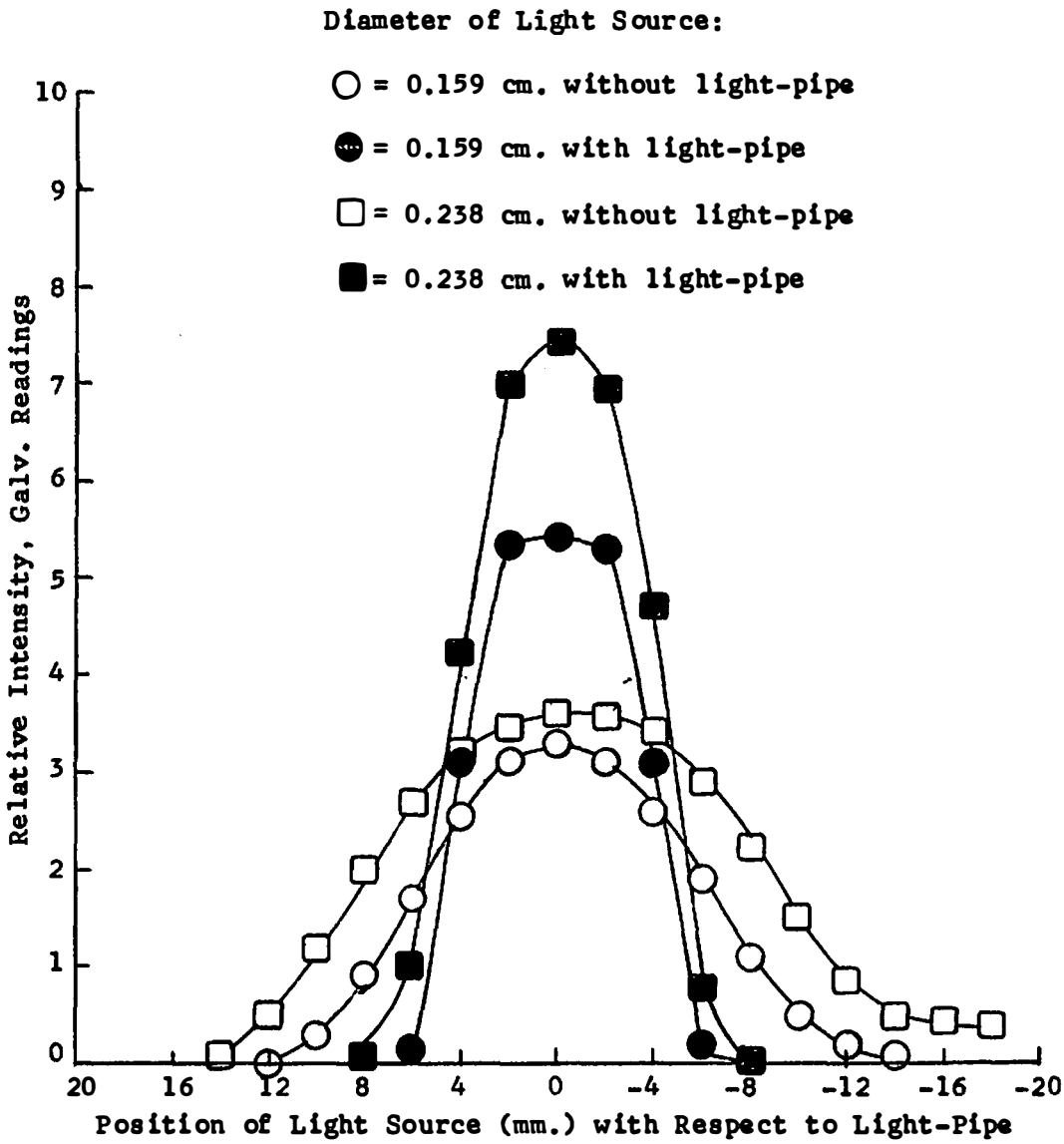

Figure 17. Plot of relative light intensity with and without the light-pipe versus the position of the light source for two light source diameters.

C. Mounting the Light-Pipe

The light-pipe was placed between the burner and the slit entrance mirror. Figure 18 illustrates the light-pipe mounting bracket which was placed between the exit port of the burner housing unit and the entrance port of the Beckman DU spectrophotometer. The bracket provided a means of adjusting the light-pipe so it would be centered on the optical axis between the burner and the entrance slit of the spectrophotometer. The mounting bracket containing the tube could be conveniently attached by swinging the burner housing to one side and placing the bracket in the proper position against the monochromator housing. A tapped hole in the slit plate enabled the bracket to be held firmly in place with a retaining screw. After the bracket was positioned the burner housing was swung back into its normal position, which also assisted in holding the bracket in place. Once the light-pipe was properly aligned, the bracket could be removed without disturbing the alignment of the light-pipe.

D. Alignment Procedure

Two alignment procedures were found to be satisfactory. In one instance the 247.8-mμ carbon line was used as a signal source. Since this carbon line is strong only in the reaction zone, its emission intensity provided a means of locating the reaction zone. First the flows of the fuel gases were set to the desired values. The burner was then positioned at an arbitrary height. The light-pipe was then adjusted

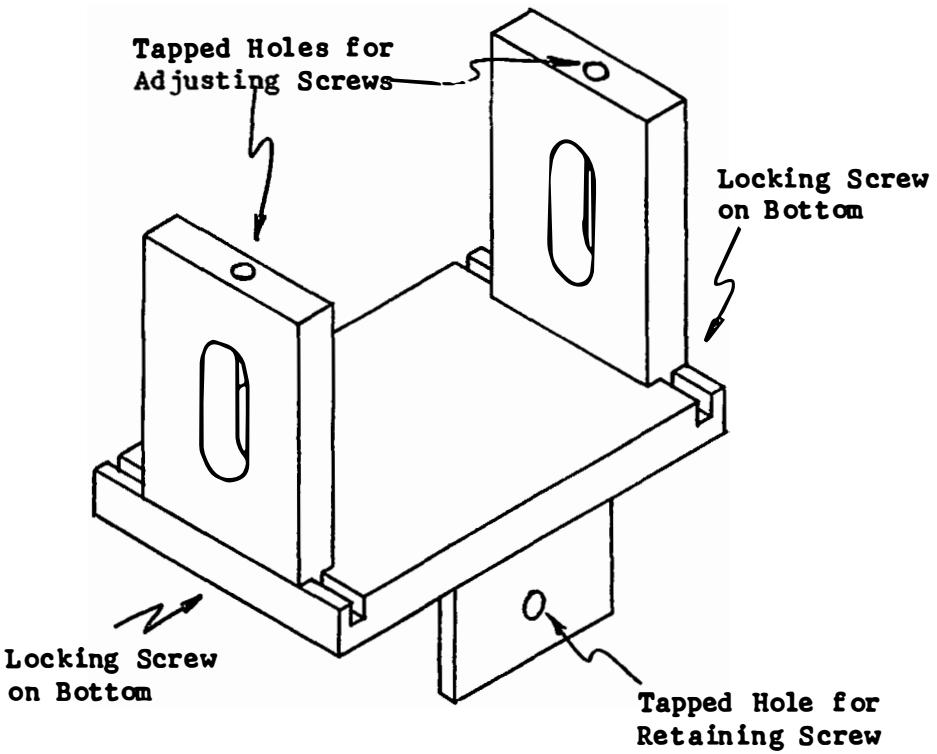

Figure 18. Light-pipe mounting bracket for Beckman Model DU spectrophotometer with flame attachment. Not drawn to scale.

vertically or laterally to obtain the maximum emission intensity for the carbon line.

A second procedure was similar to that described in the Beckman instruction manual.[27] The phototube housing and the sample compartment were removed from the monochromator chassis. Light from a tungsten bulb was projected through the exit slit of the monochromator. The light-pipe was then adjusted to transmit a perfect circular area of light as observed on a piece of paper held at the end of the light-pipe. When the light-pipe was concentric to the optical axis of the monochromator the circular light pattern was observed. Any deviation from the concentric position resulted in a distorted light pattern due to an unbalance in the distribution of the light reflected from the walls of the light-pipe, This method of alignment was necessary only when the light-pipe was initially aligned. The first method of alignment described was used frequently to allow for changes in flame geometry and for fine adjustment when the burner was suspected to be slightly out of alignment with the optical axis of the monochromator. The alignment of the tube was very critical. Vertical changes of only 1 or 2 mm. caused as much as an 80 per cent variation in the signal strength.

E. Emission Zones of Flame Spectra

1. Carbon Line

The flame spectrum of the 247.8-mμ carbon line is shown in Figure 19. The emission intensity of the 247.8-mμ carbon line when plotted versus relative flame region viewed, as shown in Figure 20,was confined

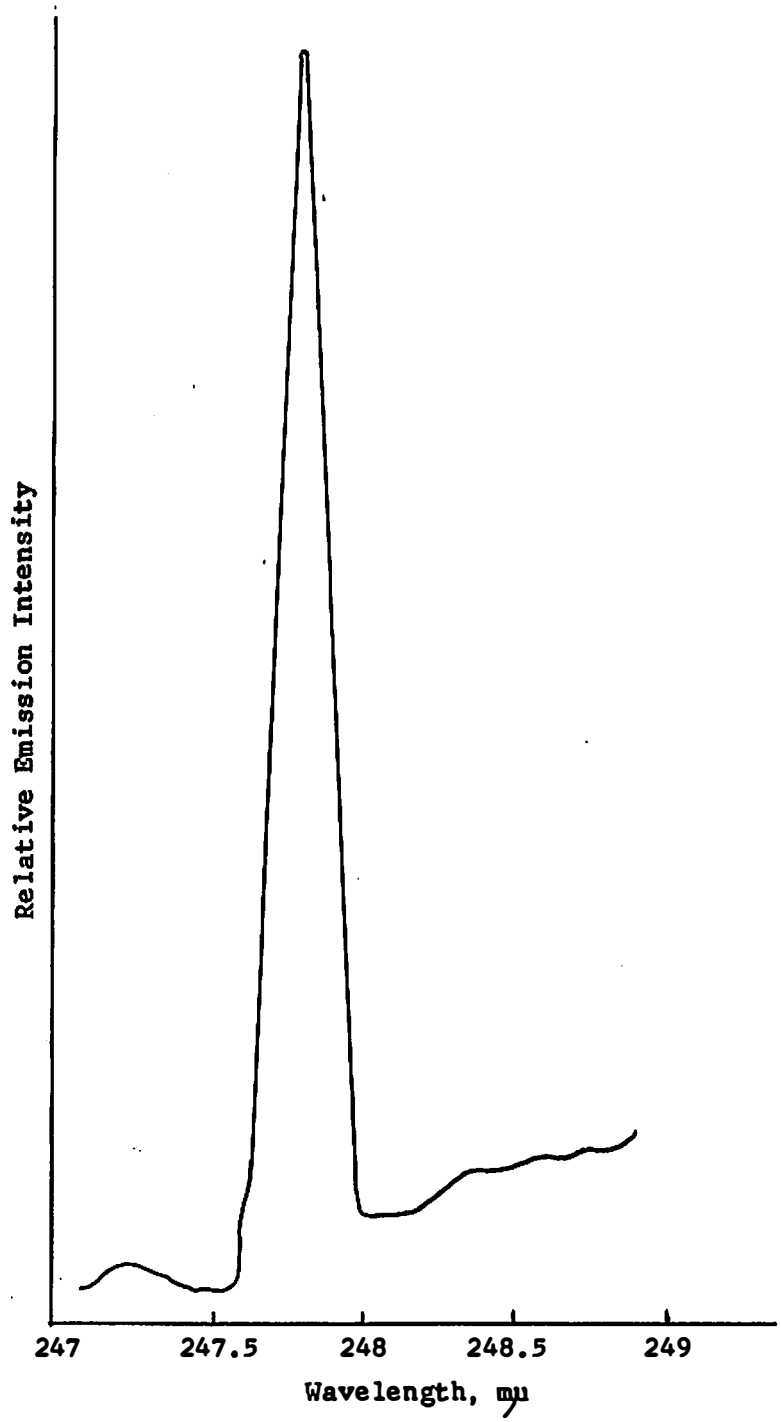

Figure 19. Flame spectrum of carbon showing the atomic line at 247.8 mμ.

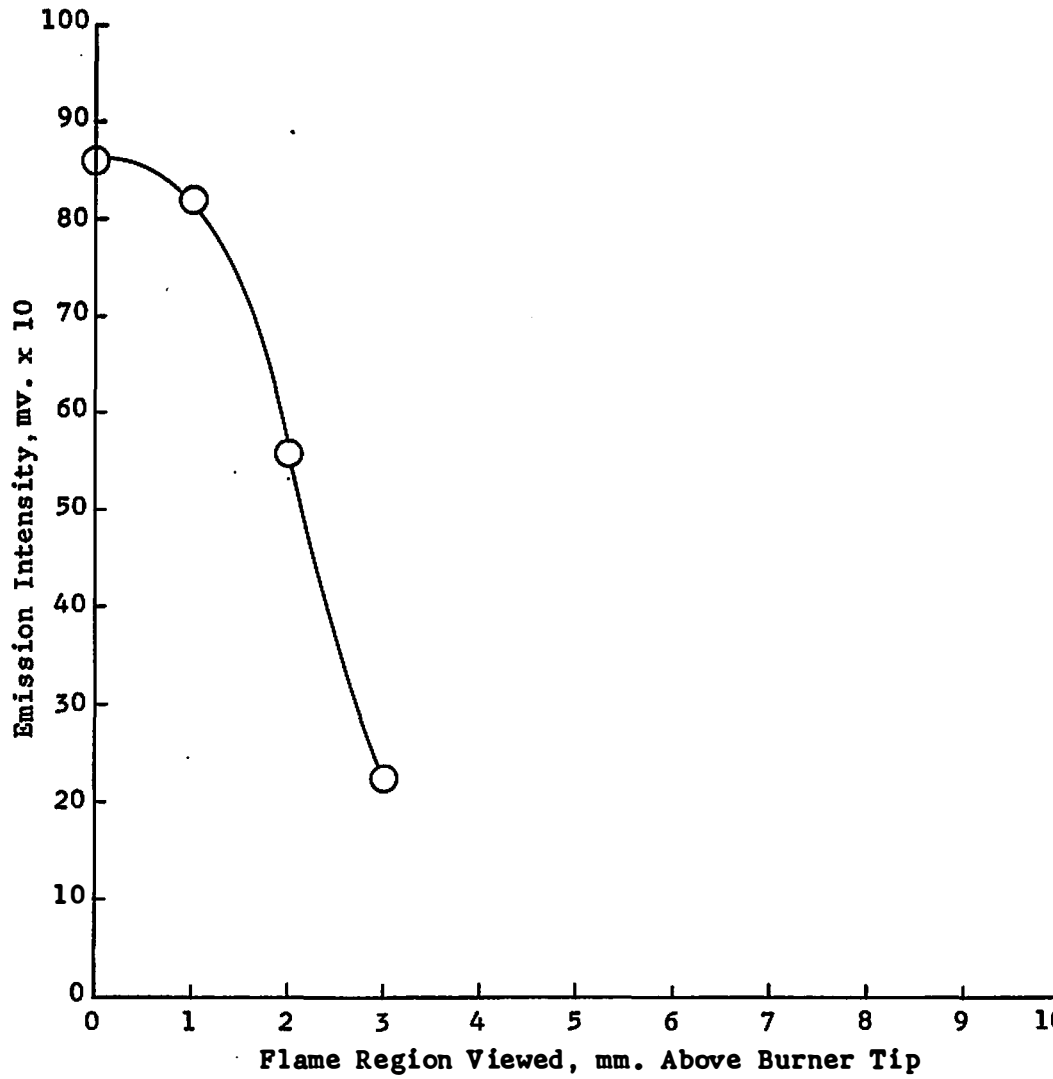

Figure 20. Plot of emission intensity of the 247.8-mμ carbon line versus relative flame region viewed.

to a very narrow region of the flame. The 247.8-mμ carbon line serves as an indication of the reaction zone region of the flame. The line emission of carbon is limited to a 3 to 4 mm. portion of the total flame height. The data shown in Figure 20 are for a ratio of oxygen flow to acetylene flow of 2.0. The instrument settings were as follows: slit width, 0.09 mm.; per cent adjust, 70.

2. CH and C_2 Band Emission

Emission from these band systems was also confined to the reaction zone. Figure 21 illustrates the very limited region of the flame in which CH and C_2 emission occurs. The 431.1-mμ CH band head intensity and the 516.5-mμ C_2 band head intensity are plotted versus the relative flame region viewed. Although the zone of emission is quite small for lean flames, the high intensity of emission and broad distribution of the bands results in a very high level of background radiation, especially in the reaction zone. The ratio of oxygen flow to acetylene flow was 2.0. The slit width was 0.01 mm. and the per cent adjust setting was 20.

3. OH Band Emission

A plot of the 306.7-mμ OH band head intensity versus the relative flame region viewed is shown in Figure 22. In this system the OH band intensity reaches its maximum just above the reaction zone. The emission extends well into the innerconal region of the flame. The ratio of oxygen to acetylene and instrument settings were idential with those used for recording the CH and C_2 band emission intensities.

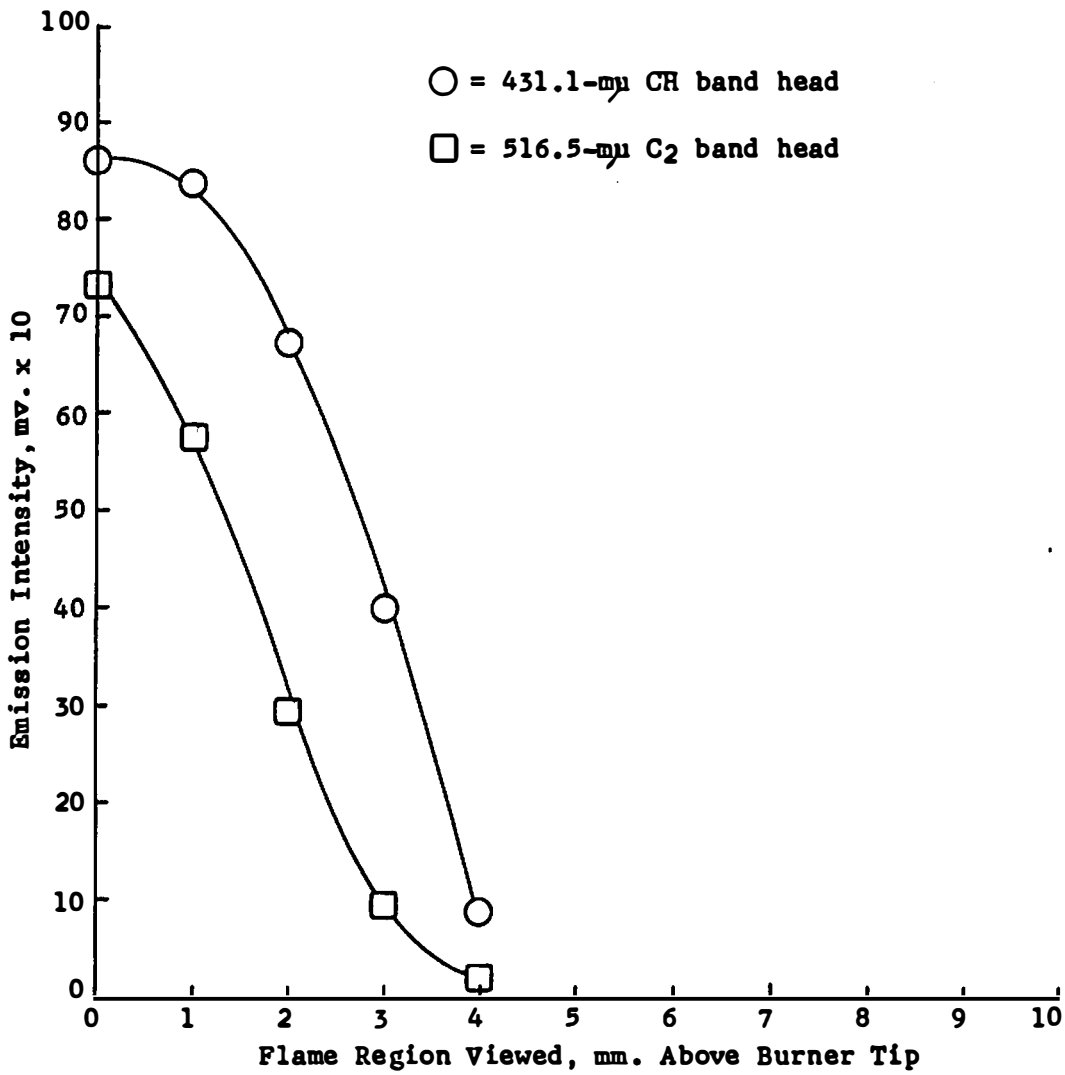

Figure 21. Plot of emission intensities of the 431.1-mμ CH band head and the 516.5-mμ C_2 band head versus flame region viewed.

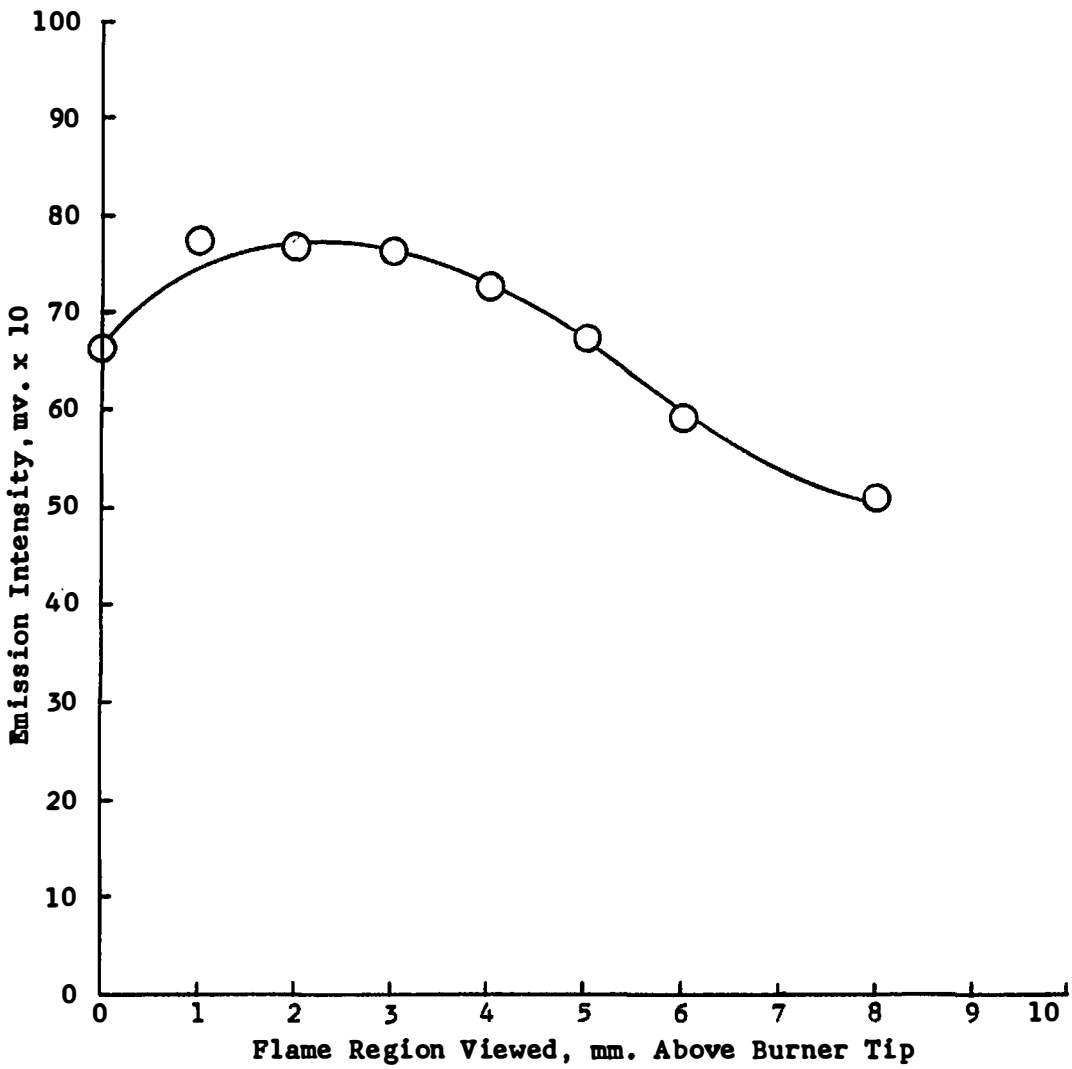

Figure 22. Plot of emission intensity of the 306.7-mμ OH band head versus flame region viewed.

F. Flame Spectra of Metals in the Reaction Zone

1. Procedure

Solutions of several metal bromides dissolved in 4-methyl pentan-2-one were prepared and aspirated into the flame. The wavelength regions were scanned where the arc lines of the metals were known to occur.

2. Instrument Settings

A 1.5 to 1 ratio of oxygen flow to acetylene flow was used to insure a thick reaction zone. The instrument settings were as follows: slit width, 0.13 mm.; sensitivity, 60 volts per dynode; per cent adjust, 50. These settings were used consistently throughout the studies made on the reaction zone, unless otherwise indicated.

3. Arsenic Spectrum

The 228.8-mμ and 234.9-mμ lines of arsenic were readily detectable in the reaction zone of the flame. The flame spectrum of the 234.9-mμ arsenic line is shown in Figure 23. Figure 24 illustrates the emission intensity of the 234.0-mμ arsenic line as a function of the flame region viewed. The arsenic emission was essentially absent above the inner cone of the flame. The optimum region for maximum emission intensity occurred from 3 to 4 mm. above the reaction zone. The emission sensitivity of the 234.9-mμ arsenic line was 2.2 ug. per ml. per per cent T (or 0.1 mv.).

4. Antimony Spectrum

Lines for antimony were observed at 231.2 mμ, 252.8 mμ, and 259.8 mμ. The flame spectrum of the 252.8-mμ line of antimony is shown in

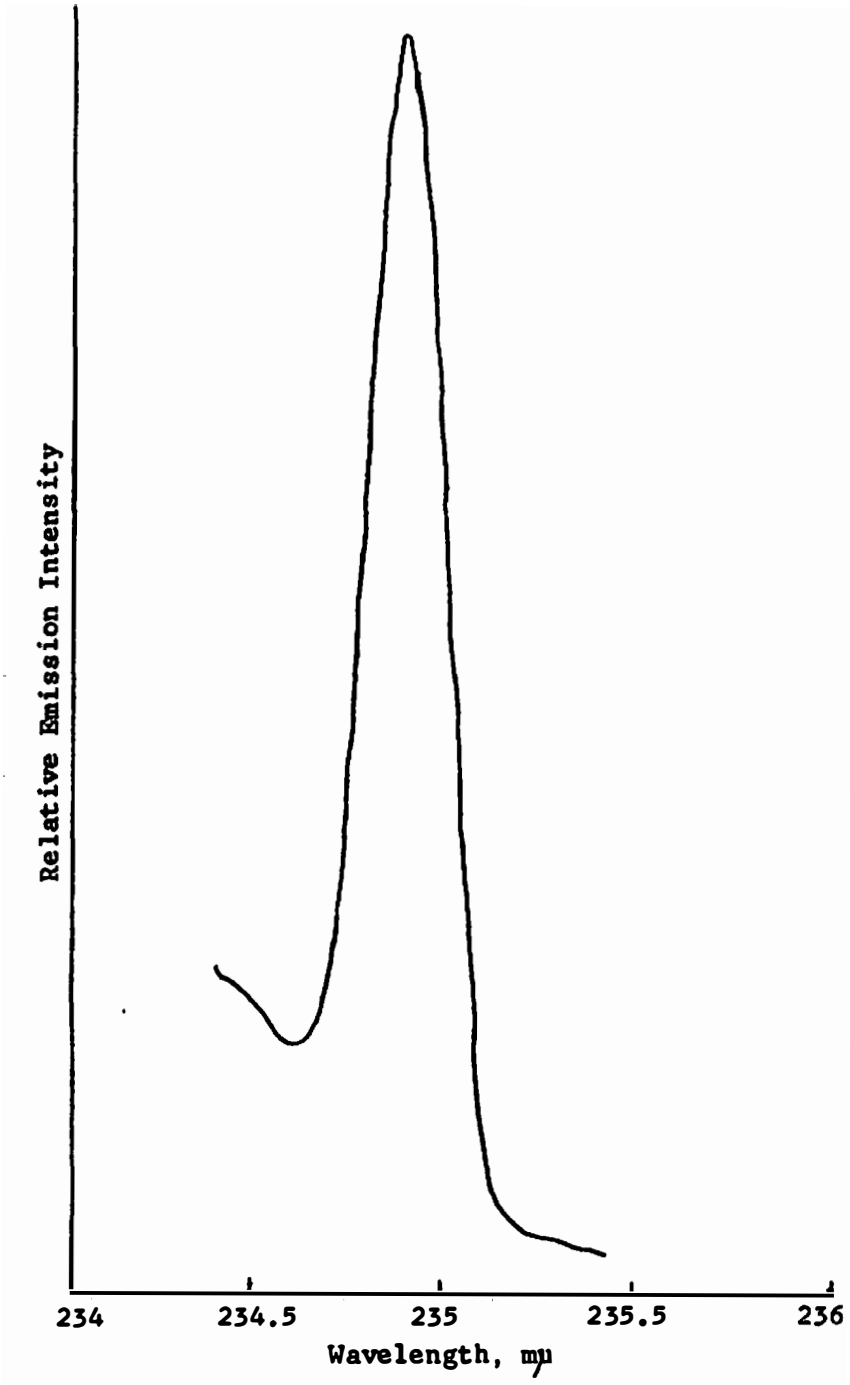

Figure 23. Flame spectrum of arsenic showing the atomic line at 234.9 mμ.

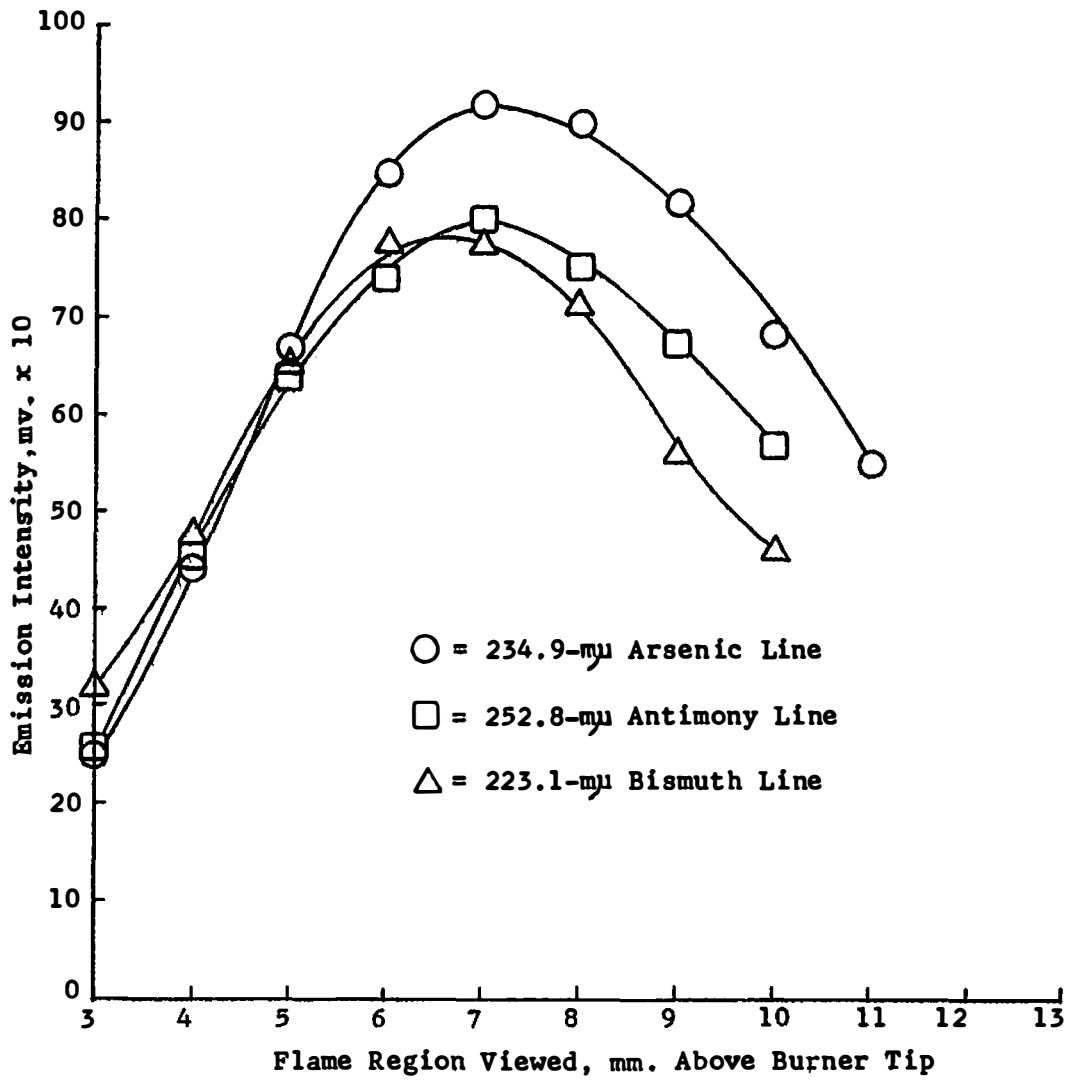

Figure 24. Plot of emission intensities of arsenic, antimony and bismuth versus flame region viewed. From a solution containing 200, 80, and 500 μg. of arsenic, antimony, and bismuth, respectively, per ml. of 4-methyl pentan-2-one.

Figure 25. The emission intensity distribution of antimony in the flame was very similar to that of arsenic (Figure 24). The emission sensitivity of the 252.8-mμ line of antimony was 1.0 μg. per ml. per 0.1 mv.

5. Bismuth Spectrum

Bismuth displayed several detectable lines in the reaction zone,* Most intense was the 223.0-mμ line. The flame spectrum of the 223.0-mμ line and the 222.8-mμ line of bismuth are shown in Figure 26. The two lines are incompletely resolved, however the slight overlap at the base of the two lines does not preclude the use of the 223.0-mμ line. The emission sensitivity of the 223.0-mμ line of bismuth was 6.4 μg. per ml. per 0.1 mv. Figure 24 shows the similarity of the bismuth emission intensity distribution curve to the curves for arsenic and antimony.

6. Tin Spectrum

The flame spectrum of tin consists of several lines of which the more sensitive are lines at 235.4 mμ and 242.9 mμ. Two ionic lines were identified at 220.9 mμ and 248.3 mμ. Figure 27 shows the emission intensity distribution of the 248.3-mμ ionic line of tin in the flame. The emission intensity distribution of the 247.8-mμ line of carbon is also shown to locate the reaction zone of the flame in relation to the tin emission. Figure 28 illustrates the emission intensity distribution of the 242.9-mμ atomic line of tin with respect to the reaction zone. The region of maximum intensity for the atomic line and the ionic line

*A complete tabulation of the lines observed for bismuth and the other metals is given in Table VI, Chapter IV of this part.

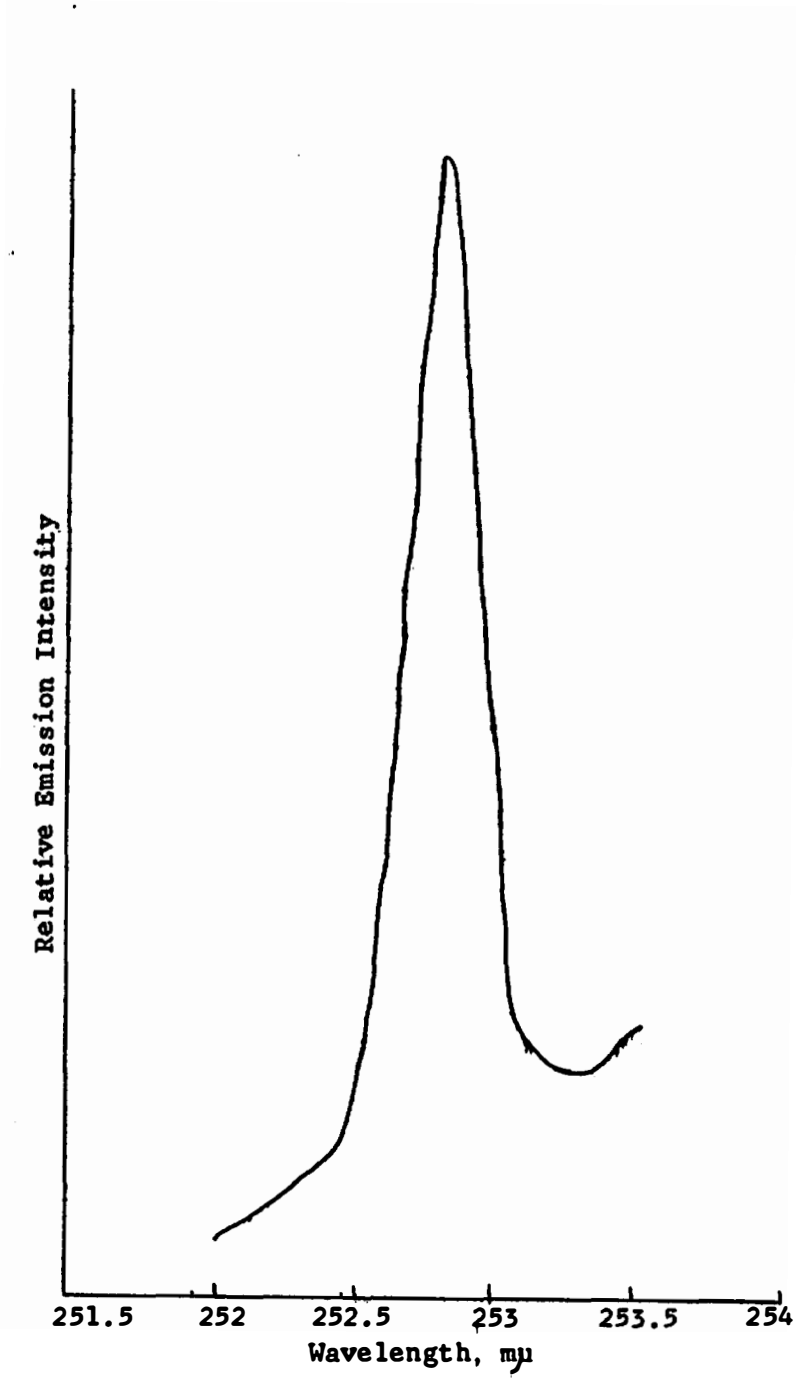

Figure 25. Flame spectrum of antimony showing the atomic line at 252.8 mμ.

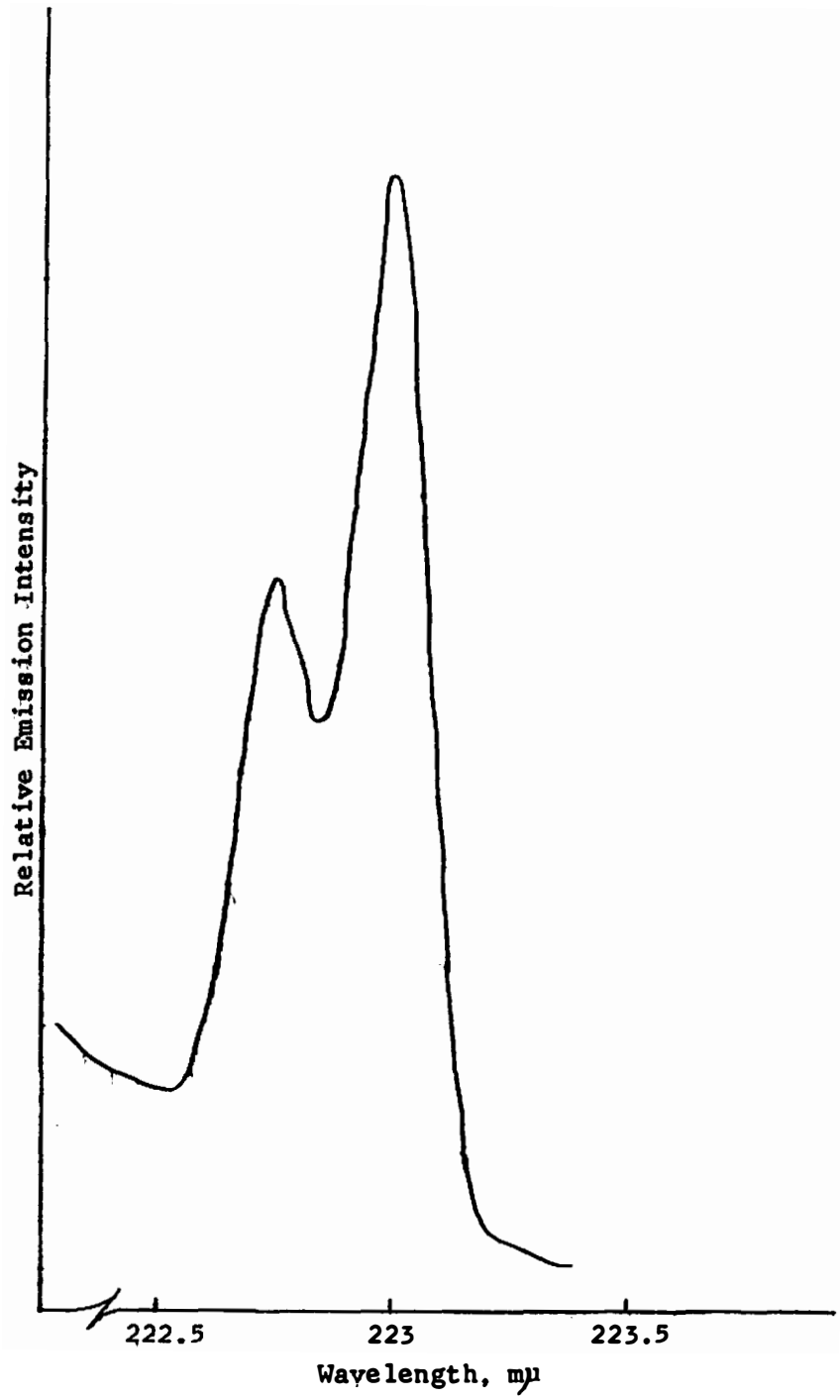

Figure 26. Flame spectrum of bismuth showing the atomic lines at 222.8 mμ and 223.0 mμ.

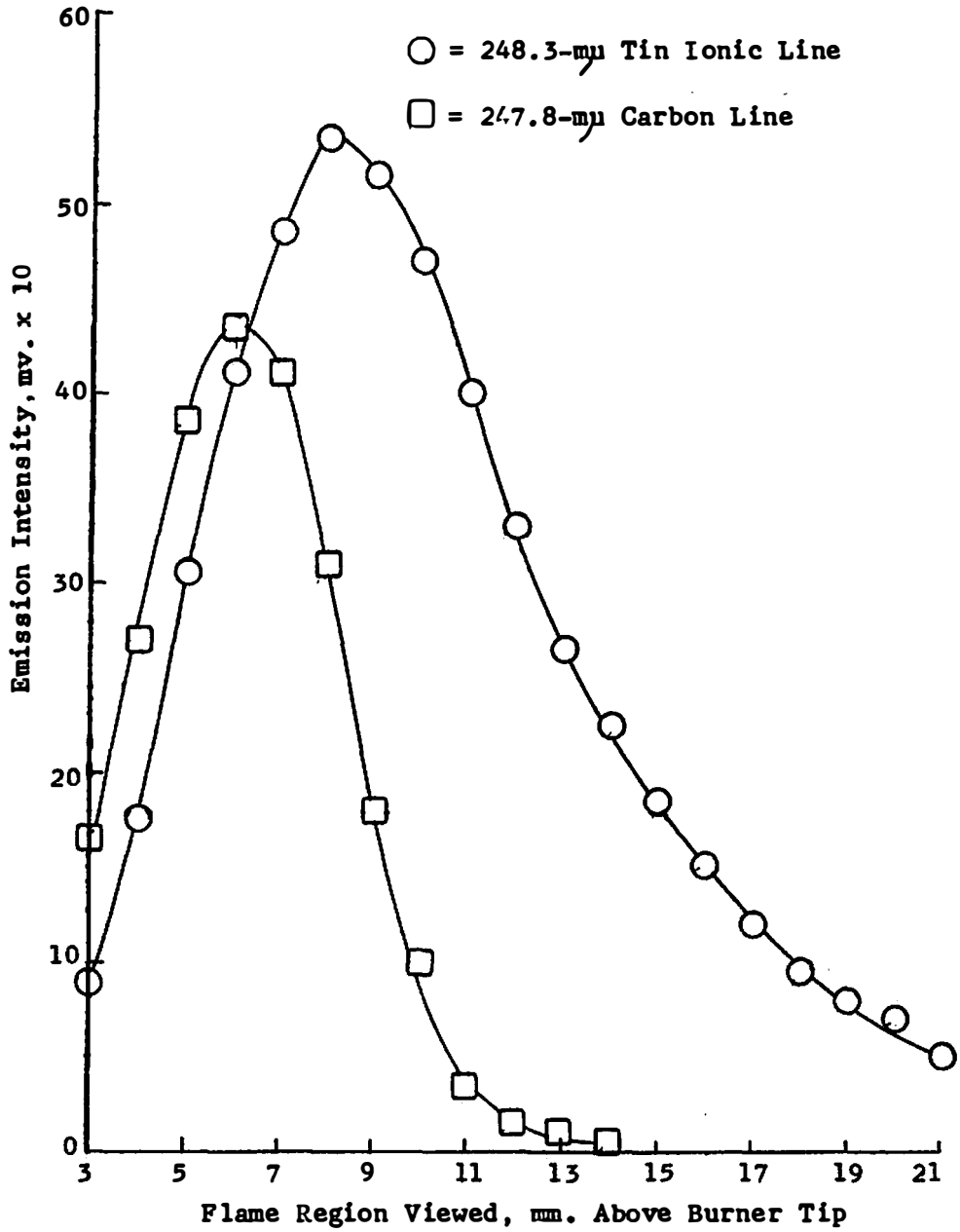

Figure 27. Plot of emission intensities of tin and carbon as a function of flame region viewed. From a solution containing 1000 μg. of tin per ml. of 4-methyl pentan-2-one.

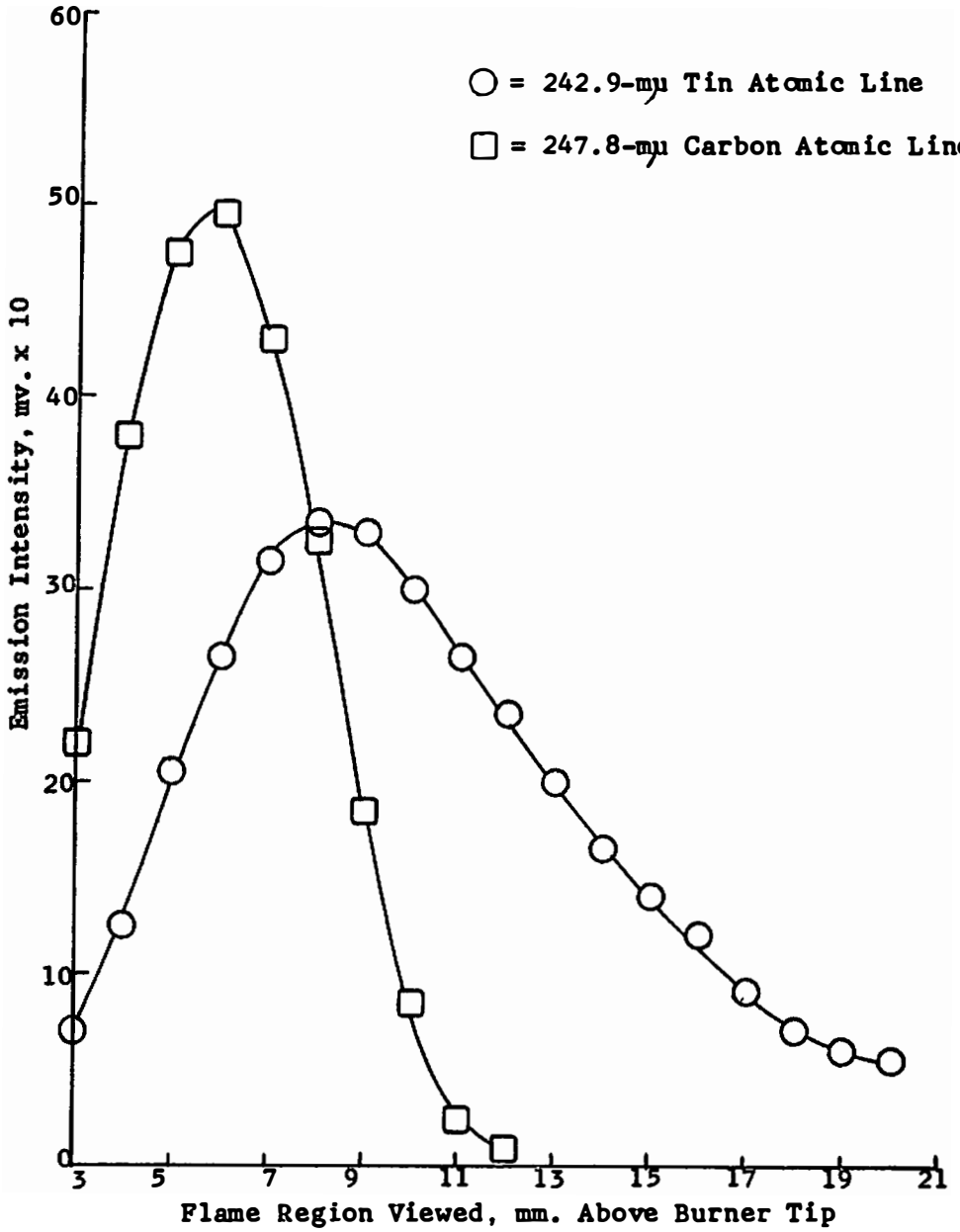

Figure 28. Plot of emission intensities of tin and carbon as a function of flame region viewed. From a solution containing 100 ug. of tin per ml. of 4-methyl pentan-2-one.

is identical. The emission sensitivities of the ionic lines and the more sensitive atomic lines are as follows:

Wavelength (mμ)	Emission Sensitivity (μg. per ml. per 0.1 mv.)
220.9 (ionic)	26
235.4	2.2
242.9	1.6
248.3 (ionic)	17

7. Zinc Spectrum

Only one weak line was observed for zinc at 213.8 mμ. The emission sensitivity was 77 μg. per ml. per 0.1 mv.

8. Cadmium Spectrum

The resonance line of cadmium at 228.8 mμ was readily observed in the reaction zone. The emission sensitivity was 4.2 μg. per ml. per 0.1 mv.

9. Mercury Spectrum

The resonance line of mercury at 253.6 mμ was observed in the reaction zone of the flame. The emission sensitivity was 2.5 μg. per ml. per 0.1 mv.

10. Platinum Spectrum

The emission spectrum of platinum was weak in the reaction zone. The atomic line of platinum at 265.9 mμ was the most sensitive line observed; its emission sensitivity was 15 μg. per ml. per 0.1 mv.

G. Interference Studies of Arsenic, Antimony, and Bismuth

1. Self-Absorption Studies

Curves of the logarithm of the emission intensity versus the logarithm of the concentration for arsenic, antimony, and bismuth are shown in Figure 29. These curves are for the 234.9-mμ line of arsenic, the 252.8-mμ line of antimony, and the 223.0-mμ line of bismuth. Antimony did not suffer from any self-absorption at least to a concentration of 200 μg. of antimony per ml. For arsenic the onset of self-absorption began at a concentration of 150 μg. of arsenic per ml. and for bismuth above 70 μg. of bismuth per ml. The linear regions of the log-log curves had slopes of 0.90, 1.1, and 1.1 for antimony, arsenic, and bismuth, respectively. The low emission sensitivity of bismuth would exclude the use of the linear portion of the bismuth emission intensity versus concentration curve.

2. Mutual Interferences

A mutual interference study was conducted on the emission intensities of arsenic, antimony, and bismuth. The presence of antimony and bismuth, at least up to 500 μg. per ml., did not effect the emission intensity of the 234.9-mμ line of arsenic. However, arsenic depressed the emission intensity of the 252.8-mμ line of antimony. For a solution containing 80 μg. of antimony per ml., the apparent concentrations of antimony in the presence of arsenic were as follows:

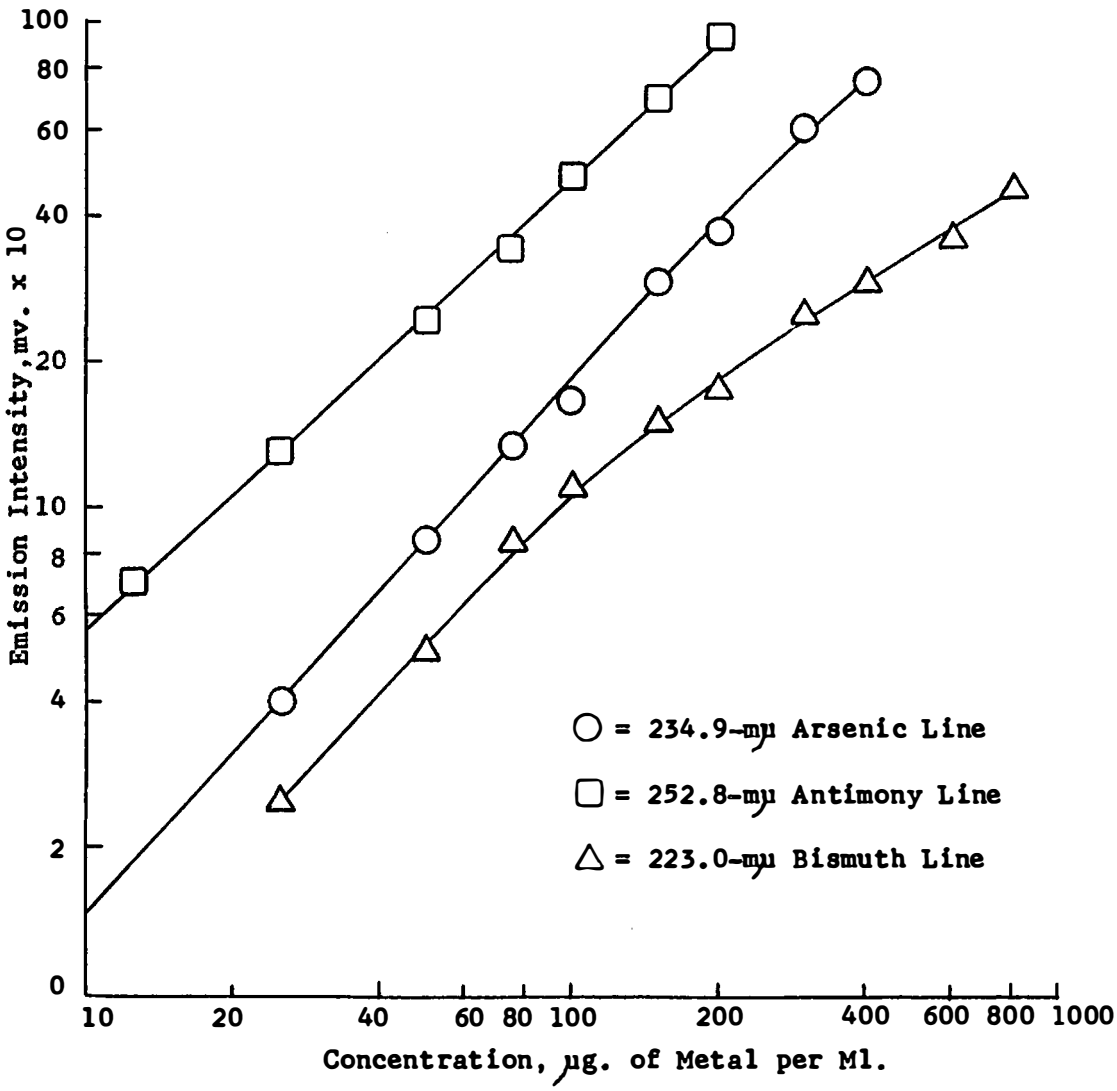

Figure 29. Plot of emission intensity versus concentration on logarithmic coordinates for arsenic, antimony, and bismuth.

Apparent Concentration of Antimony (μg./ml.)	Micrograms of Arsenic per ml.
80	0
78	100
76	200
74	300
71	500

Bismuth had only a slight repressive effect on the emission intensity of antimony. For a solution containing 80 μg. of antimony per ml. and 400 μg. of bismuth per ml., the apparent concentration of antimony was 79 μg. of antimony per ml.

The emission intensity of the 223.0-mμ line of bismuth was not affected by the presence of at least 500 μg. of arsenic or antimony per ml.

3. Effect of Tin and Zinc on the Emission Intensity of Arsenic

Tin exhibited a strong line at 235.5 mμ which was incompletely resolved from the 234.9-mμ line of arsenic. Figure 30 shows the degree of overlap between the tin and arsenic lines. It was possible to make a base line reading of the background from the short wavelength side of the 234.9-mμ line of arsenic. A concentration of at least 1000 μg. of tin per ml. had no effect upon the emission intensity of arsenic from a solution containing 200 μg. of arsenic per ml.

The 228.8-mμ line of arsenic suffered from direct spectral interference by the 228.7-mμ line of tin. The specificity factor,[28] which represents the ratio of the concentration of tin to the concentration

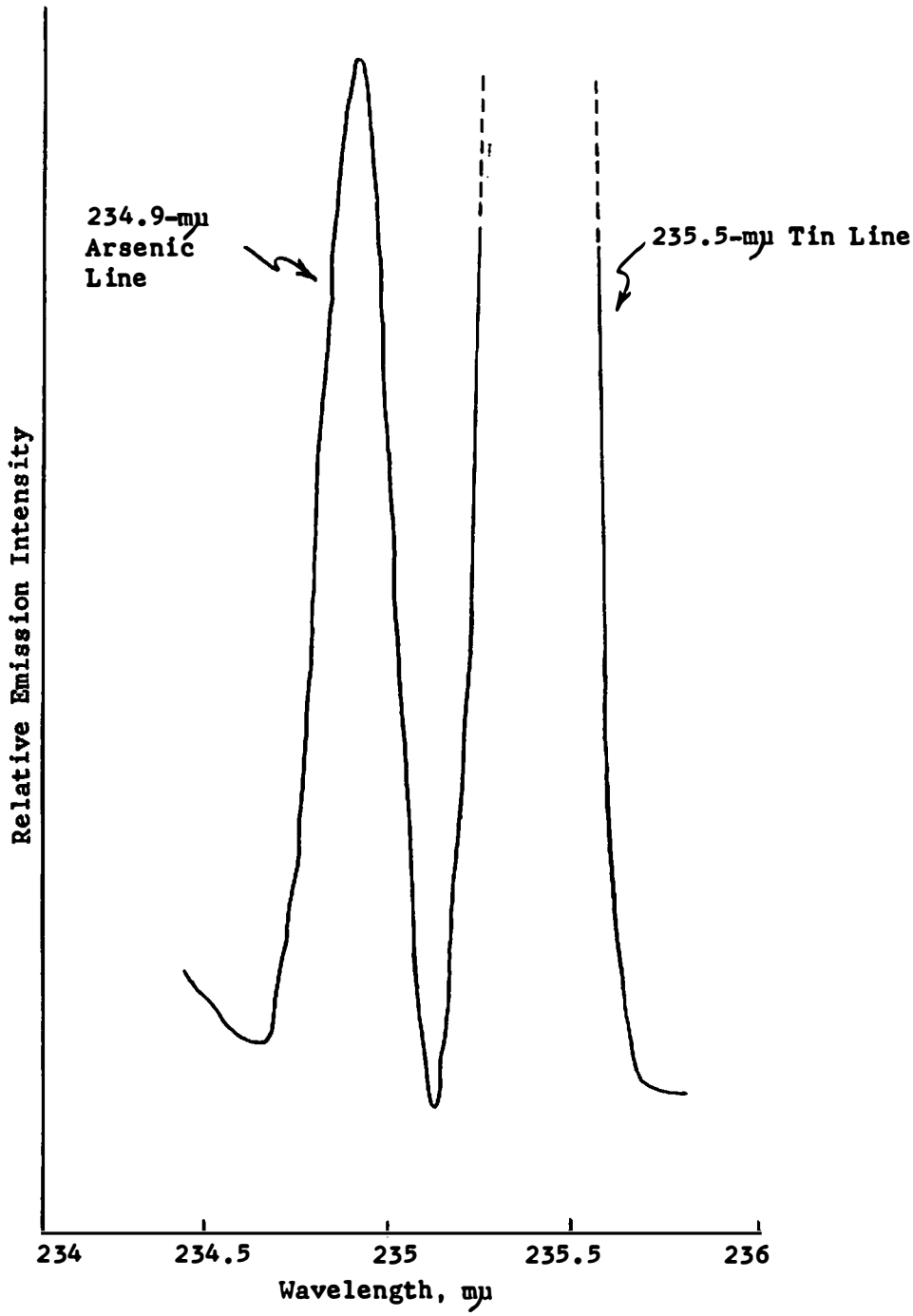

Figure 30. Flame spectrum of arsenic and tin showing the degree of resolution of the 234.9-mμ arsenic line and the 235.5-mμ tin line.

of arsenic that would each give the same emission sensitivity, was 13.3.

Zinc had a severe repressing effect upon the emission intensity of arsenic. For a solution containing 200 µg. of arsenic per ml., the following concentrations of arsenic were indicated in the presence of zinc:

Apparent Concentration of Arsenic (µg./ml.)	Micrograms of Zinc per ml.
200	0
195	200
194	400
194	600
193	800
191	1000
180	2000

H. Ratio of Signal-to-Background Using the Light-Pipe

It has been established that the use of a light-pipe proved valuable for examining various zones of the flame (Figures 27 and 28). Also a degree of amplification was obtained that was independent of the signal-receiving and -amplifying circuitry (Figure 17). For example, the intensity of the carbon line at 247.8 mµ from a dry flame, as a function of flame region viewed, is shown in Figure 31. The upper curve is the emission intensity of the carbon line observed with the light-pipe. The lower curve represents the emission intensity of the carbon line observed without the light-pipe. The mirror behind the flame was

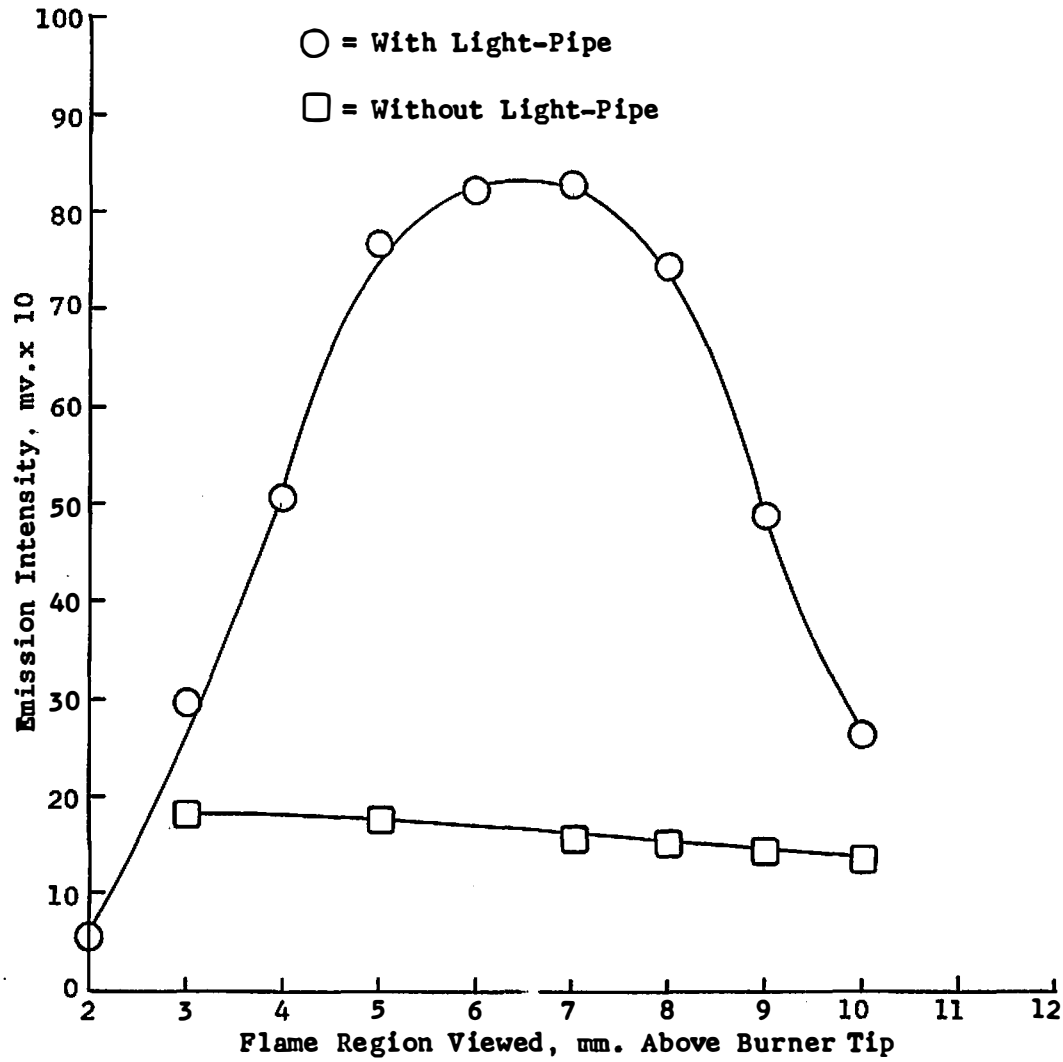

Figure 31. Plot of emission intensity of the 247.8-mμ carbon line as a function of the flame region viewed.

blocked to prevent back reflections from other regions of the flame not directly in the line of sight of the light-pipe. The instrument settings were as follows: slit, 0.09 mm.; sensitivity, 60 volts per dynode; per cent adjust, 5; ratio of oxygen flow to acetylene flow was 2.0. The emission intensity of the carbon line was increased six-fold at the region of maximum intensity. Without the light-pipe the emission intensity of the carbon line was virtually constant over the same relative region of the flame.

The signal-to-background ratio was also improved by the use of the light-pipe. It was observed that the elements arsenic, antimony, bismuth, and tin exhibited their maximum emission intensity in a very small region of the flame. The majority of the flame was emitting continuous radiation and discrete radiation from several band systems such as CH, C_2, and OH. The light-pipe enabled the burner to be positioned precisely to view only the zone of maximum emission intensity of the element. In addition, the only background signal that was observed was that from the flame region directly in view of the light-pipe. Thus a higher percentage of the total emission was the desired signal whereas the overall background intensity was greatly reduced. This fact is readily seen in Figure 32 where the emission intensity of the chromium triplet, centered about 520 mμ, and the background intensity was plotted versus the flame region viewed. The nature of the emission intensity distribution in the flame is shown when the light-pipe was used. As a comparison the emission intensity distribution is shown when the total radiation from the flame was allowed to fall on the entrance slit. At

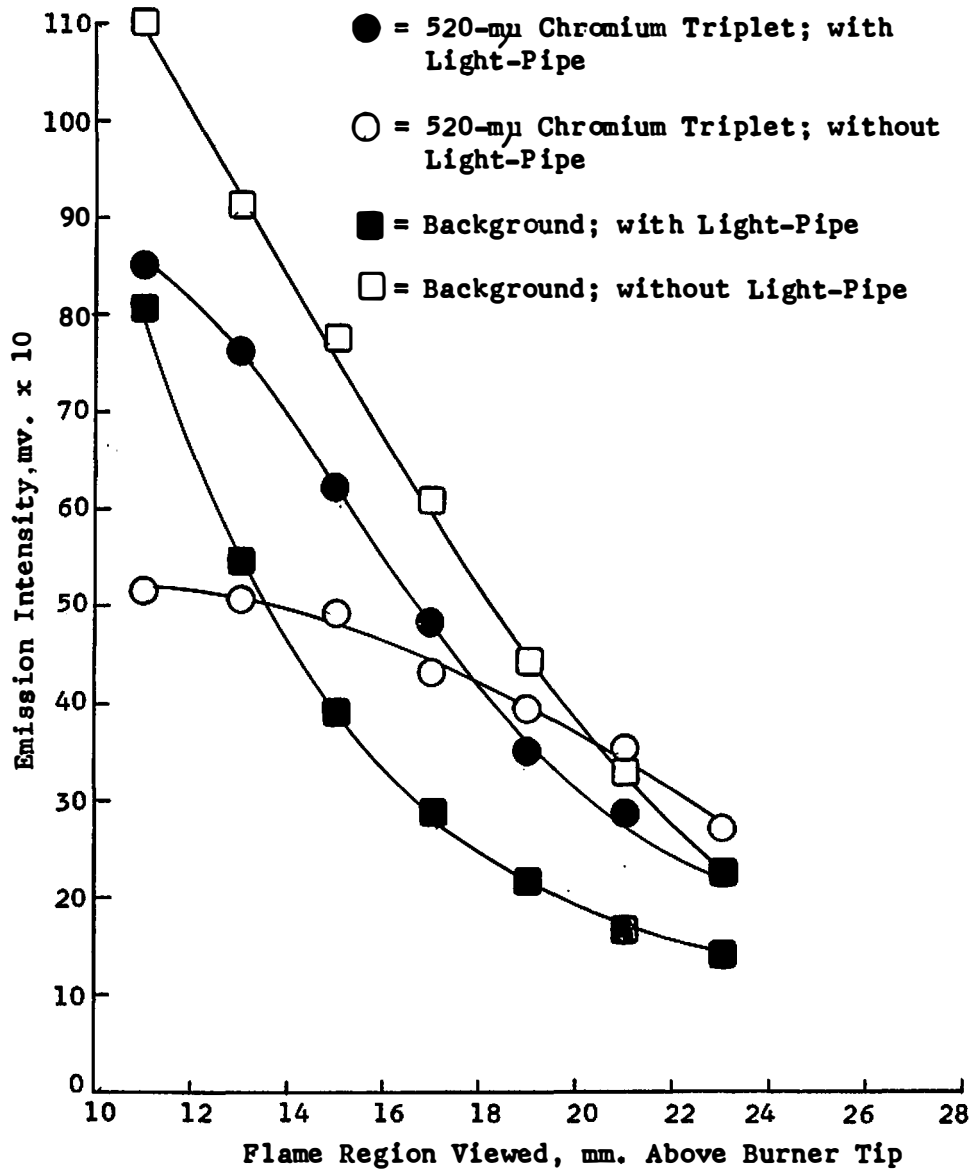

Figure 32. Plot of emission intensity of the 520-mμ chromium triplet versus relative flame region viewed.

a flame region corresponding to a burner setting of 15 mm. (normal burner position in a fixed mount) a net signal of 62 scale divisions was obtained with a signal-to-background ratio of 1.6 when the light-pipe was used. The radiation from an open flame gave a net signal of 49 scale divisions with a corresponding signal-to-background ratio of only 0.63. The instrument settings were as follows: sensitivity, 60 volts per dynode; slit, 0.03 mm., per cent adjust, 3; ratio of an oxygen flow to acetylene flow was 2.5. The background in this region of the spectrum is caused by the strong Swan bands of C_2 superimposed on the C_2 continuum. The increased signal-to-background ratio enabled the slits to be opened wider to a larger degree which in turn gave a higher emission reading. Of course, the signal-to-background ratio also depends upon the nature of the spectral and flame regions viewed. Some signal-to-background ratios are given in Table V.

I. Observations on the Emission Intensity Distribution of Calcium

An aqueous solution which contained 100 ppm of calcium was aspirated into the flame and the emission intensity of the 422.7-mμ line of calcium was observed in various regions of the flame as shown in Figure 33. The instrument settings were as follows: sensitivity, 60 volts per dynode; slit, 0.025 mm.; per cent adjust, 3; the oxygen to acetylene flow ratio was 2.5 to 1. The emission intensity distribution of the 247.8-mμ line of carbon is also shown to locate the relative position of the reaction zone. The region of maximum intensity occurred well into the innerconal region of the flame although the emission

TABLE V

SIGNAL TO BACKGROUND RATIOS AS OBSERVED WITH THE LIGHT-PIPE AND WITHOUT THE LIGHT-PIPE

Element	Wavelength, mμ	Signal-to-Background Ratios	
		With Light-Pipe	Without Light-Pipe
As	234.9	1.1	0.58
Bi	223.0	0.75	0.65
C[a]	247.8	0.88	0.26
Cr	520.6[b]	1.6	0.63

[a]Dry flame.

[b]Center line of unresolved triplet.

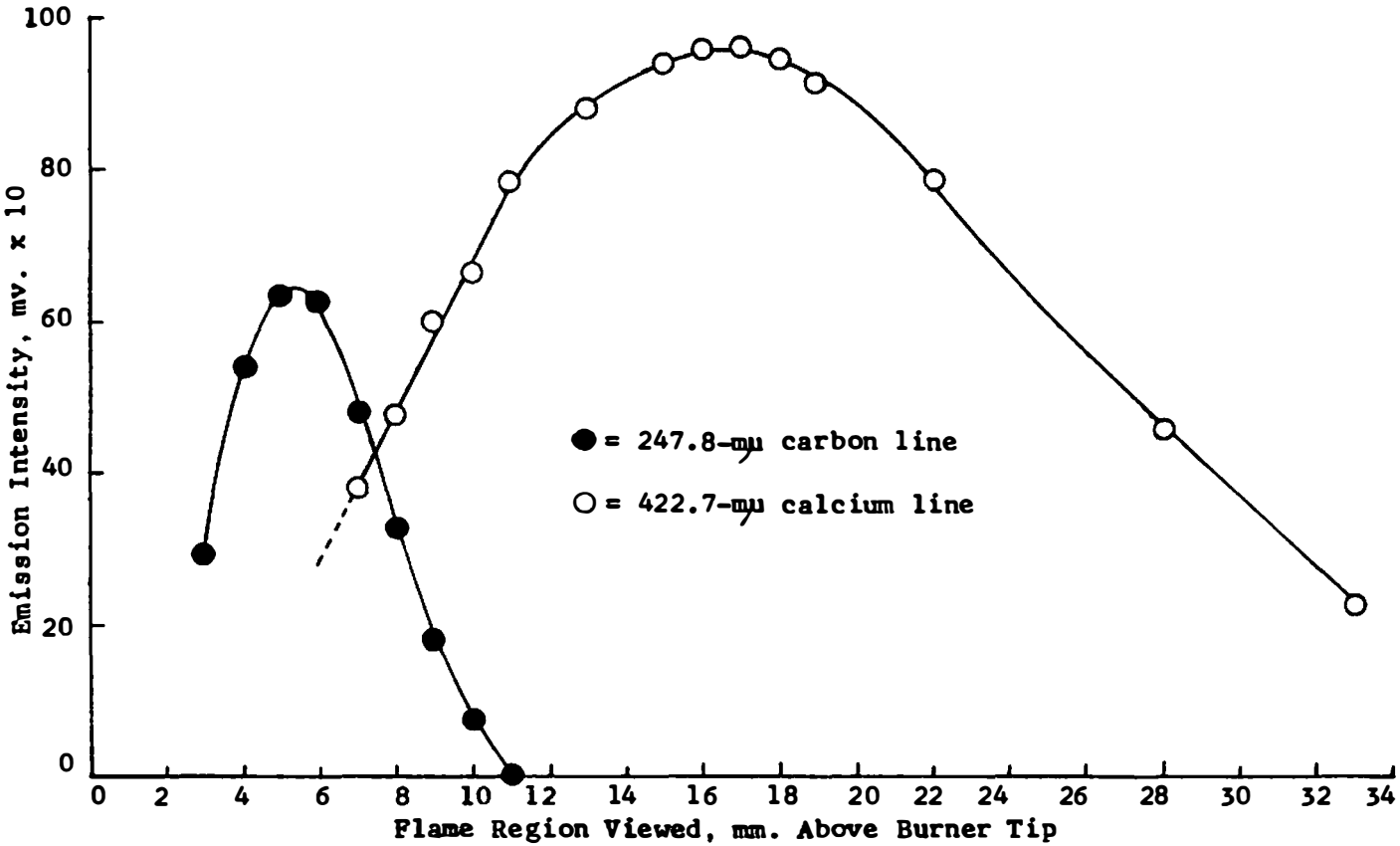

Figure 33. Plot of emission intensities of the 422.7-mμ calcium line and the 247.8-mμ carbon line versus flame region viewed.

intensity distribution was also spread throughout the flame. The distribution for calcium is contrasted with the intensity distribution of tin, shown in Figures 27 and 28. Although the initial portions of the intensity curves for tin and calcium originated in the reaction zone, the emission intensity of tin reached a maximum value much closer to the region of the reaction zone.

CHAPTER IV

DISCUSSION OF RESULTS

A. Application of the Light-Pipe to Flame Photometry

The light-pipe was useful when viewing different regions of the flame. The transmission characteristics of a reflecting and a non-reflecting light-pipe were studied. Reflections from the inner walls of the light-pipe contributed greatly to the relative intensity of the signal received by the detector. A light-pipe interposed between the flame and the entrance slit intercepted a larger portion of the luminous flux emanating from the flame. Various molecular band systems of the flame gases could be observed as different regions of the flame were viewed. The reaction zone of the flame could be defined sharply by following the emission intensity distribution of the 247.8-mμ line of carbon. The use of the light-pipe permitted the determination of the optimum flame regions for observing the emission of a particular element.

B. Flame Spectra of Metals in the Reaction Zone

A tabulation of the lines observed for several elements in the reaction zone of the flame is given in Table VI. The values of emission sensitivity are given only for the more intense lines. The lines observed are located in the ultraviolet region of the spectrum. One disadvantage when observing the reaction zone of the oxygen-acetylene flame is the unsteadiness of the background due to the intense CH and C_2 band

TABLE VI

EMISSION LINES OBSERVED FOR SOME ELEMENTS IN THE REACTION ZONE

Element	Wavelength of Lines Observed, mμ	Emission Sensitivities, μg. per ml. per % T
As	228.8	
	234.9	2.2
Bi	206.2	
	211.0	
	213.4	
	222.8	
	223.0	6.4
	227.7	
	240.1	
	289.8	
Cd	228.8	4.2
Hg	253.6	2.5
Pt	246.7	
	248.7	200
	262.8	100
	265.9	15
Sb	231.2	
	252.8	1.0
	259.8	
Sn	220.9 (ionic)	26
	224.6	
	226.8	
	231.7	
	233.4	
	235.4	
	242.2	
	242.9	1.6
	248.3 (ionic)	17
	254.6	
	257.2	
	270.6	
	284.0	
Zn	213.8	77

systems and the continuous emission of radiant energy always present in the initial stages of the combustion process. Above 260 mμ the OH band system became more troublesome as far as the nature of the background was concerned. At wavelengths below 260 mμ it was possible to open the slits to at least 0.13 mm. yet to retain a sufficient degree of resolution and signal stability. Fortunately, for the elements arsenic, antimony, bismuth, and tin, the major portion of their line spectra lie in the ultraviolet region of the spectrum which is relatively devoid of flame background emission. Spectral interferences were minimal except for the 247.8-mμ line of carbon which is found only in the reaction zone, and the intense 306.4-mμ band head of the OH system which overlaps the bismuth line at 306.7 mμ.

The emission lines tabulated in Table VI were for metal bromides dissolved in 4-methyl pentan-2-one. The emission characteristics of the elements were influenced by similar solvent and anion effects. Because the vast majority of the lines observed were resonance lines, which involve the ground state of the neutral atom, nearly all of the lines were subject to self-absorption. This was especially true for bismuth (Figure 29).

Since the excitation energy of the 247.8-mμ line of carbon is 7.68 ev., the presence of the carbon line in the reaction zone indicates that extremely energetic conditions prevail in the reaction zone of the oxygen-acetylene flame. Because only a very narrow region of the flame possesses this high energy, the emission of the more energetic atomic lines are limited to a small region immediately above the reaction zone (Figures 24 and 28).

Robinson[29] failed to detect the elements arsenic, antimony, bismuth, cadmium, mercury, platinum, and zinc from solutions which contained 1000 ppm in metal ion when employing an oxygen-cyanogen flame. This flame had a adiabatic flame temperature of 4500°C., approximately 1500° higher than the temperature of an oxygen-acetylene flame. This fact lends credence to the existance of abnormal excitation conditions in hydrocarbon flames. The C_2 band system is the only one in common to both oxygen-acetylene and oxygen-cyanogen flames, whereas CH and OH bands are always found in hydrocarbon flames. This would seem to eliminate the C_2 radical from an excitation mechanism in the oxygen-acetylene flame, although the C_2 radical may be involved in an intermediate step during the combustion process of hydrocarbon flames.

C. Interference Studies of Arsenic, Antimony, and Bismuth

The curves of emission intensity versus concentration for arsenic, antimony, and bismuth are shown in Figure 29. Appreciable self-absorption is evident for the 223.0-mμ line of bismuth, whereas arsenic and antimony exhibited linear curves, at least over the concentration of arsenic and antimony investigated. The presence of antimony and bismuth did not affect the emission intensity of the 234.9-mμ line of arsenic. The 252.8-mμ line of antimony was affected only by the presence of arsenic. The 223.0-mμ line of bismuth was unaffected by either arsenic or bismuth. Tin and zinc had a noticeable quenching effect upon the emission of arsenic. In view of these preliminary studies upon the emission

characteristics of arsenic, antimony, and bismuth, a flame spectrophotometric method of analysis appears to be feasible for the determination of these elements. Antimony and bismuth have been extracted using the sodium salt of diethyldithiocarbamate, and arsenic has been extracted using the diethylammonium salt of diethyldithiocarbamate.[30] The light-pipe would be necessary to obtain the optimum signal-to-background ratio since the emission zones in the flame for arsenic, antimony, and bismuth were very narrow.

D. Observations on the Emission Intensity Distribution of Calcium

Figure 33 illustrates the wide emission zone for calcium in the inner cone and extending out into the flame mantle. Contrast this with the emission zone for tin, shown in Figures 27 and 28. The 248.3-mμ ionic line of tin follows the same emission intensity distribution in the flame as does the 242.9-mμ atomic line of tin. Since the ionization potential for singly ionized tin is 7.3 ev., the presence of the ionic lines would be expected to be restricted to the energetic reaction zone. By contrast, the 422.7-mμ line of calcium has an excitation potential of only 2.93 ev. and the temperature of the flame is sufficiently high in the inner-conal region to allow excitation over a wider region of the flame. This fact would seem to indicate that the use of a fixed burner mounting, in the manner employed in commercially available instruments, is not always desirable. The excitation energy of the particular element determines the proper flame region from which

to obtain the maximum emission intensity.

E. Suggestions for Further Study

In this study the solvent and anion were purposely kept constant to eliminate possible effects of the solvent and the anion on the emission characteristics of the elements studied. The light-pipe permitted the reaction zone and the zone of maximum emission for a line or band to be determined quite readily. Thus a study of the effects of anion and solvent on the emission from a particular element would be possible. No attempt was made to ascertain the optimum conditions for excitation of the elements investigated. Since a flame-spectrophotometric method for these elements appears to be feasible, a more complete study of interferences, optimum excitation conditions, and methods for extraction of the metals into an organic solvent would be desirable.

The light-pipe was constructed from a length of ordinary aluminum tubing. The inner surface of the light-pipe was polished as well as possible with the limited facilities available. A mirror finish on the inside of the light-pipe would improve the efficiency of the reflecting surface. Perhaps, a more thorough study of the optical properties of the light-pipe would also be desirable.

CHAPTER V

SUMMARY

The present investigation was concerned with a preliminary study of the nature of the emission spectra of several elements in the reaction zone. Arsenic, antimony, bismuth, and tin were found to give a line emission spectra only in a very narrow region of the flame. This emission zone was related to the high energy reaction zone in that the excitation and emission were restricted to a region that was immediately above the reaction zone. The emission intensity of calcium, however, was spread throughout the flame mantle. The emission sensitivities of the elements arsenic, antimony, bismuth, cadmium, mercury, platinum, and zinc in an oxygen-acetylene flame were found to surpass the values that have been reported for these elements in an oxygen-cyanogen flame. A flame-spectrophotometric method would appear to be feasible for arsenic, antimony, and bismuth.

A light-pipe was developed which permitted the various regions of the flame to be viewed selectively apart from the remainder of the flame. The reflections from the walls of the light-pipe also provided an enhancement of the signal. The signal-to-background ratio was also greatly improved by the use of the light-pipe.

BIBLIOGRAPHY

BIBLIOGRAPHY

1. R. W. B, Pearse and A. G. Gaydon, "The Identification of Molecular Spectra," 2nd ed., John Wiley and Sons, Inc., New York, 1950, p. 79.

2. A. G. Gaydon, "The Spectroscopy of Flames," John Wiley and Sons, Inc., New York, 1957, pp. 114-136.

3. V. S. Rossikhin and I. L. Tsykor, optica i Spektroskopiya, 5, 202-204 (1958); C. A., 53, 7757 (1959).

4. W. M. Vaidya, Proc. Roy. Soc., 147, 513 (1934).

5. N. H. Kiess and A. M. Bass, J. Chem. Phys., 22, 569 (1954).

6. L. Haser, Ann. astrophys., 21, 114-116 (1958); C. A., 53, 3872 (1959).

7. H. C. Wolfe, "Temperature - Its Measurement and Control in Science and Industry," Vol. II, Reinhold Publishing Corp., New York, 1955, p. 278.

8. A. G. Gaydon and H. G. Wolfhard, Proc. Roy. Soc. (London), A 205, 118 (1951).

9. V. G. Alekseeva and S. L. Mandel'shtam, J. Exptl. Theoret. Phys. (U. S. S. R.), 17, 759-763 (1947); C. A., 42, 1503 (1948).

10. A. G. Gaydon and H. G. Wolfhard, Proc. Roy. Soc. (London), A 194, 169 (1948).

11. W. R. Kane and H. P. Broida, J. Chem. Phys., 21, 347 (1953),

12. H. P. Broida, J. Chem. Phys., 21, 340 (1953).

13. A. G. Gaydon and H. G. Wolfhard, Proc. Roy. Soc. (London), A 199, 89 (1949).

14. A. G. Gaydon and H. G. Wolfhard, Proc. Roy. Soc. (London), A 201, 561 (1950).

15. A. G. Gaydon and H. G. Wolfhard, Proc. Phys. Soc. (London), A 63, 778-780 (1950).

16. A. G. Gaydon and H. G. Wolfhard, "Flames - Their Structure, Radiation, and Temperature," Chapman and Hall, Ltd., London, 1953, p. 232.

17. Ibid., p. 235.

18. A. G. Gaydon and H. G. Wolfhard, Proc. Roy. Soc. (London), A 213, 366 (1952).

19. J. A. Dean, "Flame Photometry," McGraw-Hill Book Co., Inc., New York, 1960, p. 33.

20. J. W. Robinson, Anal. Chim. Acta, 24, 254-262 (1960).

21. G. V. Marr, Can. J. Phys., 35, 1265 (1957).

22. L. R. Koller, "Ultraviolet Radiation," John Wiley and Sons, Inc., New York, 1952, p. 140.

23. R. C. Ohlmann, P. L. Richards, and M. Tinkham, J. Am. Opt. Soc., 48, 531 (1958).

24. T. R. Harrison, "Radiation Pyrometry, and Its Underlying Principles of Radiant Heat Transfer," John Wiley and Sons, Inc., New York, 1960, p. 112.

25. P. Moon, J. Am. Opt. Soc., 30, 195 (1940).

26. P. Moon, J. Am. Opt. Soc., 31, 223 (1941).

27. Bulletin 259, Beckman Instruments, Inc., Fullerton, California, p. 2.

28. J. A. Dean, op. cit., p. 152.

29. J. W. Robinson, Anal. Chem., 33, 1226-1230 (1961).

30. G. H. Morrison and H. Freiser, "Solvent Extraction in Analytical Chemistry," John Wiley and Sons, Inc., New York, 1957, pp. 191-195.

VITA

William Joseph Carnes was born in Tucson, Arizona on December 7, 1933. He attended the elementary schools of that city through the junior year of high school. He moved to Knoxville, Tennessee in May, 1950 and was graduated from Knoxville High School in June, 1951. He entered The University of Tennessee in June, 1951 and was graduated with the Bachelor of Science degree in Chemistry in March, 1955. He entered the Graduate School of The University of Tennessee in March, 1955, where he held a graduate assistantship for two years and a teaching assistantship for one year. In April, 1958 he entered the Army and remained in the service until January, 1961. He returned to the Graduate School of The University of Tennessee in January, 1961 to complete his graduate work.

The author is a member of the American Chemical Society, Alpha Chi Sigma, and Sigma Xi.